SECOND NATIONAL CONFERENCE

ON

ELECTRON MICROPROBE ANALYSIS

June 14 - 16, 1967

Somerset Hotel

Boston, Mass.

***

Conference Chairman

Robert E. Ogilvie

***

Program Committee

R. E. Ogilvie
C. Klein
S. H. Moll
E. T. Peters
E. J. Rapperport
A. J. Saffir
T. O. Ziebold

SECOND NATIONAL CONFERENCE ON ELECTRON MICROPROBE ANALYSIS

Somerset Hotel -- Boston, Mass.

GENERAL PROGRAM

Tuesday, June 13, 1967

6:00 - 10:00 pm   Registration in the West Lobby

Wednesday, June 14, 1967

8:00 am   Registration (West Lobby)

9:00   Conference Opening (Louis XIV Ballroom)

            Technical Sessions

9:20   -- Principles and Practice of Quantitative Analysis (I)
1:30 pm   -- Principles and Practice of Quantitative Analysis (II)
3:50   -- Divergent Beam (Kossel) Diffraction

5:05   Business Meeting

6:30   Reception (Coronet Room)

Thursday, June 15, 1967

            Technical Sessions

9:00 am   -- Metallurgical Research with the Microprobe
1:30 pm   -- Geological Research with the Microprobe
3:50   -- Biological Research and Soft X-ray Analysis

7:00   Banquet (Louis XIV Ballroom)

Friday, June 16, 1967

            Technical Sessions

9:00 am   -- New Techniques and Instrumentation (I)
1:30 pm   -- New Techniques and Instrumentation (II)
4:35   -- Reports from Probe Users Groups

5:20   Conference Closing

****

All conference functions will be in the Louis XIV Ballroom.
Instrument exhibits will be in the Town and Country Room.
Message Center will be in the West Lobby (tel. 267-9000)

9:00   Conference Opening -- Prof. Robert E. Ogilvie, Conference Chairman

PRINCIPLES AND PRACTICE OF QUANTITATIVE ANALYSIS (I)

Chairman: T. O. Ziebold

Time	Author	Title	Paper Number
9:20	VIGNES, DEZ	Distribution in Depth of the Primary X-ray Emission in an Anticathode of Titanium and in an Anticathode of Lead	1
9:40	HUTCHINS, WANTMAN	Measurements of Surface Ionization of X-rays as a Function of Overvoltage and Atomic Number	2
10:00	BROWN, WITTRY	A Transport Equation Program and Its Application to Electron Microprobe Analysis	3
10:20	DUNCUMB, daCASA	Atomic Number and Absorption Corrections: Accuracy Obtained in Practice	4
10:40	WITTRY, ANDERSEN	An Evaluation of Absorption Correction Functions for Electron Probe Microanalysis	5
11:00	BARMAN	A Proposed Extension to Philibert's Absorption Correction	6
11:20	HEINRICH	The Absorption Correction Model for Microprobe Analysis	7
11:40	WARNAARS	Quantitative Analysis of Silicate Minerals	8
12:00	lunch		

PRINCIPLES AND PRACTICE OF QUANTITATIVE ANALYSIS (II)

Chairman: Peter Duncumb

Time	Author	Title	Paper Number
1:30	CRISS	Secondary Fluorescence in Terms of f( )	9
1:50	HEINRICH, YAKOWITZ	Quantitative Electron Probe Microanalysis: Fluorescence Correction Uncertainty	10

2:10	BEAMAN	A Computer Program for Quantitative Electron Probe Microanalysis	11
2:30	REED, MASON	Iterative Methods in Microprobe Correction Programs	12
2:50	FRAZER	A Computer Fit to Mass Absorption Coefficient Data	13
3:10	ANDERSEN, LATHE	Statistical Analysis of Micro-analytical Data	14
3:30	refreshments		

DIVERGENT BEAM (KOSSEL) DIFFRACTION

Chairman: R. E. Hanneman

3:50	MacKAY	An Examination of Factors Limiting Accuracy in Divergent Beam X-ray Diffraction	15
4:05	MORRIS	Lattice Parameters of Noncubic Crystals from Kossel Lines	16
4:20	FRAZER, REID	Lattice Parameters and Symmetry Information from Kossel Lines: Non-Cubic Crystals	17
4:35	UMENO, GENNAI, SHINODA	Grain Boundary Behavior of Macro-crystals in Plastic Deformation	18
4:50	VIETH, YAKOWITZ	A Novel Single Lens Kossel Pattern Generator	19

5:05 Business Meeting (Louis XIV Ballroom)

6:30 Reception (Coronet Room)

METALLURGICAL RESEARCH WITH THE MICROPROBE

Chairman: R. E. Ogilvie

			Paper Number
9:00	VIGNES, PHILIBERT, BADIA, LEVASSEUR	The Use of the Electron Microprobe for the Determination of Impurity Diffusion Coefficients	20
9:15	CALONI, FERRARI	Cu-Mn Interdiffusion Kinetics Studies by X-ray Microprobe Analyser	21
9:30	HEHENKAMP	Measurements of Transport Phenomena of Dilute Impurities in Metals	22
9:45	LIFSHIN	An Electron Microprobe Study of Diffusion in the Ni-Au System	23
10:00	RAPPERPORT, BENDER, WILDER, PEMSLER	Concentration Gradients in Cu-Ni-Mn Ternary Diffusion Couples	24
10:15	SHINODA, KAWABE, MURATA, ISOKAWA	Studies on Alpha and Beta Phases in Copper-Zinc Alloys	25
10:30	RANZETTA, SCOTT	Analysis of Fine Precipitates in a 25 Nickel-20 Chromium-0.7 Niobium Stainless Steel	26
10:45	SAWATANI, AOKI	Correction Procedures in Quantitative Electron Probe Microanalysis	27
11:00	SPENGLER, STICKLER	Electron Beam Microanalysis of "Sulfidation" Corrosion Layers on a Ni-Co-Cr Superalloy Exposed to Combustion Gases at High Temperatures	28
11:15	FISHER	The Effect of Nickel on the High Temperature Oxidation Characteristics of Copper-Bearing Steels	29
11:30	CLINE, BEATTY, GERHARD	Electron Probe Microanalysis of Laminated Metallization in Integrated Circuits	30
11:45	HART, PILNEY	Effect of Spectral Line Shift on Microprobe Data	31
12:00	lunch		

GEOLOGICAL RESEARCH WITH THE MICROPROBE

Chairman: E. J. Rapperport

1:30	BENCE, ALBEE	An Empirical Method for the Electron Microanalysis of Silicates and Oxides	32
1:50	CHODOS, SILVER	Electron Microprobe Analysis of Zircon Crystals for Trace Amounts of Lead, Uranium and Thorium	33

2:10	RUCKLIDGE, STUMPFL	Changes in the Composition of Petzite $(AuAg_3Te_2)$ During Analysis by Electron Probe	34
2:30	BOROM, HANNEMAN	Surface Damage Effects in Alkali Silicate Glasses During Electron Microprobe Analysis	35
2:50	BAYARD	Small Particle Identification by Electron Microprobe	36
3:10	TYNER, CESCAS, GRAY, LUEHRS	Iron and Manganese Distribution in Soil Concretions	37
3:30	refreshments		

BIOLOGICAL RESEARCH AND SOFT X-RAY ANALYSIS

Chairman: A. J. Tousimis

3:50	SAFFIR, OGILVIE	The Effects of Diet on the Microstructure of Teeth	38
4:05	HOGBEN, INGRAM	Electron Microprobe Display of Diffusable Constituents (K, Cl, Na) in Biological Tissues	39
4:20	CARROLL	Chemical Constitution of Bacterial Spores	40
4:35	GALLE	Electron Probe Microanalysis of Biological Ultrathin Sections	41
4:50	BAUN, FISCHER	Sample Self Absorption of Electron Excited Soft X-ray Spectra	42
5:05	OKANO, TOMURA	Light-Element Analysis with Multi-layered Pb-Stearate	43
5:20	RANZETTA, SCOTT	A Comparison of the Network Method of Pulse-Height Analysis with Crystal Spectrometry for Light Element Analysis	44

6:00   Social Hour (Anteroom of the Louis XIV Ballroom)

7:00   Conference Banquet (Louis XIV Ballroom)

NEW TECHNIQUES AND INSTRUMENTATION (I)

Chairman: S. H. Moll

			Paper Number
9:00	SKRIVANEK	Electron Microscope-Microprobe for Analysis of Small Particles	45
9:20	KOFFMAN, SCHIPPERT, MOLL, HAMILL	An X-ray Spectrometer Attachment for the Philips EM-200 Electron Microscope	46
9:40	CONTY, FINLEY	Design and Application of a Combined Instrument "Electron Microprobe Electron Microscope	47
10:00	SCHIPPERT, MOLL OGILVIE	Analytical Applications of a Combined Electron Microscope/Electron Microanalyzer	48
10:20	COOKE, DUNCUMB	Applications of a Combined Electron Microscope and Electron Probe Microanalyser-EMMA	49
10:40	KYSER, McCOY, WITTRY	Some Optical Signal Detection Techniques for Electron Microprobe Instruments	50
11:00	GREER, WHITE	Microprobe Attachment for Quantitative Studies of Cathodo-luminescence	51
11:20	ICHINOKAWA	Microanalysis of Electron Microscope Images with a New Type Electron Velocity Analyzer	52
11:40	KIMOTO, HASHIMOTO, TANAKA	Observation of the Transmitted Electron Image of Thin Films with a Scanning Electron Microscope	53
12:00	lunch		

NEW TECHNIQUES AND INSTRUMENTATION (II)

Chairman: E. T. Peters

1:30	RAPPERPORT	Deconvolution: A Technique to Increase Electron Microprobe Resolution	54
1:50	SPIELBERG	Mechanism of Gain Shift in Proportional Counters	55

2:10	HEINRICH, GILES, VIETH	Pulse Height Programmed X-ray Wavelength Scanning	56
2:30	MOLL, BRUNO	Gas Jet Sample Decontamination in the Electron Microprobe	57
2:50	McMILLAN	Statistical Evaluation of Photographic, Optical and Electronic Integration of X-ray Scans	58
3:10	KIMOTO, HASHIMOTO, TADA	A Specimen Heating Device for an Electron Probe Microanalyzer	59
3:30	refreshments		
3:50	ROBINSON, MITCHELL	A Simple Camera for Taking Stero Projection X-ray Micrographs with an Electron Microprobe	60
4:05	BEAMAN, DIEHL	On the Use of a Focusing Spectrometer with a Cambridge Electron Probe	61
4:20	BROWNING,COOKNELL, HEATHCOTE,OPENSHAW, WILLIAMS, WRIGHT	Progress in Fully Automatic Scanning Electron Probe Microanalysis	62

REPORTS FROM PROBE USERS GROUPS

Chairman: R. E. Ogilvie

4:35	FISHER, FISCHER, NOETZEL, SUTKOWSKI	Report of the New York Metropolitan Probe Users Group on Analysis of Fe-Ni and Fe-Cr Standards	63
4:50	BEAMAN	Report on the Activities of the Midwest Electron Probe Users Group	64
5:05	BÄCKERUD	Report of the Scandinavian Association of Microprobe Users	65

5:20   Conference Closing

INDEX OF AUTHORS AND THEIR AFFILIATIONS

INDEX OF AUTHORS AND THEIR AFFILIATIONS

INDEX OF AUTHORS AND THEIR AFFILIATIONS

SUMMARIES

OF

PAPERS

I

DISTRIBUTION IN DEPTH OF THE PRIMARY X-RAY EMISSION IN AN ANTICATHODE OF TITANIUM AND IN AN ANTICATHODE OF LEAD

A. Vignes and G. Dez

The distribution in depth (below the specimen surface) of the primary X-ray emission $\phi(\rho z)$ has been determined experimentally at various electron accelerating voltages for two elements -- lead and titanium.

The technique used is that previously used by Castaing and Descamps [1] for copper and gold. In order to separate from the total emission of the anticathode that of a particular layer, an artifice is used which consists in replacing the layer dz in the massive anticathode A by a thin layer of an element B close to element A and whose properties are substantially the same as regards diffusion and deceleration of the electrons. Layer B then acts as a "tracer" whose characteristic B emission can be easily separated by the spectrometer from the A emission of the anticathode as a whole.

The distribution in depth of the characteristic $L\alpha_1$ line of lead has been determined with the help of a tracer of bismuth at 29 and 33 KV. The distribution in depth of the characteristic $K\alpha_1$ line of titanium has been determined with the help of a tracer of vanadium at 17, 20, 25 and 29 KV. The experimental curve at 29 KV is compared with the curve calculated from the distribution in depth and energy of the incident electron computed by Bishop [2]. The agreement between experimental and theoretical results is good.

The value of $\phi(\rho z)$ for zero depth, $\phi(0)$, which is mainly due to back-scattering of the electrons, has also been determined for copper with a tracer of nickel at 17, 20, 25, 29 and 35 KV. This initial value $\phi(0)$ appears to be a function of the atomic number of the anticathode and the accelerating voltage. The data are compared with an expression proposed by Hutchins [3]

$$\phi(0) = 1 + 2 \eta$$

where η is the back-scattered electron fraction.

From the experimental curves of distribution in depth of the characteristic emission, the X-ray absorption correction curves, $f(\chi)$, for titanium and lead have been computed at 17, 20, 25 and 29 KV. The parameter $\chi = (\mu/\rho) \cosec \theta$, where μ is the linear absorption coefficient and θ is the take-off angle. These curves are compared with the curves predicted by the "Philibert correction" [4].

----

1. R. Castaing, J. Descamps, J. Phys. Rad., 16, 304 (1955); R. Castaing, Advances in Electronics and Electron Physics, Academic Press, N. Y., 1960, vol. 13, p. 317.

2. H. E. Bishop, Thesis, University of Cambridge.
3. G. A. Hutchins, The Electron Microprobe, McKinley et al (eds.) Wiley and Sons, N. Y., 1966, p. 390.
4. J. Philibert, Metaux Corrosion Industries, No. 465, May 1964; Third Int'l. Conf. on X-Ray Optics and Microanalysis (Stanford 1962), Academic Press, N. Y., 1964, p. 379.

2

MEASUREMENTS OF SURFACE IONIZATION OF X-RAYS AS A FUNCTION OF OVERVOLTAGE AND ATOMIC NUMBER

Gudrun A. Hutchins and Richard D. Wantman

In some samples, the x-radiation of interest is emitted only from a thin surface layer. Examples are very thin films on a substrate and soft x-rays in a highly absorbing matrix. For such samples, the total distribution of x-ray emission with depth is of little interest, but ϕ_0, the value of the ionization function at the surface must be accurately known.

From Castaing's early work, it is known that ϕ_0 is a function of the backscattered electron fraction and, therefore, a function of atomic number. As discussed by Duncumb and Melford [1,2], ϕ_0 is also a function of the ionization cross-section (dependent on the overvoltage U_0) of the particular radiation measured, and hence a function of the energy distribution of backscattered electrons. This means that ϕ_0 will not be the same for x-radiation of different wavelengths even if they are measured in the same matrix or the same thin films.

A set of curves of ϕ_0 as a function of U_0 and Z has been calculated [2]. However, there are few actual measurements, especially in the region of high U_0 and Z. The purpose of this paper is to discuss the measurement of this quantity and to make available new and extensive data.

Most previous determinations of ϕ_0 have been made by comparing the radiation from a film supported by a grid and a film on a substrate. Thin grid-supported films tend to buckle and tear under electron bombardment; thick films contribute significantly to the electron scattering. The authors have, therefore, found the following method to be preferable.

A number of substrates were mounted and polished together and subsequently coated with an evaporated film. The x-ray intensities emitted by the film on various substrates were measured and plotted as a function of Z. This curve was then extrapolated to Z = 0 to give the intensity corresponding to $\phi_0 = 1$ (Castaing's notation). The measured intensities on all substrates were then divided by this extrapolated value to give the higher ϕ_0 values directly. The figure gives an indication of typical data and error limits.

It was found that moderately thick films lowered the measured ϕ_0 curve. Therefore, it was necessary to use films thin enough to scatter only a few electrons and yet thick enough to yield statistically significant data. Precautions were taken to assure film uniformity, non-interference of spectral lines and substrate flatness. The data measured cover the range from Z = 4 to Z = 83 and from $U_0 = 1.5$ to $U_0 = 32$.

- - - - - - - - - - - - - - - - - - - -

1. P. Duncumb, D. A. Melford, Fourth International Congress on X-ray Optics
   and X-ray Microanalysis, Orsay, France, 1965.
2. P. Duncumb, D. A. Melford, First National Conference on Electron Probe
   Microanalysis, College Park, Md., 1966.

Typical Data Cu Film $U_0 = 3.4$

3
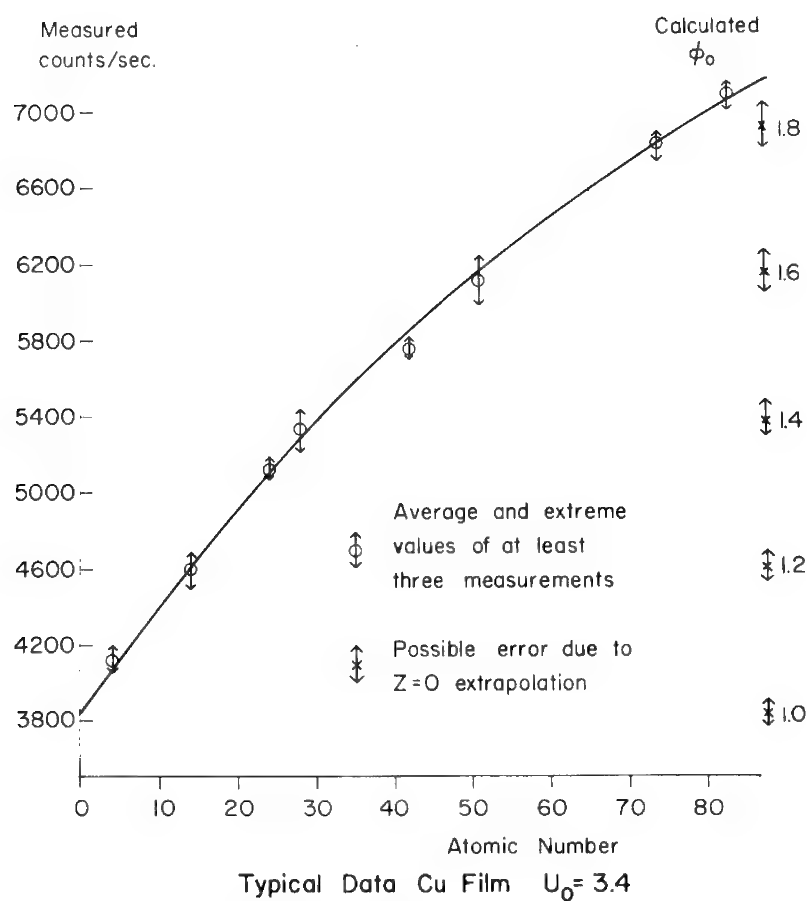
A TRANSPORT EQUATION PROGRAM AND ITS APPLICATION TO ELECTRON MICROPROBE ANALYSIS*

D. B. Brown and D. B. Wittry

Brown and Ogilvie [1] have described the use of a Boltzmann equation for electron transport to predict electron scattering and X-ray production in a semi-infinite specimen bombarded with 5 to 50 kev electrons. This paper will 1) outline refinements to this transport equation program (TEP); 2) compare predictions of the TEP with experimental data for the energy distribution of backscattered electrons, for the distribution in depth of primary x-radiation, and for the variation with voltage of emerging X-ray intensity; 3) discuss the use of the TEP to calculate microprobe calibration curves (intensity ratio versus composition). With respect to the latter, it will be shown that a correction for fluorescence due to the continuum is not generally negligible.

The three most interesting modifications of the TEP are as follows: First, Bethe, Rose and Smith [2] have shown how to treat electron transport as a diffusion problem when the propagation directions have become sufficiently random. This approach is now used in the TEP after the electrons have lost "memory" of their original direction. This reduces the mathematical treatment from a three dimensional to a two dimensional problem, thus significantly cutting computation time, especially for high Z where scattering is greatest.

Second, the initial stages of scattering are now treated more carefully. The principal result of this change is that the energy distribution of backscattered electrons does not approach zero for energy approaching that of the incident electron beam. This is in agreement with the experimental results of Kulenkampff and Spyra [3] and of Bishop [4].

Third, in calculating the relation between the mean energy of an electron and the range that it has traveled it is usual to assume the continuous-slowing-down-approximation. According to this model one may say $dx/dV = (dV/dx)^{-1}$. That is, one takes dV/dx according to Bethe, takes its reciprocal, and integrates this to find range versus energy. Spencer and Fano [5] have shown how to treat this problem more rigorously. The most striking result of Spencer-Fano theory is that dx/dV peaks up in the region of the initial voltage. This means that electrons lose energy more slowly in the early portion of their travel than the continuous slowing model predicts. The introduction of Spencer-Fano theory in the TEP has moved the peak of the backscattered electron energy distribution to higher energy, in better agreement with experiment.

The TEP has been used to predict the intensity of radiation leaving an Al specimen at 15.5 degrees for several voltages. This has been compared with experimental work by Brown and Ogilvie [6]. Agreement was very good. This

may be to some degree fortuitous since both the mass absorption coefficient and the fluorescence yield factor are uncertain.

The TEP has been used to calculate a calibration curve for Cu-Au alloys at 30 kev with a takeoff angle of 52.5 degrees. This system has a well-known "atomic number effect." In order to get good agreement with experiment [7] it has been found necessary to correct for secondary ionization due to the continuum. The fraction of emerging Au $L\alpha$ radiation due to fluorescence is calculated to be of the order of 10% for this system.

----

1. D. B. Brown, R. E. Ogilvie, J. Appl. Phys., 37, 4429 (1966).
2. H. A. Bethe, M. E. Rose, L. P. Smith, Proc. Am. Phil. Soc., 78, 573 (1938).
3. H. Kulenkampff, W. Spyra, Z. Phys., 137, 416 (1954).
4. H. E. Bishop, Fourth Int. Cong. (Orsay), op. cit.
5. L. V. Spencer, U. Fano, Phys. Rev., 93, 1172 (1954).
6. D. B. Brown, R. E. Ogilvie, J. Appl. Phys., 35, 309 (1964).
7. T. O. Ziebold, Ph.D. Thesis, Massachusetts Institute of Technology, 1965.

ATOMIC NUMBER AND ABSORPTION CORRECTIONS: ACCURACY OBTAINED IN PRACTICE

P. Duncumb and C. da Casa

Numerous mathematical models have been proposed to permit the calculation of corrections in electron probe microanalysis, ranging from basic Monte Carlo studies to empirical fits of microprobe data. Although much can be learned from these two extremes, the former is normally too complicated for routine application, and the latter is often lacking in generality. The best compromise must be based on a model which is sufficiently simplified to permit rapid calculation, if necessary without the aid of a computer, and yet well tested by a wide variety of practical measurements to ensure generality.

Philibert [1] has proposed a model of the electron scattering process and Duncumb and Shields [2] have modified this to take account of the critical excitation potential of the analysed elements. Although this gives a good representation of the X-ray absorption correction in a given target, it does not describe well the correction to be made to the ratio of generated intensities from two targets of different atomic number. To allow for this, it is strictly necessary to make a numerical integration of the intensity generated along the track of an electron in each target. Integration can be avoided, however, by an approximation first suggested by Thomas [3] and we have now established the range over which this can be applied. To take account of the ionization loss due to back-scatter, a set of curves for the quantity R (the fractional loss being 1 - R) is obtained from Bishop's [4] measurements of energy distribution and total back-scatter.

The above model makes use of the Bethe relation for electron energy loss, in which the mean ionization potential J is not accurately known for the energies used in probe analysis. J is therefore left undefined until last, and fitted as a function of target atomic number to experimental data obtained with the probe itself. It is this fitting of the least well known parameter which permits the final matching between theory and experiment to be carried out with precision.

To test the theory, probe measurements on over 150 alloys of known composition have been processed. In 40 of these cases, the atomic number correction was dominant, and these were used to establish the function J. Using the values for J so obtained, agreement between theory and experiment was found to be better than 5% (relative error) for over 80% of all the measurements made, despite a strong absorption correction in many cases and possible experimental errors in chemical and microprobe analysis. The choice of mass absorption coefficient is important, and results are shown comparing the values listed by Heinrich [5] with those of Theisen [6]. Where necessary, correction for fluorescence from characteristic radiation was made by Castaing's formula as modified by Reed [7]. Fluorescence from the continuum was found to be negligible.

----

1. J. Philibert, Third, Int. Symp. (Stanford), op. cit.
2. P. Duncumb, P. Shields, The Electron Microprobe, op. cit.
3. P. M. Thomas, Brit. J. Appl. Physics, $\underline{14}$, 397 (1963).
4. H. E. Bishop, Thesis, University of Cambridge (1966).
5. K. F. J. Heinrich, 1964, The Electron Microprobe, op. cit.
6. R. Theisen, Private Communication, (1967).
7. S. J. B. Reed, Brit. J. Appl. Physics, $\underline{16}$, 913 (1965).

5

AN EVALUATION OF ABSORPTION CORRECTION FUNCTIONS FOR ELECTRON PROBE MICRO-ANALYSIS

David B. Wittry* and C. A. Andersen

One of the most important corrections required in quantitative electron probe microanalysis is the correction for absorption of radiation by the specimen. Heinrich [1] emphasized the importance of more accurate methods to correct for absorption, and several authors [2,3] have noted that the usual correction procedures [4] for quantitative analysis fail to give satisfactory results when the accelerating voltages are low or the mass absorption coefficients are large.

A comparison of various experimental data is of immediate practical interest in quantitative electron probe microanalysis, particularly for cases of large absorption. A more accurate absorption correction will also clarify the atomic number effect and provide a better basis for evaluating theories of quantitative analysis. While experimental data for the absorption correction have often been compared, a systematic comparison that might draw attention to unreliable data has never been made.

In the present work, experimental data for $f(\chi)$ are compared by assuming that the absorption correction function depends on the product of χ and the mean depth of X-ray production. This comparison is expected to yield accurate results only if the mean depth of ionization is greater than $1/\chi$ so that changes in the shape of the excitation distribution function are not important. The dependence of the mean depth of X-ray production on accelerating voltage is determined from experimental data for which $V/V_k \gg 1$. Since the effect of varying V/V_k and varying atomic number are often obscured by errors in the experimental data, variation of the mean depth of ionization with these parameters is estimated from Bishop's Monte Carlo calculations. With the basis for comparison, it is found that the majority of the experimental data for $f(\chi)$ have a systematic variation with the accelerating voltage, excitation ratio V/V_k, and atomic number Z. Notable exceptions are explained by experimental errors, errors in absorption coefficients, or by fluorescence excitation. In this comparison, data for which the beam strikes the specimen at angles significantly different from 90 degrees are excluded because of possible errors due to changes in the backscattering [5].

For further comparison of existing experimental data, a special scale for $f(\chi)$ based on a Gaussian approximation to $\phi(\rho z)$ is used. On this scale $f(\chi)$ will plot as nearly a straight line function of $\ln \chi$ and can then be used to extrapolate the absorption correction to small $f(\chi)$. In this extrapolation the possibility that the mean depth of ionization must be replaced by an "effective mean depth of ionization" is examined in the light of experimental results, and the results of Monte Carlo calculations. Data for ultra-soft X-rays are then used to check the predicted variation of intensity with voltage and the relative intensity of nearby lines.

----

1. K. F. J. Heinrich, First National Conference (College Park) op. cit.
2. C. A. Andersen, ibid.
3. P. Duncumb, D. A. Melford, Fourth Int. Cong. (Orsay), op. cit.
4. D. B. Wittry, STP 349, Amer. Soc. for Test. and Mat'ls., Phila,, 1964.
5. R. A. Abelmann, R. Jones, J. Appl. Phys., 37, 4507 (1966).
6. R. Castaing, J. Henoc, Fourth Int. Cong. (Orsay), op. cit.
7. H. E. Bishop, ibid.

OBSERVED* AND CALCULATED VARIATION OF CKα INTENSITY FROM DIAMOND AS A FUNCTION OF ACCELERATING POTENTIAL (θ = 20°)

Calculated intensities at 10 KV: (1) Philibert's exponential model (full expression) as given by Duncumb and Melford [3], (2) Proposed correction model, linear extrapolation of function from large f(x) region, (3) Proposed correction model as based on experimental determinations of Castaing and Henoc [6], (4) Monte Carlo model as determined by Bishop [7].

*Observed intensities from Duncumb and Melford [3].

6

A PROPOSED EXTENSION TO PHILIBERT'S ABSORPTION CORRECTION

Mervyn L. Barman

In his original paper [1] Philibert derived the function

$$F(\chi) = \frac{1}{1+h(1=\underline{\chi})} \left[\frac{1}{1+\frac{\chi}{\sigma}} +h \frac{R_o}{R_\infty}\right] \qquad (1)$$

as an absorption correction factor. He then found that he could curve fit to some experimental data by proper choice of certain constants, along with setting $R = o$, by using the approximate function

$$F_a(\chi) = 1/ \left[1+\frac{\chi}{\sigma}\right] \left[1+h(1+\frac{\chi}{\sigma})\right]. \qquad (2)$$

Now, the above two functions are quite similar (assuming appropriate constants for each case) for small values of (χ/σ), but for light element work, where (χ/σ) may be very large, they are quite different functions. (As a matter of fact Philibert himself pointed out that equation 2 lacks physical content.) In working with light elements particularly it therefore seems advisable to use the full Philibert expression and find a means of evaluating the ratio R_o/ R_∞. The present paper represents an attempt to do this, and must be taken only as a first and highly tentative effort.

In Philibert's paper R_o and R_∞ are extreme values of the geometric efficiency function:

$$R(\rho z) = r(\rho z)/<|\cos\omega|> \qquad (3)$$

where ρz is the mass depth within the sample. Here $r(\rho z)$ is a function such that if there are n electrons moving downwards, then there are rn electrons moving both upwards and downwards. Also, ω is the angle which an electron path makes with the vertical, and the angular brackets represent an average at the given mass depth.

Let the subscripts U and D refer to electrons moving in the upward and downward directions, respectively. Then we can take a weighted average over the two hemispheres and write

$$<|\cos\omega|> = \{|<\cos\omega_D>| +(r-1) |<\cos\omega_U>|\} /r \qquad (4)$$

At great depth (subscript infinity) we will assume that the electrons have their velocity vectors isotropically distributed in space so that $r_\infty = 2$ and $|<\cos\omega>| = 1/2$, making $R_\infty = 4$. (Actually, at very low accelerating voltages it may happen that before this state of complete "diffusion" has taken place many of the electrons have already lost so much energy that they are no longer capable of generating X-rays. In this case R_∞ would be slightly less than 4.)

1. K. F. J. Heinrich, First National Conference (College Park) op. cit.
2. C. A. Andersen, ibid.
3. P. Duncumb, D. A. Melford, Fourth Int. Cong. (Orsay), op. cit.
4. D. B. Wittry, STP 349, Amer. Soc. for Test. and Mat'ls., Phila,, 1964.
5. R. A. Abelmann, R. Jones, J. Appl. Phys., 37, 4507 (1966).
6. R. Castaing, J. Henoc, Fourth Int. Cong. (Orsay), op. cit.
7. H. E. Bishop, ibid.

OBSERVED* AND CALCULATED VARIATION OF CKα INTENSITY FROM DIAMOND AS A FUNCTION OF ACCELERATING POTENTIAL (θ = 20°)

Calculated intensities at 10 KV: (1) Philibert's exponential model (full expression) as given by Duncumb and Melford [3], (2) Proposed correction model, linear extrapolation of function from large f(x) region, (3) Proposed correction model as based on experimental determinations of Castaing and Henoc [6], (4) Monte Carlo model as determined by Bishop [7].

*Observed intensities from Duncumb and Melford [3].

6

A PROPOSED EXTENSION TO PHILIBERT'S ABSORPTION CORRECTION

Mervyn L. Barman

In his original paper [1] Philibert derived the function

$$F(\chi) = \frac{1}{1+h(1=\underline{\chi})} \left[\frac{1}{1+\frac{\chi}{\sigma}} + h \frac{R_o}{R_\infty} \right]$$

(1)

as an absorption correction factor. He then found that he could curve fit to
some experimental data by proper choice of certain constants, along with set-
ting $R = o$, by using the approximate function

$$F_a(\chi) = 1/ \left[1+\frac{\chi}{\sigma}\right] \left[1+h(1+\frac{\chi}{\sigma})\right].$$

(2)

Now, the above two functions are quite similar (assuming appropriate constants
for each case) for small values of (χ/σ), but for light element work, where
(χ/σ) may be very large, they are quite different functions. (As a matter of
fact Philibert himself pointed out that equation 2 lacks physical content.)
In working with light elements particularly it therefore seems advisable to
use the full Philibert expression and find a means of evaluating the ratio
R_o/ R_∞. The present paper represents an attempt to do this, and must be taken
only as a first and highly tentative effort.

In Philibert's paper R_o and R_∞ are extreme values of the geometric efficiency
function:

$$R(\rho z) = r(\rho z)/<|cos\omega|>$$

(3)

where ρz is the mass depth within the sample. Here $r(\rho z)$ is a function such
that if there are n electrons moving downwards, then there are rn electrons
moving both upwards and downwards. Also, ω is the angle which an electron
path makes with the vertical, and the angular brackets represent an average at
the given mass depth.

Let the subscripts U and D refer to electrons moving in the upward and down-
ward directions, respectively. Then we can take a weighted average over the
two hemispheres and write

$$<|cos\omega|> = \{|<cos\omega_D>| +(r-1) |<cos\omega_U>|\} /r$$

(4)

At great depth (subscript infinity) we will assume that the electrons have
their velocity vectors isotropically distributed in space so that $r_\infty = 2$ and
$|<cos\omega>| = 1/2$, making $R_\infty = 4$. (Actually, at very low accelerating voltages
it may happen that before this state of complete "diffusion" has taken place
many of the electrons have already lost so much energy that they are no longer
capable of generating X-rays. In this case R_∞ would be slightly less than 4.)

At the surface (subscript zero) the downward moving electrons are all moving in a vertical direction so that $\cos_D = 1$. Since the upward moving electrons here are all the result of backscattering at random angles, we will assume their paths to be isotropically distributed in space so that $\cos_U = 1/2$. Equation 4 then becomes

$$R = 2\, r^2/(r+1) \tag{5}$$

If the sample is biased positively (say by a 67 volt battery) so that all secondary electrons return to it, we can write

$$1/r = \text{sample current/beam current} \tag{6}$$

In conformity with Philibert we write

$$h = 3.5\, A/Z^2 \tag{7}$$

and tentatively use [2] for the Lenard coefficient

$$= 4.72 \times 10^5/(V^{1.7} - V_c^{1.7}) \tag{8}$$

V and V_c being the accelerating and critical voltages (in KV), respectively. Also, we use only the backscatter factor in the atomic number correction, since it seems at the present time that the effect of stopping power is adequately represented through the terms r, , and cos . That is, strong scattering produces both great stopping power and a large scattering angle. Stopping power shows up both as backscattering expressed in r and as an effective current decrease expressed in , while the term cos expresses the average result of multiple large angle scattering. However, while r and show the effect of backscattered electrons in generating X-rays within the target, the total loss must still be expressed as an overall multiplying factor.

So far we have only applied this correction to the case of carbon radiation from silicon carbide. In Table 1 are shown the errors resulting from using the full function F along with those found from using the approximate function F_a.

The author wishes to thank Christian Anderson, Alan Joncich, and David Wittry for many helpful discussions.

----

1. J. Philibert, Third Int. Symp. (Stanford) op. cit.
2. Birkoff, Hdbk. d. Phys., Geiger and Schul (eds.), vol. 30; D. Wittry private communication.
3. J. V. Smith, J. Geol., 73, 830 (1965).

Table 1. Errors in Calculated Wt. % Carbon in Silicon Carbide

KV	% Error Using F	% Error Using F_a
4	4.5	53
5	5.1	47
6	2.5	21
7	5.4	18.5
8	7.6	25
9	2.2	30.5
10	0.1	23

Notes: 1. Pyrolytic graphite standard.

2. Atomic number effect multiplier taken as equal for both sample and standard from an extrapolation of Green's curve (3). The error in doing this is significantly less than the differences shown above.

3. In computing F_a the Duncomb and Shields formula for σ is used. Cf. "The Electron Microprobe" by McKinley, Heinrich and Wittry. John Wiley, 1966.

THE ABSORPTION CORRECTION MODEL FOR MICROPROBE ANALYSIS

Kurt F. J. Heinrich

Experimental evidence concerning the attenuation of X-rays within the target is obtainable through tracer experiments [1,2] and measurements with variable X-ray emergence angle [3,4,5]. Quantitative electron probe microanalysis with the aid of elemental standards requires a generalized expression for this effect. Of several proposed analytical models [6,7,8], that of Philibert [9], modified by Duncumb and Shields [10] is in closest agreement with the experiments. In this model, which can be written as follows:

$$I/I' = 1/f = (1 + \chi/\sigma)(1 + a\chi/\sigma) \tag{1}$$

the ratio of the generated counting rate $\underline{I}$ (within the solid angle of observation) to the emerging counting rate $\underline{I}'$ is expressed as a function of three variables, χ, σ, and a. The first variable is

$$\chi = \mu.\text{cosec } \theta \tag{2}$$

where μ is the mass attenuation coefficient of the observed radiation within the specimen, and θ the emergence angle. Similar expressions can be developed for oblique electron beam incidence [11]; such a geometry is not considered further in this paper. The term

$$a = 6A/(5Z^2 + 6A) \tag{3}$$

depends exclusively upon the atomic number Z and the atomic mass A of the target, and the term

$$\sigma = 2.39 \times 10^5 / (V^{1.5} - E^{1.5}) \tag{4}$$

is a function of the operating voltage V and the minimum excitation potential E.

Yakowitz and Heinrich showed [12] that the value of 1/f should be kept small in order to minimize the errors due to faulty input parameters. For moderate values of 1/f, equation 1 can be rewritten as follows:

$$1/f = 1 + (1 + a)(\chi/\sigma) + a(\chi/\sigma)^2 \simeq 1 + (\chi/\sigma)(1 + a) \tag{5}$$

The suppression of the quadratic term [13] does not introduce serious errors unless 1/f is unacceptably big. It will be shown that Green's data show linearity for 1/f within the useful range, and that plotting 1/f as a function of χ permits a better way of extrapolating to ($\chi = 0$) than the plot of log f used by Green. The absorption correction can thus be reduced, for hand cal-

culation, to the simple form

$$k_a = k \ (\sigma + \bar{b}'\mu)/(\sigma + b^{*'}\mu^*)$$ (6)

In this equation, k is the observed intensity ratio, k_a is the absorption corrected ratio, $\bar{b}' = (1 + \bar{a}) \ \mathrm{cosec} \ \theta$, $b^{*'} = (1 + a^*) \ \mathrm{cosec} \ \theta$ and $\bar{a}$ and a^* are the values of a according to equation 3, for specimen and standard; $\bar{\mu}$ and μ^* are the mass attenuation coefficients for specimen and standard, respectively. Observation of 1/f as a function of χ shows that the present uncertainties of the absorption correction are essentially uncertainties in the slope of

$$1/f - 1 = b\chi/\sigma$$ (7)

This equation permits calculating values of σ from experimental data of 1/f as a function of χ, and assuming that the value of b derived from Philibert's equation holds. A study of the values of σ obtained in this manner permits drawing the following conclusions:

a. The general model proposed by Philibert and Duncumb describes well the variation of the absorption correction as a function of atomic number, operating voltage, minimum excitation potential, and mass attenuation coefficient.

b. The value of b derived from Philibert's equation, $b = (5Z^2 + 12A)/(5Z^2 + 6A)$, describes adequately the variation of the absorption correction with atomic number.

c. The following expression for voltage dependence was found to be most adequate:

$$\sigma = 4.5 \times 10^5/(V^{1.65} - E^{1.65})$$

The exponent 1.65 is identical to that proposed by Andersen and Hasler; however, the coefficient differs from that used by these authors. It should also be pointed out that this expression yields analysis results very similar to those obtained with the value of σ proposed by Duncumb and Shields, except for low voltages and low atomic numbers.

d. Very poor fit of the absorption function is obtained for radiation of short wavelength (e.g. Ag and MoKα, ULα). This is attributed to the effects of fluorescence by continuous radiation. The discrepancy is of no practical consequence for the absorption correction, since the absorption correction for such radiations is trivial. This is not equivalent to saying that the entire correction for fluorescence from the continuum can always be neglected.

----

1.   R. Castaing, J. Descamps, J. de Phys. Rad., 16, 306-17, (1955).
2.   R. Castaing, J. Henoc, Fourth Int. Conq. (Orsay), op. cit.
3.   R. Castaing, Doctoral Thesis, U. Paris, (1951).
4.   M. Green, Third Int. Symp. (Stanford), op. cit.
5.   D. B. Brown, Doctoral Thesis, M. I. T., Cambridge, Mass., (1965).
6.   L. S. Birks, J. Appl. Phys., 32, 387 (1961).
7.   C. A. Andersen, M. F. Hasler, Fourth Int. Conq. (Orsay), op. cit.
8.   R. Theisen, EUR-I-1, Report, Centre Commun de Recherche Nucleaire,
     Etablissement d'Ispra - Italy, (1961).
9.   J. Philibert, Third Int. Symp. (Stanford), op. cit.
10. P. Duncumb, P. K. Shields, The Electron Microprobe, op. cit.
11. T. A. Taylor, Master's Thesis, Stanford University, (1965).
12. H. Yakowitz, K. F. J. Heinrich, submitted to Mikrochim. Acta.
13. J. A. Belk, Proc., Fourth Int. Cong. (Orsay), op. cit.

QUANTITATIVE ANALYSIS OF SILICATE MINERALS

F. W. Warnaars

For the quantitative analysis of unknown minerals it is recommended to use standards which have a chemical composition as identical as possible to the mineral to be determined. As it is hardly possible to have standards for all kinds of minerals, it is more practical to use the same standards for all analyses.

With a Norelco microprobe, 35 different minerals have been analysed for Na, Mg, Al, Si, Ca, Ti, Fe and Ni. These minerals are of simple composition or have been analysed already by wet chemical methods (pyroxenes, feldspars, amfiboles, olivines and garnets). For all analyses the same standards have been used:

Albite ($NaAlSi_3O_8$) for sodium radiation

Olivine ($(MgFe)_2SiO_4$) for magnesium radiation

Kyanite Al_2SiO_5 for aluminium radiation

Sphene $CaTiSiO_5$ for titanium radiation

Wollastonite $CaSiO_3$ for silicium and calcium radiation

Fe-rich cummingtonite ($FeMgSiO_3$) for iron radiation and pure Mn and Ni

Comparisons from the wet chemical analyses have a reproducibility of about 3 percent.

The low take-off angle of the Norelco probe (15°) makes it a very useful instrument to study absorption. Different methods of absorption corrections were compared, such as those described by Philibert [3], Birks [1], and Smith [4]. (The last author modified the parameter "h" of Philibert's method as shown in Figure 1.)

Making use of the overvoltage correction as suggested by Duncumb and Shields [2], theoretical curves were drawn in $f(\chi)$ vs χ diagrams at constant excitation potential for different pure elements by varying the take-off angle. Results are given in Figure 2. The values of $f(\chi)$ of the different minerals have been plotted in these diagrams together with their average Z. These values correspond to the theoretical curves of the different elements with an accuracy of 1 to 2 percent (see Figure 3). For example, by measuring aluminium in a mineral with an average Z of 13 the value of $f(\chi)$ for that mineral fits the theoretical curve for Z = 13. If Z = 14 it corresponds to the curve Z = 14.

In these diagrams the parameter "h" of the minerals has been assumed to be a function of the average Z of the mineral and is not the average $\overline{h}$ determined

from the weighted mass-concentration of the sample. The values of f(χ) of the minerals calculated with the average $\bar{h}$ do not correspond to the theoretical curves. (See Figure 4.)

----

1. L. S. Birks, 1963, Electron Probe Microanalysis: New York, Interscience Publishers.
2. P. Duncumb, P. K. Shields, The Electron Microprobe, op. cit.
3. J. Philibert, Third Int. Conf. (Stanford), op. cit.
4. J. V. Smith, "X-ray Emission Microanalysis of Rock-Forming Minerals," J. of Geol., 830-864 (1965).
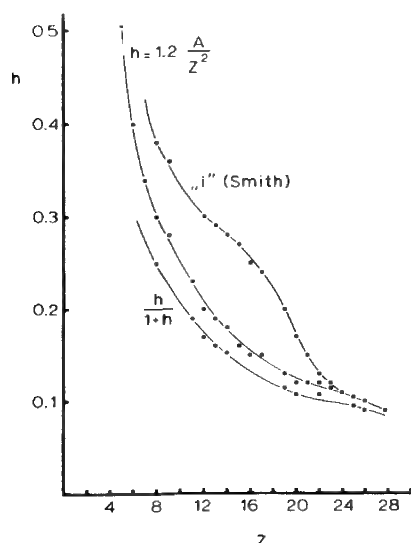
Figure 1   The electron-scattering-parameters of Philibert and of Smith with atomic number of the target.
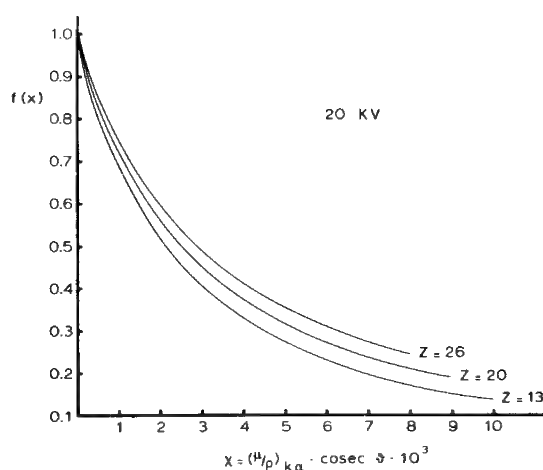
Figure 2   Theoretical curve of the fractional transmission at constant KV.
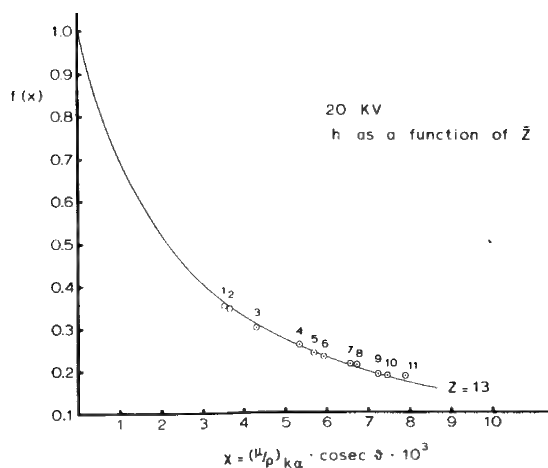
Figure 3   The f(χ) of AlK of minerals with different Z with the theoretical curve for Z=13.
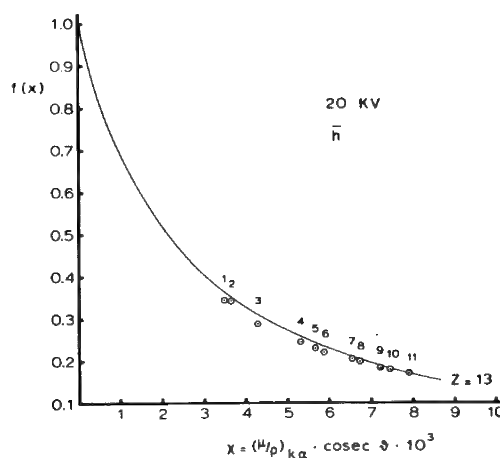
Figure 4   Same as Figure 3 except that parameter h is the average calculated from the weighted mass-concentration of the minerals.

9

John W. Criss

Fluorescence by characteristic lines has been expressed in terms of $f(x)$, thus eliminating the separate consideration of $\phi(\rho Z)$. The expression has a precision limited only by uncertainties in $f(x)$ and other physical parameters, and has closed mathematical form whenever $f(x)$ is represented by a rational function, e.g. Philibert's expression.

The derivations of previous formulae have shown that secondary fluorescence depends on a triple integral involving $\phi(\rho Z)$, the production of primary radiation as a function of depth. The approach until now has been to represent $\phi(\rho Z)$ by a mathematical expression that permitted integration in closed form. Such treatments introduce uncertainties in approximating $\phi(\rho Z)$.

The new formula described here results from a different arrangement of terms, substitution of variables, and order of integration. The function $f(x)$, rather than $\phi(\rho Z)$, must be represented mathematically. The relative X-ray intensity of some element, A, including the effect of fluorescence by another element, B, is found to be

$$R_A = \frac{G_A \, f_A \, (x) + G_B \, S_{AB} \, (x)}{G_A^\star \, f_A^\star \, (x^\star) + G_B^\star \, S_{AB}^\star \, (x^\star)}$$

where

$$S_{AB}(x) = \frac{1}{2} C_A K_A \quad \mu_{AB} \times \left[\frac{f_B(x)}{x} \ln\left(1 + \frac{x}{\mu_{MB}}\right) + \int_{\mu_{MB}}^{\infty} \frac{f_B(x) - f_B(t)}{t \, (t - x)} \, dt \right]$$

Here f_A and f_B are the familiar absorption correction functions for electron-excited characteristic radiation of elements A and B; x has the usual definition, and in every term applies to the measured element, A. The factors G_A and G_B represent total electron-excited radiation of A and B, generated throughout the specimen and not corrected for absorption. These factors would be proportional to mass fractions C_A and C_B, but for atomic number effects. Symbols with asterisks are similar quantities in the comparison standard. The mass absorption coefficients μ_{AB} and μ_{MB} are for the absorption of element-B radiation by element A and by the whole specimen. The factor K_A is $\omega(1 - 1/J)$, ω and J being the fluorescence yield and absorption edge jump-ratio for element A. If another element, D, also fluoresced element A, then additional terms $G_D S_{AD}(x)$ and $G_D^\star \, S_{AD}^\star (x^\star)$ would be added to numerator and denominator in the formula for relative intensity.

This formula is convenient for analysis whenever the integral in the expression for $S_{AB}(x)$ can be evaluated in closed form. Such is the case whenever $f_B(t)$ is a rational function. For example, one might use the Philibert expression,

$$f_B(t) = \frac{1 + h}{(1 + t/\sigma)\,[1 + h(1 + t/\sigma)]}$$

where h and σ correspond to the production of element-B radiation. The integral then reduces to

$$\frac{1 + h}{\sigma + X}\,\ell n\,(1 + \frac{\sigma}{\mu_{MB}}) + \frac{h^2}{(1 + h)\sigma + h}\,\ell n\left[1 + \frac{\sigma}{\mu_{MB}} + \frac{1}{h\mu_{MB}}\right]$$

where χ, as before, applies to element A.

Until now, equations including secondary fluorescence required knowledge of both f(χ) and Φ(ρZ). For the present formula, only f(χ) is needed.

QUANTITATIVE ELECTRON PROBE MICROANALYSIS: FLUORESCENCE CORRECTION UNCERTAINTY

Kurt F. J. Heinrich and Harvey Yakowitz

In order to determine the uncertainties in the evaluation of the fluorescence correction, the effects of microprobe operational variables, such as X-ray emergence angle and operating voltage, as well as model input parameter errors, such as fluorescence yield factors and mass attenuation coefficients, were investigated. To do this, both the Castaing [1] and Reed [2] models accounting for the effects of photons produced by K-characteristic line fluorescence within a microprobe specimen were subjected to error propagation analysis in much the same fashion as the function $f(\chi)$ was examined to determine the absorption correction uncertainty [3].

The analytical expression relating the true weight fraction, C_A, of a combined element in the matrix AB in which B excites fluorescence of A to the relative X-ray intensity will be:

$$C_A = k_A \left[1/(1+r_f) \right] \tag{1}$$

where k_A is the measured relative intensity appropriately corrected for any effects of absorption and atomic number differences which may or may not be present and r_f is the fluorescence correction factor as deduced from the relation of Castaing or alternately, that of Reed. If Equation (1) is subjected to propagation of error procedures, the relative error in the composition, $\Delta C_A / C_A$, will be given by:

$$\Delta C_A / C_A = (\Delta r_f / r_f) \left[r_f / (1+r_f) \right] \tag{2}$$

The task of error analysis is simplified by noting that Castaing's relation for r_f may be transformed to Reed's relation through multiplication by the factor $\left[(U_B-1)/(U_A-1) \right]^{1.67} (\lambda_A^E / \lambda_B^E)$ in which λ_A^E and λ_B^E are the K absorption edge wavelengths for elements A and B respectively and U_A and U_B are the overvoltage ratios for elements A and B respectively. By making use of this factor, only one extra term is obtained in the error analysis when using Reed's model rather than that of Castaing.

The effect of errors in the mass attenuation coefficients can be quite significant. In the error propagation analysis of the factor r_f, six of nine input parameter errors are caused by uncertainties in mass attenuation coefficients. Of the remaining terms, one is concerned with error in the X-ray emergence angle, θ, while one is concerned with the fluorescence yield factor, ω_B, and the final term has to do with the coefficient σ, which is assumed to describe the electron absorption as a function of voltage. It is found that errors in the absorption jump ratio as well as small operating voltage errors can be neglected. Assuming that the present models are basically correct, the largest single source of error in r_f arises from the uncertainty in the flourescence yield factor, ω_B. More accurate fluorescence yield factor data are definitely required [4].

As far as operational variables are concerned, the magnitude of the correction term r_f decreases as the X-ray emergence angle, θ, and the operating voltage decrease. However, the critical factor in the choice of emergence angle becomes the possible error in the emergence angle, $\Delta\theta$, when the compositional error ($\Delta C_A/C_A$) is considered. It is found that the same small absolute error in the value of the emergence angle will lead to a greater compositional error at θ of 15° than at θ of 60°.

Regardless of the value of the emergence angle, lower operating voltages reduce the magnitude of the fluorescence correction factor, r_f. Reducing the voltage reduces the depth of primary X-ray emission and hence the effects of error associated with the corresponding correction term, $[\ell n(1+v)]/v$, in the Castaing or Reed model. In fact, at high voltages, the input parameter uncertainties are larger than the differences between the Reed and Castaing models. A case for which this is true is the analysis of iron in 50Fe-50Ni alloy performed with an operating voltage of 30 kV.

The entire foregoing discussion refers to a nearly homogeneous specimen. For the case of a small precipitate or a highly segregated specimen in which fluorescence effects occur, no satisfactory model appears to be available. It has been suggested by Castaing that lower X-ray emergence angles coupled with low operating voltages will tend to diminish the analytical error in such cases [5].

----

1. R. Castaing, Thesis (1951).
2. S. J. B. Reed, Brit. J. Appl. Phys., 16, 913 (1965).
3. H. Yakowitz, K. F. J. Heinrich, Submitted to Mikrochimica Acta.
4. R. W. Fink, R. C. Jopson, H. Mark, C. D. Swift, Revs. Mod. Phys., 38, 513 (1966).
5. R. Castaing, Adv. Elect. and Elect. Phys., 13, 317 (1960).

II

A COMPUTER PROGRAM FOR QUANTITATIVE ELECTRON PROBE MICROANALYSIS

D. R. Beaman

In this program the chemical concentration of the analyzed element, C_1, is calculated from the measured X-ray intensity ratio, k, in an iterative process using the expression:

$$k = C_1 \left(\frac{F(0)'}{F(0)^0} \right) \left(\frac{f(\chi)'}{f(\chi)^0} \right) \left(1 + \frac{I_f'}{I_p'} \right) . \tag{1}$$

The symbols have the meanings normally encountered in electron probe micro-analysis and the superscripts prime and zero refer to the alloy and standard materials respectively. The absorption correction can be made using the techniques of Philibert, Duncumb and Shields, Green, Thomas, or Tong (modified). The latter two techniques correct for absorption and atomic number effect.

In the modified Tong procedure $F(\chi)$ is calculated from the expression:

$$F(\chi) = \frac{1}{\frac{z}{A}} \quad \frac{1}{1 + \frac{\chi}{\sigma_0}} \quad - \frac{1 - \frac{\phi(0)}{K}}{1 + \frac{\chi}{\sigma_0} + \frac{z}{m}} . \tag{2}$$

$\phi(0)$ is the value of $\phi(\rho z)$ at $z = 0$; K has a value of 3 or 4 depending on the overvoltage; and m and σ_0 are functions of the acceleration potential only. This expression has been found to give good results at low atomic number.

The Green $f(\chi)$ curves have been fitted to a Philibert type expression for $f(\chi)$ and a set of σ values determined along with an s value of 40; s appears in the Philibert expression for h where $h = sA/z^2$. The program will only use this technique if $\chi < 1200$, because the experimental $f(\chi)$ data for Cu exists for the range, $60 < \chi < 1000$.

Divergence has been found to accompany iteration in some multicomponent systems when using the Thomas expression. The program circumvents this problem by constructing, when divergence occurs, a pseudo-binary system in which the atomic number of the unanalyzed component is given by

$$\sum_{i=2}^{n} C_i z_i / (1 - C_1)$$

where n is the number of components. When using any of the above mentioned techniques the input data consists of the acceleration potential, take-off angle, choice of technique, atomic numbers of the components, and the measured intensity ratios.

Characteristic fluorescence effects are corrected for using either Castaing's or Reed's technique. Reed has derived two expressions, one exact and one approximate, both of which are incorporated into the program. The program can be used to correct for KK, LL, KL or LK fluorescence (L exciting K) and also for fluorescence arising from excitation by $K\beta$ or $L\beta$ radiation.

In iterating the concentration of the analyzed element, C_1, is taken to be the value midway between the previously assumed and calculated concentrations and a new concentration is calculated using equation 1. The concentrations of the unanalyzed elements are given by:

$$c_j = \frac{k_j}{\sum\limits_{i=2}^{n} k_i} (1 - c_1) \quad j \geqslant 2. \tag{3}$$

This is the only point where any normalization occurs within the program.

The program has been written in such a way as to minimize the amount of input data but still allow the investigator to maintain some contact with the problem; e.g., the investigator must calculate the intensity ratios and must decide when fluorescence occurs; however, atomic weights, fluorescence yields, absorption jump ratios, mass absorption coefficients, Thomas' backscatter and stopping power data, Reed's J(A) values, etc., are part of the permanent input data. The program is written in Algol 60 for use with a Burroughs 5500 computer. Additional programs using other correction techniques (Belk, Theisen, Tong) have also been written.

ITERATIVE METHODS IN MICROPROBE CORRECTION PROGRAMS

S. J. B. Reed and P. K. Mason (Mrs)

In calculating corrections for microprobe data, the difficulty that true concentrations are required before true correction factors can be obtained has generally been overcome by using an iterative procedure. Most commonly this has been "simple iteration," in which a set of corrected concentrations is calculated in each cycle from the concentrations obtained from the previous cycle. An alternative method sometimes used, which differs only in detail, is "Gauss-Seidel iteration." The limitations of these iterative procedures, and the relative merits of more sophisticated procedures for use in computer programs for calculating corrections, have not so far been considered.

Analysis of the convergence properties of simple iteration with binary specimens shows that divergence may occur when corrections are very large. In general only the absorption correction can be large enough to have this effect. General analysis of iterative behaviour with ternary and higher specimens is not practicable, so a set of imaginary ternary specimens with large absorption corrections was devised, and used to test the behaviour of simple iteration, together with several other iterative procedures. These include an "averaging method" in which concentrations from the last two cycles are averaged for each element, before being used for calculating the correction factors in the next cycle, which has the effect of damping any tendency to oscillate. Two general mathematical methods were tested: Aitken's delta-squared method and Wegstein's method. Finally the method proposed by Criss and Birks (Electrochemical Society Symposium, Washington, 1964), based on the hyperbolic form of correction curves for binary systems, was also included.

It was found that Wegstein's method gave the best results. Aitken's delta-squared method gave almost equally good results, but required more iterations. The averaging method was found to be less suitable for general use, since it did not give reliable results with monotonic convergence behaviour, which is quite often encountered. The Criss and Birks method, though ideal for binary systems, is not so suitable for ternaries. Of the methods tested, simple iteration was the least successful, and gave unsatisfactory results in over 40 percent of the test cases, compared with a nil failure rate for Wegstein's method. In many practical cases the corrections are not large enough for there to be a great advantage in using this method rather than simple iteration, but it is important that a computer program for corrections should give reliable results for all specimens likely to be encountered. It is clear from these investigations that the use of Wegstein's method is of considerable overall benefit, in extending the range of specimens for which correct results can be obtained, and reducing the number of iterations required. The cost in terms of added program complexity and increased storage requirements is very small, and in most cases there is a net reduction in computing time because fewer iterations are required.

A COMPUTER FIT TO MASS ABSORPTION COEFFICIENT DATA*

Jane Z. Frazer

Inaccurate values for mass absorption coefficients (μ/ρ) are one of the several sources of error in correcting for absorption in electron probe microanalysis. Without good μ/ρ values we cannot hope to refine absorption correction schemes currently in use or even evaluate their validity. Because experimental data are not available for all elements at all wavelengths, interpolation and extrapolation are necessary. Various authors have proposed empirical relations for calculating μ/ρ. The tabulation probably most used in probe analysis is that of Heinrich [1], which is based on the formula $\mu/\rho = C\lambda^n$, with values of C and n for each element assigned to fit measured values of μ/ρ. Differences between calculated and measured values appear sufficiently large to warrant a new attempt at obtaining values for C and n which provide a better fit to experimental values. In addition, it is desirable to extend the range of wavelengths for which the values are applicable.

Experimental data taken into consideration in this project consists of 2700 measurements on 33 elements, Be to Pu, from 18 different experimenters. Included in these data are recent measurements which were not taken into account in previous tabulations.

Two basic assumptions were made: that μ/ρ can be expressed by the function $C\lambda^n$, and that the degree to which an experimenter's values fit a function of this form is a reasonable measure of the accuracy of his experiments. These assumptions were also basic to Heinrich's tables. We fit the values of each experimenter within each region (e.g., below the K absorption edge, or between the K and L_1 edges) of each element to establish their internal consistency. But instead of using an all-or-nothing method of accepting or rejecting a set of data, we used standard statistical procedures to assign a weight to each measurement. Thus Allen's data from 1924-26 were not omitted, but in most cases they received very little weight.

Then all data for a given region of a particular absorber were fit by the least squares method and values of C and n found for each. At this point we made the further assumption that for each region all c's can be fit with a smooth curve as a function of Z, the atomic number, and n's likewise. The resulting equations enable one to calculate μ/ρ as a function of Z and λ.

All fitting was done by least squares methods with a digital computer. This is more accurate than graphical fitting as well as more convenient. Since almost all presently available data is now on punched cards, one can easily add new data as they become available and rerun the appropriate computer programs to revise the formulas whenever it appears desirable.

----

1. K. F. J. Heinrich, "X-Ray Absorption Uncertainty," The Electron Micro-
    probe, op. cit.

STATISTICAL ANALYSIS OF MICROANALYTICAL DATA

C. A. Andersen and R. F. Lathe

Microanalysis can be extended to studies of microstructures smaller in size than the resolving power of the microanalyzer. The correlation of elements, to each other and to position within the sample, can be investigated as can the chemical relationships between various members of a general population. The interpretation of the data gathered in such an investigation can be aided greatly through the use of statistical analysis. These various analytic approaches combined with the data handling capabilities of the computer provide an important tool for the study of complex, submicroscopic systems.

It is often of basic interest to know, for example, if two elements under investigation are spatially related and if they are correlated, that is, if they are functions of each other's concentration. If it is established that the elements are correlated then it is of interest to make some judgments as to their possible chemical combination. A statistical approach useful in such an analysis is the correlation plot. This is constructed by plotting the concentration of one element as a function of the concentration of the second element, when the two sets of data are taken from simultaneous measurements of selected points in the sample. A regression line can be calculated for the data which will indicate the fraction of the measurements which are correlated. The slope of this line for well correlated elements indicates a possible chemical combination for the elements when considered in terms of known compounds. Confidence limits can be placed on the slope of the line to help in interpreting the possible chemical compound. In addition a further statistical test can be applied which will indicate the possibility that such a group of measurements could be related purely by chance.

A second question of basic interest is concerned with the relationships of selected members of a general population. For instance, it might be desirable to know if all the chemical entities bearing element x are related. If they are not related is it possible to separate them into groups in which they are interrelated. The cumulative frequency plot is a useful approach to such a problem. The data points are plotted as a cumulating frequency of arbitrary intensity intervals. A least squares line can then be drawn through the points and used in conjunction with a statistical χ^2 test to judge the normality of the plotted distribution. If the points are judged to be representative of a single normal distribution the standard deviation of the distribution can be determined and compared to what would be expected solely from counting statistics. In this way information about the variation of the stoichiometry of the chemical combination or the size distribution of the microstructures bearing element x is gained. If the points do not represent a single normal distribution it may be possible to decompose the measured population into separate groups which are interrelated. The bases on which the measured population is divided to produce the separate interrelated groups indicate important facts about the chemistry of the sample (i.e. divided on basis of concentration or sample position etc.).

The frequency distribution plot is another useful statistical approach. It has the facility of grouping the data as functions of concentration, elemental ratio, or sample position. It is most often used in the present schemes of analysis as a preliminary data grouping step.

AN EXAMINATION OF FACTORS LIMITING ACCURACY IN DIVERGENT BEAM X-RAY DIFFRACTION

K. J. H. Mackay

An increasing number of papers are being published on the use of the divergent beam X-ray diffraction technique, particularly since the advent of electron-beam instruments has made production of the necessary point-source of X-rays an elementary procedure. The technique can be made to produce results of high intrinsic accuracy, of the order of 10 p.p.m. However, such measurements must depend on the accuracy with which the X-ray wavelengths employed are themselves known, and the absolute value of these cannot at present be taken to be much better than 40 p.p.m. [1] The question arises therefore whether the high (relative) accuracies obtained can be utilized to establish absolute standards for X-ray measurements.

The divergent beam diffraction pattern has the supreme characteristic of simplicity of production. Employing a single crystal specimen with few restrictions on dimensions, the method calls for no moving parts, and yields photographic records in exposures of minutes, or even seconds.

The photographs are both striking and significant. Study of the recorded pattern can lead - without physical measurements of any kind - directly to a determination of the lattice parameters of the crystal to a high degree of precision, such as was formerly obtainable only after laborious measurement, computation and graphical extrapolation.

It is important to examine closely the extent to which errors can affect the overall accuracy. Confining ourselves to those errors arising in using absorption conics, we observe that they fall under three general headings:

1. Errors arising in all divergent-beam methods.
    1.1 X-ray source
        -- Diameter of focal spot.
        -- Chemical and isotopic constitution of target.
        -- Value of wavelength assumed for radiation.

    1.2 Specimen
        -- Composition; degree of homogeneity.
        -- Degree of crystalline perfection.
        -- Temperature.
        -- Refraction effects.

    1.3 Photographic Emulsion
        -- Grain of film; thickness of emulsion.
        -- Angle of incidence between X-rays and plate.

    1.4 Diffraction Effects
        -- Line width; line symmetry
        -- Orders of intersecting conics.
        -- Choice of well-conditioned pairs of intersections (when two lattice parameters are to be found).

2. Errors additionally affecting applications which require measurements to be made on the films.

   2.1 Dimensional stability of film.

   2.2 Conversion of linear measurements on the film to angular relationships in space.

3. Errors similarly affecting applications which require measurements to be made on the experimental apparatus.

Before the highest accuracy can be obtained, particular attention must be paid to the following: 1) The precision of one's standards, 2) the observed line profiles, 3) the choice of well-conditioned intersections, 4) the conversion of linear measurements on film or plate, to spatial relations.

A divergent-beam pattern, by virtue of its similar degree of symmetry to the crystal causing it, contains much more information than is strictly necessary for solving the crystal parameter problem. In the pattern from a cubic crystal for instance, eight equivalent intersections may occur on the same photograph. If each is studied, independently, one gains a corresponding increase in confidence in the lattice parameter. Even more promising, perhaps, is the method which compares the reliability of results calculated from non-equivalent intersections, and derives an optimized value.

The divergent-beam technique, though capable of producing results to a high degree of precision, must be used with care if the cumulative effect of errors from a variety of sources is to be avoided. Since no intrinsic check is involved in the calculations, it is particularly important that - before publication - values of lattice parameter obtained by this technique should be compared with previously published values where possible, and any discrepancy satisfactorily accounted for.

----

1. G. D. Rieck, Section 2.2 in "International Tables for X-ray Crystallography" Vol. III (I.U.C., Kynoch Press, Birmingham, 1962).

LATTICE PARAMETERS OF NONCUBIC CRYSTALS FROM KOSSEL LINES

William G. Morris

The extension of precision parameter measurements to noncubic materials involves three steps. First, a procedure is developed which will select intersections and wavelengths that may be suitable for precision parameter determination in any crystal system. Second, each intersection length measurement from the film, L, must be converted to the corresponding angle, Γ. Third, the lattice parameters (six in the case of monoclinic crystals) are related to the angles, Γ_{ij}, of the intersections. Most of the error in precision parameter determinations arises in the second step where accurate lineal measurements are required.

In order to select sensitive intersections, all possible combinations of diffraction cones from a given crystal (approximate values of the lattice parameter are required) and set of wavelengths must be checked to see if a suitable intersection arises. The reciprocal lattice is used in these calculations since it simplifies the computation of angles between poles as well as the semi-angles of the diffraction cones. If the diffraction cones from two planes intersect but do not overlap more than 6 degrees, then the pair of planes is probably suitable for lattice parameter determinations and the lens intersection angle Γ is calculated. A FORTRAN computer program has been written to perform the necessary calculations. The technique of using metal and alloy foil overlays on a crystal permit the use of a wide range of wavelengths, some of which will give sensitive intersections.

The quantity which is read from the film and used in subsequent calculations is $\text{Sec}\Gamma$, where 2Γ is the angular length of the lens intersection. In general, the lens will not lie in the center of the film nor will it bear any particular relationship to the center of the film. Therefore, $\text{Sec}\Gamma$ is related to four lineal measurements: (1) the length of the lens intersection, (2) the source to film distance, (3) and (4), the distances from the center of the pattern to the two points of intersection on the lens. The nature of the lens intersection is such that the accuracy of the final lattice parameter determination is usually an order of magnitude better than the accuracy of the film measurements. Thus, film measurements accurate to one part in 1000 will typically yield a lattice parameter accurate to one part in 10,000. Improved accuracy can be achieved in special cases.

Lattice parameters in noncubic crystals can be determined by several independent intersections and using a "least squares" fitting procedure. One intersection must be measured for each lattice parameter to be determined (two for tetragonal and hexagonal crystals, three for orthorombic, etc.) and the intersections must be linearly independent. The calculations are again done by a FORTRAN program. Starting with approximate values of the lattice parameters, values of Sec are calculated for each intersection. These are then compared with the measured values from the film and the initial approximation is changed to give better agreement. One or two iterations in this manner usually give sufficiently accurate values for the lattice parameters.

LATTICE PARAMETERS AND SYMMETRY INFORMATION FROM KOSSEL LINES: NONCUBIC CRYSTALS*

Jane Z. Frazer and Arch M. Reid

Gielen et al [1] have described the use of lenses formed by two Kossel conics to determine precisely the lattice parameters of cubic crystals. Morris [2] has shown theoretically how this procedure can be extended to crystals of lower symmetry. In practice, however, it is sometimes difficult to find enough of the right kind of lenses in the right locations.

A particularly difficult problem is the detection of very small changes in symmetry which may or may not be accompanied by changes in cell volume. This type of problem is encountered in the study of superconductors. For example, two Kossel patterns were made of V_3Si, one above and one below the critical temperature. The patterns are clearly different, but it is not obvious whether the change reflects a phase transition in which the crystal changed from cubic to tetragonal with an a/c ratio $\leqslant 1.002$, or a change in the size of the cubic unit cell due to thermal contraction. We have not been able to make this distinction by measuring lenses.

In general, very high precision measurements of one single lattice parameter are of doubtful value if one is not sure that the associated structure is cubic. Many approximately cubic structures, when investigated with high enough precision, prove to be of lower symmetry of show interesting transitions to a lower symmetry having very small deviations from cubic structure. The establishment of the true symmetry in such systems is consequently a problem of general importance. While lens ratios remain the most precise measure of a cubic lattice parameter, supplementary techniques are often necessary if one is to extract the most information from a Kossel pattern.

In situations where it is not convenient to determine lattice parameters by measuring only lenses, other features of the Kossel pattern may be used. For example, there are persistent nodes [3]: Intersections of three or more conics which are independent of lattice parameters, wavelength, and crystal orientation but which depend on the symmetry of the crystal. Certain of these nodes exist for cubic crystals only; others persist for all orthogonal systems but break up if the crystal becomes non-orthogonal.

The study of such features and determination of precise lattice parameters from them is simplified if one considers a given point on the film as the intersection of a vector with the film plane. The vector which represents an intersection of any two absorption cones can be easily calculated, and the angle between any two vectors can then be expressed as a distance on the film. Computer programs have been written to perform these calculations.

Another program has been written to combine measurements from all or a selected number of conics and calculate the lattice parameters that best fit the entire

Kossel pattern. The program promises to be particularly useful in cases where the crystal under investigation cannot be oriented.

----

1. P. Gielen, H. Yakowitz, D. Ganow, R. E. Ogilvie, J. Appl. Phys., $\underline{36}$, 1965, p. 773.
2. W. G. Morris, General Electric Technical Information Series Report No. 66-C-217, July, 1966.
3. J. Z. Frazer, G. Arrhenius, Optique des Rayons X et Microanalyse, R. Castaing, P. Descamps and J. Philibert, (eds.), Editions Scientifiques Hermann, Paris, 1967.

GRAIN BOUNDARY BEHAVIOR OF MACROCRYSTALS IN PLASTIC DEFORMATION

Masataka Umeno, Norio Gennai and Gunji Shinoda

Grain boundary behavior of aluminum and zinc macrocrystals have been studied by EPMA-Kossel techniques using Mo, Cu and Zn $K\alpha$ radiation.

Neighboring grains are observed to influence the slip modes that are operative in the grain boundary regions of a grain. When the neighboring grains are incoherent, complicated distortion of Kossel patterns peculiar to the grain boundary region is observed. When certain slip systems of the first crystal becomes active, the slip systems in the second crystal which are activated locally under the influence of the first crystal are usually determined by the Schmid factor of the second crystal for the direction of tension caused by the slip system in the first crystal. Sometimes, relative rotations of both crystals were found in a boundary region and it was observed that the amount of rotation was slightly larger in a place about 200μ away from the grain boundary than in the place very close to it. Distortions of Kossel lines due to planes parallel to the grain boundary are more significant than those due to planes perpendicular to the grain boundary.

When the thickness of the specimen is small, the influence of neighboring grains are reduced. This is confirmed by the use of longer wavelengths, such as Cu and Zn $K\alpha$. The optimum specimen thickness for aluminum is about 0.5 mm for these radiations, which corresponds to about one third of that for Mo $K\alpha_1$. Therefore, there will exist a surface layer of a few hundred microns whose plastic behavior is different from that of the inner region of the specimen. For smaller crystals, nearly one mm of grain size in average, distortions of Kossel patterns are insignificant, which might show that in the extreme case minute crystallites flow without any deformation.

In zinc macrocrystals, deformation twins are usually generated in appropriately oriented crystals. Figure 1 is a Kossel pattern obtained at the twin boundary of a zinc crystal; lines are present which correspond to both matrix and twin regions. In this figure, the effect of slip in the deformation twin is observed in the (002) line of the twin.
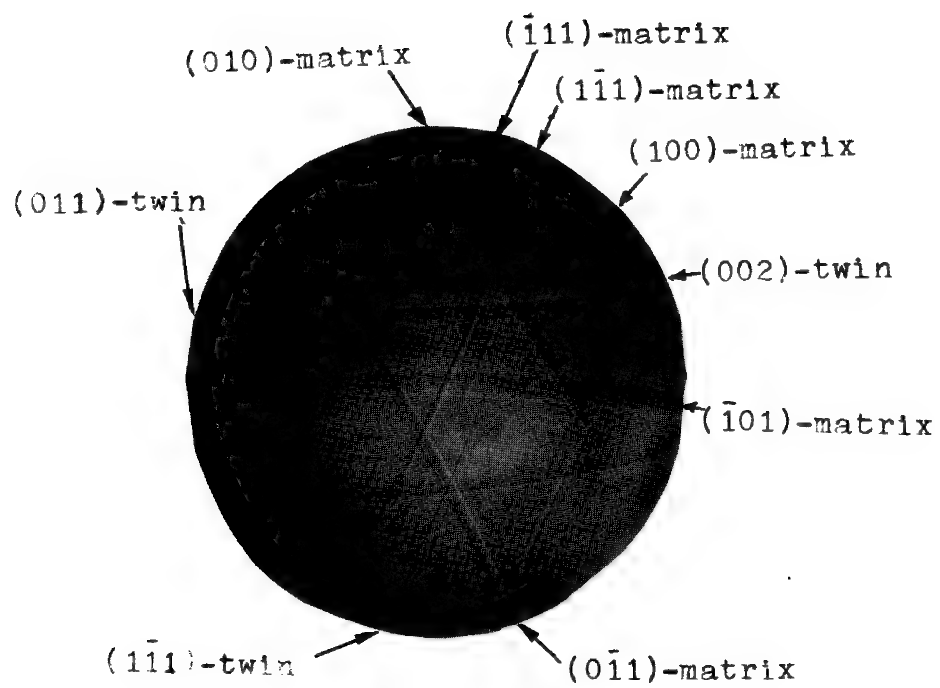
Figure 1   Kossel pattern obtained from a deformation twin
boundary in a zinc crystal.

A NOVEL SINGLE LENS KOSSEL PATTERN GENERATOR

D. L. Vieth and Harvey Yakowitz

The divergent beam X-ray diffraction technique has the advantage of being one of the most versatile techniques in addition to possessing very high spatial resolution. Until recently, two major factors inhibited the development of the technique to its fullest extent. These factors were the lack of a straight-forward mathematical technique for the reduction of experimental measurements and the lack of instrumentation development.

A significant advancement in the instrumentation for Kossel microdiffraction was demonstrated by Castaing in 1950 [1] when high quality Kossel patterns were obtained by means of the electron microprobe. Since that time consider-able effort has been expended in developing cameras to fit existing micro-probes.

Reduction of experimental measurements to crystallographic data was simplified when a straightforward mathematical procedure was developed in 1964 [2,3]. However, the mathematical procedure for the rigorous reduction of data requires that certain experimental conditions be fulfilled. Although the requirements are straightforward, the instrumentation required is somewhat more sophisticated than that being used previously.

To take full advantage of the versatility and high spatial resolution and to fulfill the requred experimental conditions, the following design concepts were considered essential:
1. Movement of the specimen in orthogonal directions
2. Capability of observing the specimen
3. Capability of orienting the specimen by means of a microgonimeter and facilities for controlling the goniometer from outside the vacuum
4. Capability of marking the center of the pattern
5. A specimen-to-film distance of 5 to 11 cm
6. An X-ray divergence angle of at least 56°
7. A camera which maintains the specimen in vacuum and the film in air.

An attempt was made to adapt a camera to an existing electron probe micro-analyzer [4] but the physical limitations made it impossible to build a camera having all the desired design features.

To overcome the limitations imposed by the instrument to which the camera was attached, a separate instrument was designed. The resulting instrument is a one electromagnetic lens [5] unit containing reflecting light optics and a transmission Kossel camera. The electromagnetic lens has a working distance of 50 mm with a C_s value of 67 cm and is capable of producing an intense spot of less than 10μ diameter. The light optics consists of a 50X reflecting objective with a numerical aperture of 0.56. It is possible to move the speci-men a total of 1/2 inch in both X and Y directions with a total vertical motion of 3/8 inch. The built-in goniometer is capable of being tilted ±12° about two axes and controlled from outside the vacuum system. A specimen-to-film distance of 10 cm is used; this results in an X-ray divergence angle of

70°. Patterns are obtained on either 5" x 7" film or glass plates. For ease of operation, the specimen is maintained in vacuum while the photographic film is in air.

----

1. R. Castaing, Thesis, U. Paris, 1951.
2. P. Gielen, H. Yakowitz, D. Ganow, R. E. Ogilvie, J. App. Phys. 36, No. 3 (Part 1), 773-782, March 1965.
3. H. Yakowitz, The Electron Microprobe, op. cit.
4. D. L. Vieth, H. Yakowitz, Rev. Sci. Instr. 37, 206-209, February 1966.
5. V. E. Cosslett, W. C. Nixon, H. E. Pearson, X-ray Microscopy and Micro-radiography, Academic Press, New York, 1957, p. 96.

THE USE OF THE ELECTRON MICROPROBE FOR THE DETERMINATION OF IMPURITY DIFFUSION COEFFICIENTS

A. Vignes, J. Philibert, M. Badia, and J. Levasseur

Diffusion is a rate-controlling process in a large number of metallurgical reactions, and the phenomenon can be measured in a wide variety of ways. The electron microprobe has been used mainly for measurements of the chemical interdiffusion coefficient in a binary alloy. The intrinsic diffusivity of a solute A, present in extremely dilute concentration in a pure metal B, is mostly measured by radioactive tracer techniques. A thin layer of radioactive isotope of the metal A is deposited on the surface of a single crystal of metal B by electroplating or evaporation. After the diffusion anneal, the specimen should be carefully sectioned and the activity in each section can be counted by a variety of techniques.

In the present study, the electron probe has been used for the determination of impurity diffusion coefficients. With an electron probe, concentrations of the order of 100 ppm can be measured, point analyses can be made in a volume of 1 to 2 cubic microns, and the penetration curve can be determined step by step each 5 microns, with no error in the distance measurements, so that accurate determinations of impurity diffusion coefficients can be made.

Two methods have been used, the thin film method and the diffusion couple. The thin film method has been used for the determination of the diffusion coefficient of copper into gold not previously determined by any method. A thin layer (1_μ) of copper is deposited on the surface of a crystal of gold by evaporation. After the diffusion anneal, analysis of a section of the specimen allows the precise determination of the "concentration-penetration curve" down to a concentration of copper of 0.0005. The concentration-penetration curves have been determined from 700 to 900°C. The data obtained follow the law

$$D^\circ_{Cu(Au)} = 0.105 \exp [- 40,600/RT] \ cm^2/sec$$

With a diffusion made of welded specimens of metal A and B, the "Hall method" of analysis of the concentration-penetration curve of each element allows the precise determination of the impurity diffusion coefficients of A in B and B in A at each end of the diffusion zone. This method has been used for the determination of the following impurity diffusion coefficients between 1100°C and 1400°C and the data obtained follow the laws:

$$D^\circ_{Fe(Ni)} = 0.28\exp [-60,500/RT] \qquad D^\circ_{Ni(Fe)} = 0.6\exp [-62,600/RT]$$

$$D^\circ_{Co(Ni)} = 0.16\exp [-(60200\pm1000)/RT] \qquad D^\circ_{Ni(Co)} = 0.128\exp [-(64500\pm1000/RT]$$

$$D^\circ_{Fe(Co)} = 0.11\exp [-60,500/RT] \qquad D^\circ_{Co(Fe)} = 0.17\exp [-67,000/RT]$$

The data obtained compared well in some cases ($D^\circ_{Co(Ni)}$, $D^\circ_{Fe(Ni)}$, $D^\circ_{Fe(Co)}$) with the results obtained by tracer radioactive techniques. In other cases ($D^\circ_{Ni(Fe)}$, $D^\circ_{Ni(Co)}$), discrepancies between the two sets of results are attributed to impurities present in the base metal in the radioactive tracer measurements.

The impurity diffusion coefficient of element B in metal A can also be determined by using A/AB couples. The B concentration in the AB alloy must be sufficiently dilute when B has a limited solubility in A -- so that the solution obeys Henry's law -- or when the diffusion coefficient varies rapidly with concentration. This method has been used for the determination of Al, Si and As diffusivities in B.C.C. iron between 800 and 1400°C.

In the case of aluminium, the diffusivity does not vary with concentration, and the Hall method has been used:

$$D^\circ_{Al(Fe)} = 5.9 \exp\left[-(57,700 \pm 1000)/RT\right]$$

In the case of silicon, the diffusivity varies appreciably with concentration, and the Matano analysis has to be used. However, the activation energy has been found to be fairly constant, so that the results may be extrapolated to infinite dilution

$$D^\circ_{Si(Fe)} = 8 \exp\left[-(59,500 \pm 1000)/RT\right]$$

$$D^{4\% \ Si}_{Si(FeSi)} = 17 \exp\left[-(59,500 \pm 1000)/RT\right]$$

$$D^{5\% \ Si}_{Si(FeSi)} = 17 \exp\left[-(59,100 \pm 1000)/RT\right]$$

$$D^{8\% \ Si}_{Si(FeSi)} = 35 \exp\left[-(59,400 \pm 1000)/RT\right]$$

In the case of arsenic only preliminary results have been obtained at the present time, and it is intended to compare more complete results with tracer measurements (As[76]). In the case of elements such as Al or Si, the microprobe determination seems quite promising since "good" tracers are not available.

The impurity diffusion coefficients have been in the past exclusively determined by radioactive tracers methods, while microprobe analysis has been mainly devoted to chemical diffusion studies. However, determination of impurity diffusivities, which are of considerable interest for solid solution theory, could be extended to many other systems with the help of the microprobe.

CU-MN INTERDIFFUSION KINETICS STUDIES BY X-RAY MICROPROBE ANALYSER

Olivo Caloni and Alberto Ferrari

Cu-Mn alloys have recently proved to be very interesting in different fields of application thanks to their particular properties. A study of the interdiffusion of these two elements is of particular technological interest. Diffusion of manganese in copper single crystals have been studied by some investigators with tracers utilizing a compositional gradient approaching zero [1,2]. These investigations are of primary importance from a theoretical viewpoint, since practical problems involve diffusion under significant concentration gradients.

In our experiments the diffusion coefficient was obtained on elementary copper and Cu-28% Mn alloy couples. These couples were put into intimate physical contact by a screw-press. Thermal diffusion treatments were carried out in a vacuum between 640°C and 820°C for times varying from 2 to 32 hours. The temperature was kept constant within $\pm$ 2°C. Less than 5 minutes were required to heat or cool the sample. Diffusion layers were analysed with an ARL electron microprobe. The concentrations of Cu and Mn elements were calculated by making the fluorescence and absorption corrections in intensity ratios of X-radiation emitted by samples and pure standards [3].

The time-penetration curves show that experimental results follow, in the range of temperature explored, an equation of the type: $x^n = Kt$ with $n = 2.11$. According to the results obtained, the volume diffusion process prevails, and interdiffusion in the Cu-Mn system exhibits almost symmetrical penetration curves.

The calculation of diffusion coefficients were made by the Grube's method. If one plots $x/2 \sqrt{Dt}$ as a function of x, one obtains a linear relationship as shown in Figure 1. This indicates that D is independent of concentration. The linear relationship was employed to calculate the diffusion coefficients.

Figure 2 shows log D as function of the reciprocal of absolute temperature. The straight line fitted by the least squares calculation is expressed as:

$$D = 0.58 \exp [-42,390/RT] \quad cm^2/sec$$

The activation energy of the diffusion process has also been calculated from time-penetration curves. The value obtained is consistent with the above.

----

1. C. D. Mackliet, Phys. Rev. 102, (1958).
2. Kushima, J. Phys. Soc. Japan 14, III (1959).
3. J. Philibert, Metaux Corrosion Industries, No. 465, 466, 468 (1964).

Figure 1

$$D = D_0 \exp(E_D/RT)$$
$$D_0 = 0.58 \, cm^2/sec$$
$$E_D = 42,390 \, cal/mol$$

Figure 2

22

MEASUREMENTS OF TRANSPORT PHENOMENA OF DILUTE IMPURITIES IN METALS
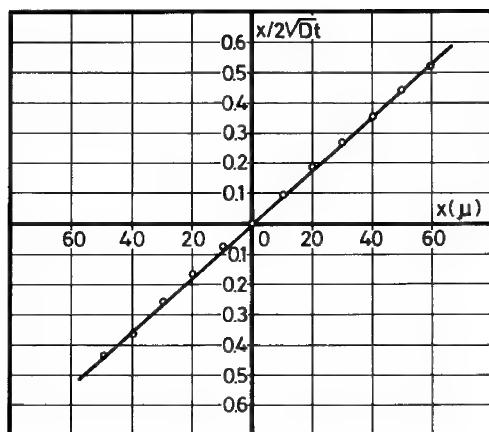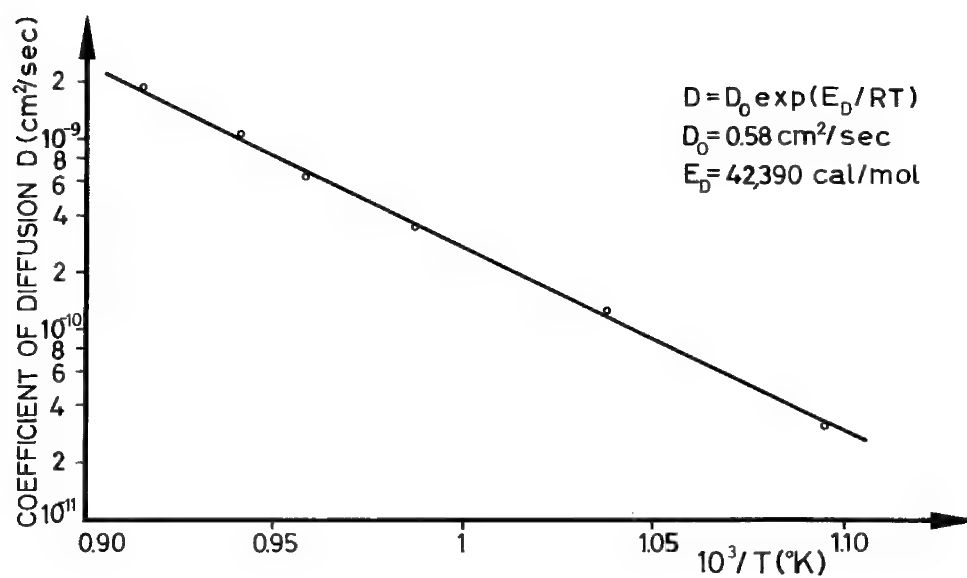
Theodor H. Hehenkamp

Radioactive tracers have been used to measure mass transport in metals, such as electromigration or the Soret effect. Such measurements are based on solutions of a transport equation for appropriate boundary conditions. By determination of a concentration profile, one obtains the mobility in terms of the diffusion coefficient D. The shift of this profile -- relative to a space fixed reference system -- produced by the driving forces yields information on the transport velocity, and from this the physically important properties, such as effective charges, can be derived. Since this shift often is in the order of only 10 to 100 microns, its precise measurement requires much better spatial resolution of the local concentration analysis than can usually be provided by tracers and conventional sectioning techniques.

Whereas this latter procedure is still necessary for measurements of self transport in pure metals, the situation for transport of impurity atoms in a matrix can be greatly improved by using an electron microprobe for analysis. From several points of view, application of this instrument seems to be quite favorable. It provides much better linear resolution and facilitates exact positioning of the measured profile with respect to the reference system by means of the internal optical microscope. As will be discussed in detail, application of a microprobe for this purpose is also quite justified from the standpoint of the possible analytical errors, most of which cancel for the usual experimental conditions. Since, for theoretical reasons, one measures these transport effects mostly in dilute solid solutions, the detectability of very low impurity concentrations is a necessity. Measurements of the limit of detectability show that the microprobe used met all requirements and is able to compete favorably with common tracer techniques, even in this respect. Another feature is the possibility of measurements in cases where no suitable tracer exists. Measurements are also repeatable with the same sample after further treatment since analysis with the microprobe is nondestructive.

For the first time an electron microprobe has been used for transport measurements of this type. The results obtained in some dilute copper and aluminum base alloys are presented. Diffusion coefficients obtained by this method agree quite well with those determined previously by radioactive tracer methods. The accuracy of measurements of the transport controlling physical properties could be considerably improved. In evaluating the shifts of the concentration profile, an electronic method has been developed to read the shifts from the screen of the cathode ray oscilloscope.

AN ELECTRON MICROPROBE STUDY OF DIFFUSION IN THE NI-AU SYSTEM

Eric Lifshin

Interdiffusion in the Ni-Au system has been studied by analysis of incremental diffusion couples using a Cambridge Mark II microprobe. The instrument was modified to automatically step-scan samples and to transmit measured X-ray intensity data to a time-shared computer. Computer programs were written to analyze these data and to obtain composition profile, which were subsequently used to determine interdiffusion coefficients by Matano's analysis. Diffusion coefficients were determined as functions of composition at 850, 875, 900, and 925°C.

Conversion of X-ray intensity to composition was done by experimentally measuring both Ni-Kα and Au-Lα intensities from six standards of intermediate compositions. The corrected relative intensity data and sample compositions were then used to obtain values of the parameters a_{AuNi} and a_{NiAu} by at least squares fit of the data to the Ziebold equation [1]:

$$(1-K)/K = a(1-C)/C$$

where C is the weight fraction composition, K is the corrected relative intensity, and a is the appropriate deviation parameter.

Figure 1 shows the resulting calibration curves obtained from the Ziebold equation as well as the individual data points measured. This equation provided a convenient method for the conversion of X-ray data to composition in the computer. Figure 2 is a composition profile obtained from an incremental couple annealed for 9.60 x 10^5 sec. at 925°C. These data and the data obtained from other incremental couples covering the entire composition range from pure Au to pure Ni were used as input for the Matano analysis program which calculated the results presented in Figure 3. Activation energies and pre-exponential factors for interdiffusion were also determined as functions of composition.

Self-diffusion coefficients and thermodynamic data obtained from the literature were used with the experimental values of diffusion coefficients to evaluate the Darken equation [2]:

$$\widetilde{D} = N_1 D_2^* + N_2 D_1^* [\partial \ell n a_1 / \partial N_1]$$

where $\widetilde{D}$ is the interdiffusion coefficient, D_1^*, D_2^* are the self-diffusion coefficients, N_1, N_2 are the mole fractions of elements 1 and 2, and a_1 is the activity of component 1.

In addition, the Hilliard theory [3], which relates the activation energies for self-diffusion to those for interdiffusion was evaluated. Good agreement was found for both these theories except at high Ni compositions where activation energies could not be readily determined. Except at high Ni compositions, good agreement was found with previous work done by another technique [3].

----

1. T. O. Ziebold, R. E. Ogilvie, Anal. Chem., 36, 322 (1963).
2. L. S. Darken, Trans. AIME, 175, 184 (1948).
3. J. E. Reynolds, B. L. Averbach, M. Cohen, Acta Met., 5, 29, (1957).
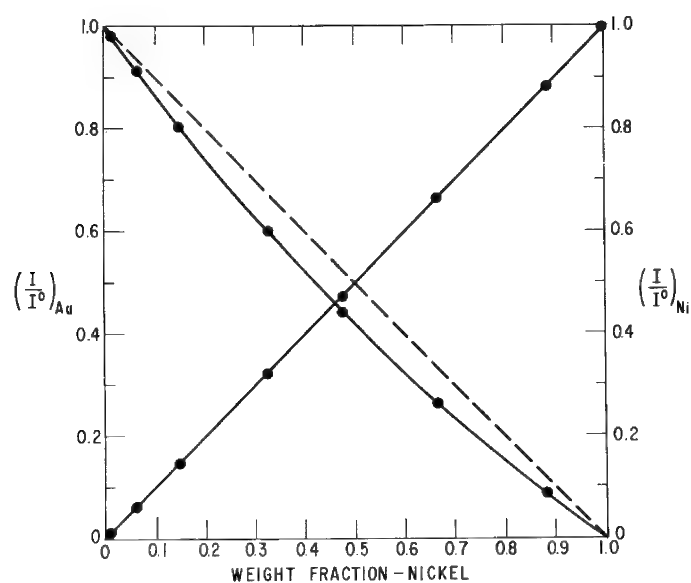
Figure 1
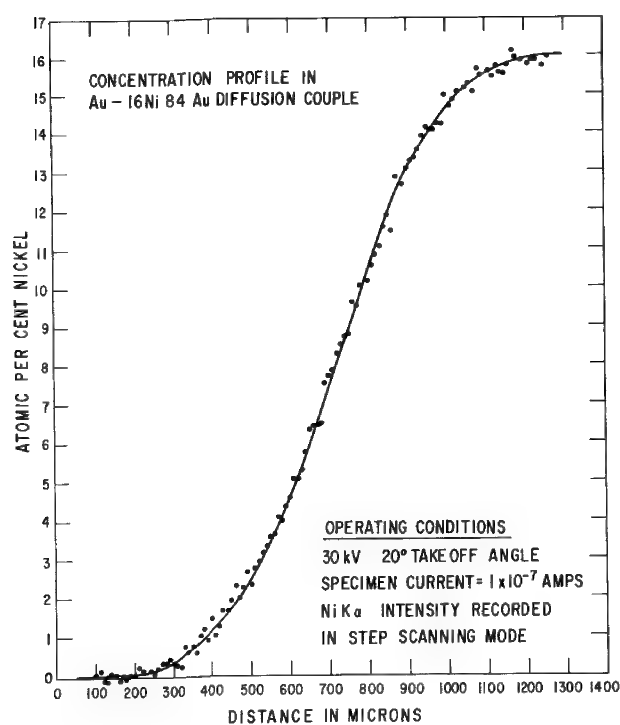
Figure 2
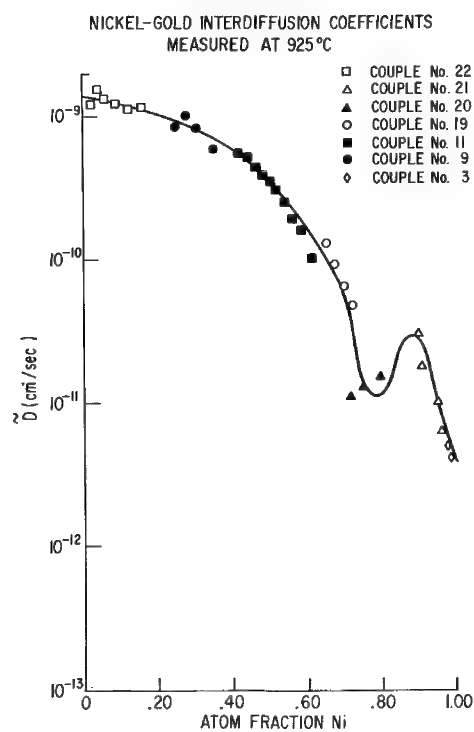
Figure 3

CONCENTRATION GRADIENTS IN CU-NI-MN TERNARY DIFFUSION COUPLES

Eugene J. Rapperport, Stephen L. Bender, and Thomas C. Wilder

A study of the relationship between physical diffusion coefficients and experimental thermodynamic activities is being conducted on the non-ideal system Cu-Ni-Mn. Of primary concern in this work is the conversion of measurements of the characteristic X-ray intensities of the constituent elements at a number of points within the diffusion zone to accurate ternary compositions. This must be done in order to establish reliable concentration gradients from which to compute diffusion coefficients.

The basis for the analysis of ternary compositions is the microprobe analysis of the three binary systems involved. The alloys of these three binary systems (Cu-Ni; Cu-Mn; and Ni-Mn) were fabricated by rapid solidification from binary melts in evacuated silica tubes using an inert gas as a pressure medium. Homogenization of the cast binary alloys was achieved by 16 hour anneals at 845°C. Electron probe measurements of relative characteristic X-ray intensities indicated that homogeneity within the overall reproducibility of the X-ray intensities had been attained.

Ternary diffusion couples were made using selected pairs of the binary alloys cited above by bonding metallographically polished wafers in a molybdenum clamping device at a temperature of 600°C for one hour. Microprobe examination of sectioned bonded couples showed that less than one micron of diffusion had occurred during bonding. Ten couples selected to give concentration gradients within the large solid solution region adjacent to the Ni-Cu binary were diffused at 800°C for 336 hours.

A number of ternary alloys in this same solid solution region were also prepared, in a fashion similar to the binary alloys described above. These alloys were used for two purposes: as electrodes in fused electrolyte EMF measurements to determine the thermodynamic activity as a function of composition in the solid solution region of interest; and as standards to verify the accuracy of the computation of ternary concentrations from binary data.

The problem of accurately converting X-ray intensities to concentrations in a ternary system is a straightforward one if homogeneous binary and ternary standards are available. The method of Ziebold and Ogilvie [1] is useful if one can demonstrate that each of the three pairs of binary calibration curves can be accurately described by a single empirical parameter. This condition holds for the Cu-Ni, Cu-Mn and Ni-Mn binary systems. Assuming that the calibration curve of one element in a ternary alloy will be shifted in direct proportion to the weight fraction ratio of the other two elements, the compositions of the ternary standards were computed from their relative X-ray intensities and the binary parameters. The computed concentrations agreed with the wet chemical values within the reproducibility of the X-ray intensities.

Curves of concentration vs distance for couples with compositions lying
entirely within the solid solution region adjacent to the Cu-Ni binary display
startling evidence of the drastic non-ideal thermodynamic behavior found in
EMF measurements. In particular, "up-hill" diffusion is found in which Mn
diffuses from a level of 21.5 atomic percent to a band of 33.9 atomic percent.
This apparent anamaly may be understood when coupled to a knowledge of the
activity variation within the diffusion couple. An activity plot vs distance
for the same data set shows a monotonic decrease, which is the expected
behavior.

----

1. T. O. Ziebold, R. E. Ogilvie, Anal. Chem., 36, 322 (1964).

STUDIES ON ALPHA AND BETA PHASES IN COPPER-ZINC ALLOYS

Gunji Shinoda, Hideaki Kawabe, Kenji Murata, and Kenji Isokawa

It was found from an electron probe microanalysis study on cast 55% copper - 45% zinc alloy that alpha and beta phases coexist, that the concentration of copper in precipitated alpha is quite close to that of the beta matrix, and that some kind of martensitic transformation at the initial stage of alpha precipitation is expected. Naturally, the concentration of copper in the alpha phase decreases gradually by thermal diffusion to an equilibrium state. The initial alpha phase has a much higher concentration of copper than can be expected from the equilibrium diagram. Rather the compositions of the alpha and beta phases coincide with those obtained by extrapolating the liquidus and solidus to lower temperature side.

Frequently, denuded zones near grain boundaries and massive alpha in an inner part of a grain are observed. Figure 1 is an example of an analysis near a denuded zone. Apparently the grain boundary is composed of alpha phase, while in the denuded zone, the concentration of copper is almost the same as that in the beta matrix and a slight orientation variation is observed. In the copper-zinc system the atomic numbers of both elements are quite close to each other, so that the change of the specimen current does not correspond to that of atomic number, but rather to the difference of the orientations of each crystal.

Figure 2 is an example of an analysis of massive alpha. Fluctuations in concentration are not observed in this region. Further, the specimen current indicates that when massive alpha is formed, the change should be abrupt and its crystal orientation relation would be similar to that in martensitic transformations found in this alloy system.
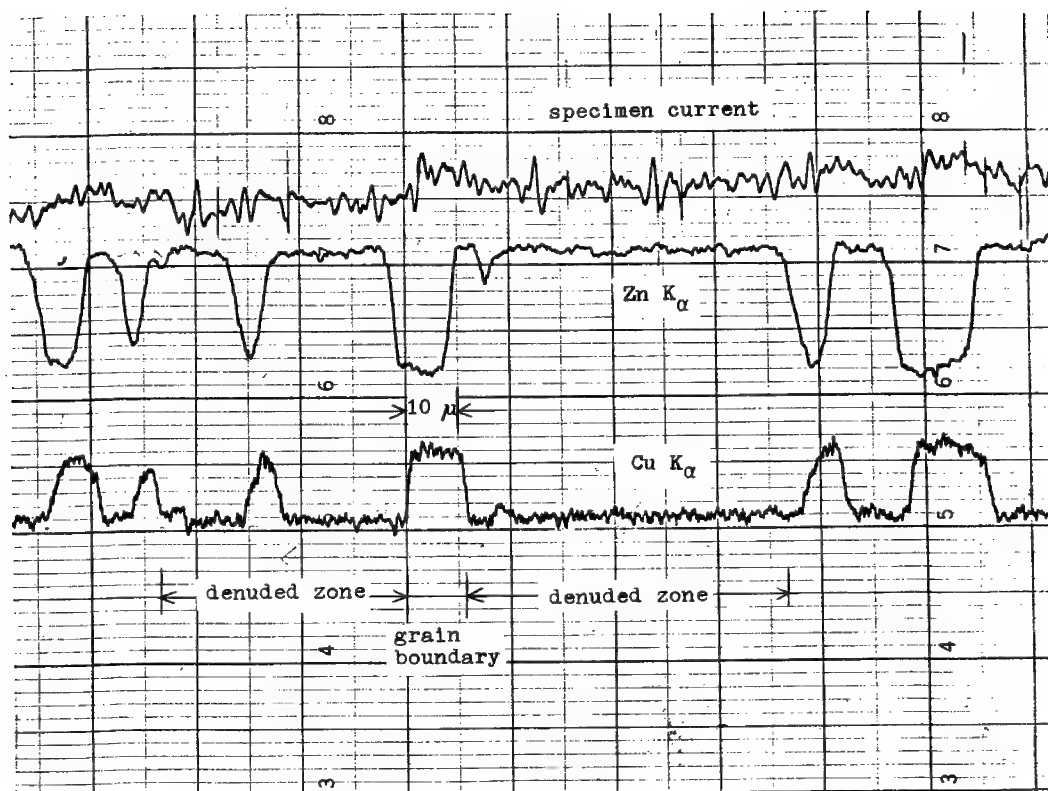
Figure 1   An analysis near denuded zone
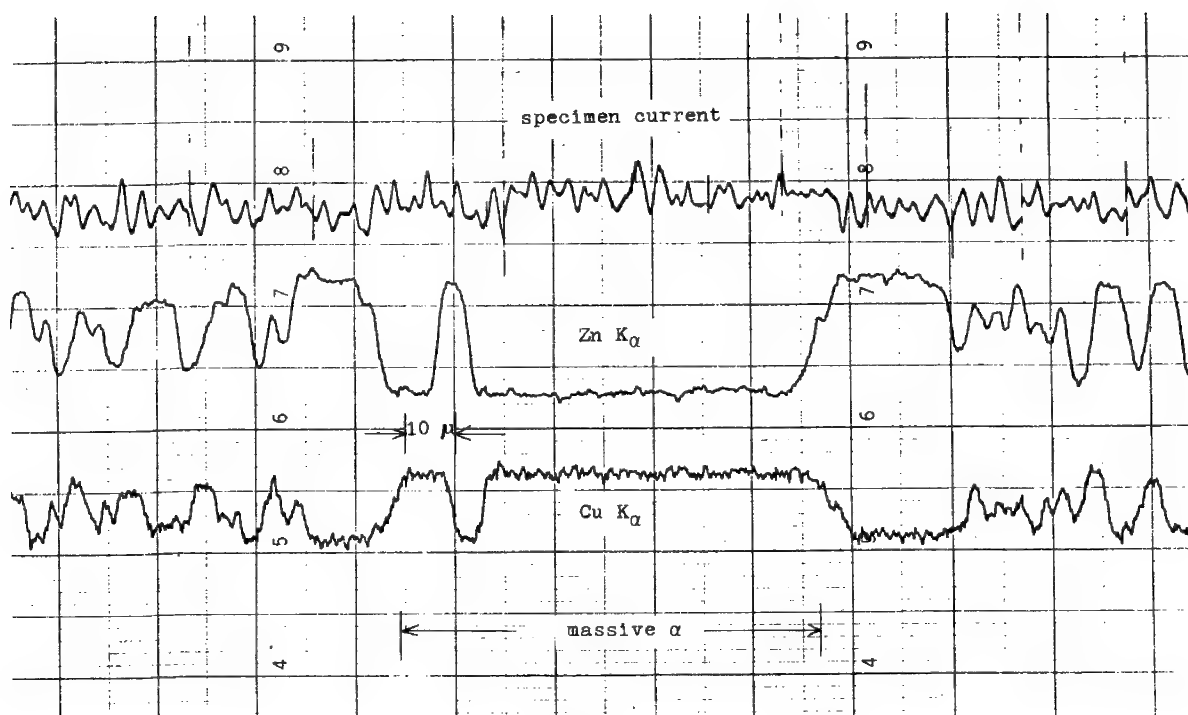
Figure 2   An analysis of a massive α

ANALYSIS OF FINE PRECIPITATES IN A 25 NICKEL-20 CHROMIUM-0.7 NIOBIUM STAINLESS STEEL

G. V. T. Ranzetta and V. D. Scott

Electron microscopy of a 25 nickel-20 chromium-0.7 niobium stainless steel had revealed the presence of two types of precipitate, which electron diffraction tentatively indicated as carbides of the MC and M_6C form respectively. Such data, however, gave no positive indication of the relevant metallic elements M, as many carbides have structures with similar lattice dimensions, and a real need remained to characterize completely the precipitating phases.

Although electron probe microanalysis has been widely and successfully used for the composition analysis of fairly large precipitates in solid samples, its extension to the sub-micron range raises difficulties due to the fact that X-ray generation occurs in a volume of material of several cubic microns, leading to some averaged value for the precipitate and matrix. This difficulty has been overcome in the present work by using specimens consisting of extraction replicas. Furthermore, since the microanalysis data could be directly correlated with electron microscopy and diffraction results, morphological, compositional and crystal lattice information has been collected on individual as well as on aggregates of small particles.

In general, the steel contained two distinct types of precipitate -- a fine dispersion distributed throughout the material and a coarse precipitate situated mainly at grain boundaries. Only niobium among the metallic alloying elements was located in the fine precipitate and this information, together with the electron diffraction data, identified it as niobium carbide. The coarse precipitate contained niobium and nickel, together with a trace of iron and chromium. The crystal structure of the phase was found to be face-centered-cubic with a cell size of 11.4 angstroms, which rules out any of the possible intermetallic compounds and indicates a η-carbide of the M_6C composition. The high nickel content and low chromium content eliminates the Cr_3Nb_3C phase, which was earlier suggested on the basis of the diffraction data alone, thus leaving for consideration carbides based on Ni_3Nb_3C (η_1) and Ni_2Nb_4C (η_2).

Measurements were then carried out on a number of the coarse precipitates in order to determine the ratio of the metallic elements and the values normalized to 100% in order to take into account the small size of the particles. The niobium content was in this way estimated at 59 weight percent and the nickel (inclusive of chromium and iron) at 38 weight percent, close to the expected value for η_1-carbide of 60 and 38 weight percents respectively. It is, therefore, concluded that the structure is $[(Fe + Cr),Ni]_3Nb_3C$, analagous to the previously reported $(V,Ni)_3Nb_3C$.

The advantages of jointly applying microanalysis and electron diffraction to the identification of fine precipitates, particularly in complex materials, is thus evidenced since many possible ambiguities can be removed. Certainly such a combined approach is essential if precipitation behavior in alloy steels is to be fully understood.

ıd V. D. Scott

of a 25 nickel-20 chromium-0.7 niobium stainless steel had
ce of two types of precipitate, which electron diffraction
ed as carbides of the MC and M_6C form respectively. Such
no positive indication of the relevant metallic elements
have structures with similar lattice dimensions, and a
to characterize completely the precipitating phases.

ırobe microanalysis has been widely and successfully used
ı analysis of fairly large precipitates in solid samples,
ıe sub-micron range raises difficulties due to the fact that
:curs in a volume of material of several cubic microns,
ıraged value for the precipitate and matrix. This diffi-
ʳcome in the present work by using specimens consisting of
ɨ. Furthermore, since the microanalysis data could be
ɨ with electron microscopy and diffraction results, morpho-
ɔnal and crystal lattice information has been collected on
as on aggregates of small particles.

eel contained two distinct types of precipitate -- a fine
uted throughout the material and a coarse precipitate sit-
ain boundaries. Only niobium among the metallic alloying
.ed in the fine precipitate and this information, together
diffraction data, identified it as niobium carbide. The
ɨ contained niobium and nickel, together with a trace of iron
ɨ crystal structure of the phase was found to be face-
ːh a cell size of 11.4 angstroms, which rules out any of the
ıllic compounds and indicates a n-carbide of the M_6C composi-
ickel content and low chromium content eliminates the Cr_3Nb_3C
ɨarlier suggested on the basis of the diffraction data alone,
ɔonsideration carbides based on Ni_3Nb_3C (n_1) and Ni_2Nb_4C

then carried out on a number of the coarse precipitates in
e the ratio of the metallic elements and the values normal-
rder to take into account the small size of the particles.
ɨnt was in this way estimated at 59 weight percent and the
ɨ of chromium and iron) at 38 weight percent, close to the
ɨ of n_1-carbide of 60 and 38 weight percents respectively. It
ɨr ıncluded that the structure is $[(Fe + Cr),Ni]_3Nb_3C$, analagous
ɨ reported $(V,Ni)_3Nb_3C$.

ɨ jointly applying microanalysis and electron diffraction to
ɔn of fine precipitates, particularly in complex materials, is
ince many possible ambiguities can be removed. Certainly such
ach is essential if precipitation behavior in alloy steels is
rstood.

hi h have been used at
aken into account the
t characteristic radia-
ɨo ption correction by
tic radiation by
ıı ɨ purpose [1]. The
ɨi ɨ using 1) the Web-
⁻ ʳelation between
ı's expression [3]
rı ırmed for iron-base
hɨ experiment has been

-a uminum intermetallic
⁻ ed intensity ratios
ɨɨ ʷere made with an
ɨ 5 KV. These results
ʰɔ effect due to the
ıce each other's

ıalysis of the non-
uɨ ons usually inter-
eı ˈsample a single
saki, Kusaka and
.. ections (10μm in
ɨ e electron probe
ɔɔ sible to clarify
h aid of both
ɨ ɨs been presented
ɨh ɔugh electron probe

ʌ 66 (1965) and

(1 ɨ61).

ars, 5, 324 (1965).
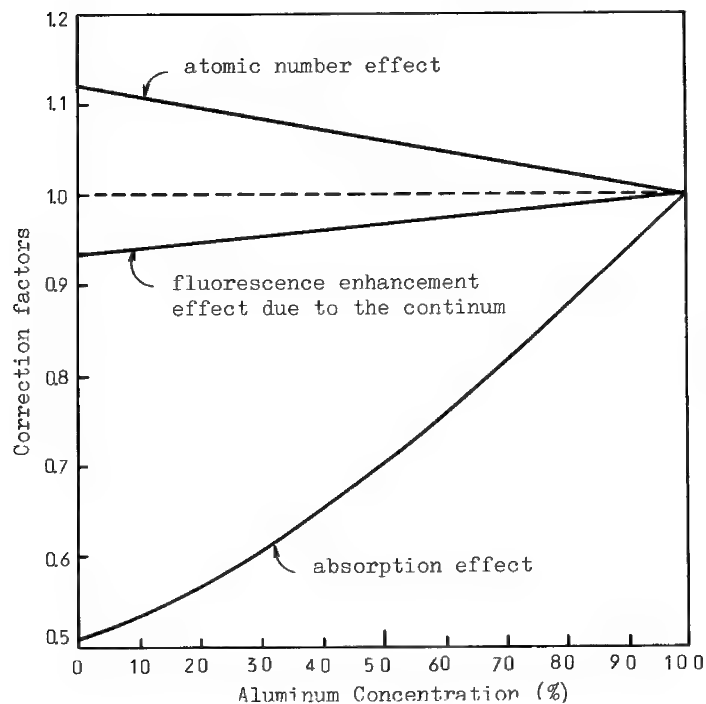
Figure 1   The comparison of the calculated cor-
rection factors of the various effects
in Al-Fe alloy. (Al Kα line, accelera-
ting voltage = 15 Kv, and take-off
angle = 52.5°)
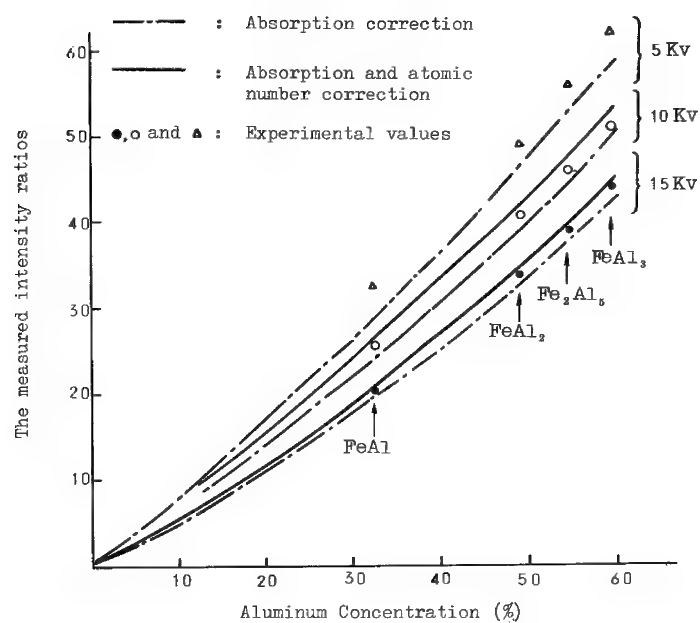
Figure 2   The comparison between the proposed
correction curves and the measured
intensity ratios for a series of
aluminium compounds.

ELECTRON BEAM MICROANALYSIS OF "SULFIDATION" CORROSION LAYERS ON A NI-CO-CR SUPERALLOY EXPOSED TO COMBUSTION GASES AT HIGH TEMPERATURES

Charles J. Spengler and Roland Stickler

This investigation was performed to determine the microstructure of corrosion layers on a superalloy of base composition 48Ni-28Co-15Cr both on accelerated test, laboratory, and field-corroded specimens. The accelerated tests were performed in two different apparatus. Specimens were precoated with a simulated slag of Mg-Na-sulfate. Table 1 lists the operating conditions. The field-corroded specimens were from gas turbines operated for extended periods in different locations and with various fuels.

The specimens were metallographically mounted in epoxy cement and polished under kerosene to preserve the fragile layers and the chemically unstable phases. The specimens were examined by light microscopy, electron-beam microanalysis, X-ray diffraction, electron diffraction, and electron microscopy to establish the morphology, distribution, chemistry, and crystal structure of the phases.

Table 1 summarizes the results. Most of the specimens were in the heat-treated and aged condition and consisted of a matrix of Ni-Co-Cr solid solution bulky precipitates of (Ti, Mo)·(C, N), fine intra-crystalline precipitates of Ni_3(Ti, Al), and massive $M_{23}C_6$ on grain boundaries and most twin boundaries.

Most of the specimens exhibited an affected alloy region covered with scales of several layers of non-metallic compounds. In the laboratory-tested specimens the first effect of the corrosion attack was the disappearance of the $M_{23}C_6$ grain-boundary precipitate. A finely dispersed Ti-sulfide phase was revealed by electron beam microanalysis along the denuded grain boundaries where concurrently the Ni_3(Ti, Al) disappeared from the neighboring regions. Chromium depletion was detected in the matrix only after all Ni_3(Ti, Al) had vanished. The microstructure of the Ni-rich matrix in these regions was not related to the original microstructure in the sample.

The oxide layers on the laboratory specimens tested in high SO_3 atmospheres consisted of a mixture of simple oxides and non-coherent spinel layers. The specimens tested in low SO_3 atmospheres generally had a scale of simple oxides. A similar sequence of corrosion layers existed in some of the field-corroded samples; however, others had oxide scales immediately bordering an apparently unaffected alloy. Ni-sulfide-rich scales in other specimens indicated periodic turbine operation in a reducing environment. The accelerated laboratory tests yield corrosion microstructures in the affected alloy layer comparable with those field samples in which the oxidation rate of this layer was relatively low. The evaluation of corrosion tests and the correlation with corrosion during service exposure requires careful consideration of the distribution, chemistry, and crystal structure of the phases present.

Table 1. Identification and Distribution of Phases in Corroded 48Ni-28Co-15Cr Specimens

Specimen	Base Alloy	Affected Alloy Layer I	Affected Alloy Layer II	Scale I	Scale II	Scale III
A	(Ni,Co,Cr) $(Ti,Mo)C$ $Ni_3(Ti,Al)$	(Ni,Co) $(Cr,Ti)S_x$		$CoO.Cr_2O_3$* $MeSO_4$ $(Ni,Co)O_x$	Cr_2O_3* $(Ni,Co)O_x$	
B	(Ni,Co,Cr) $(Ti,Mo)C$ $Ni_3(Ti,Al)$ $Me_{23}C_6$	(Ni,Co) TiS_x	Ni Al_2O_3	CrO_x TiO_x	$(Ti,Al)O_x$ $MeSO_4$	MgO* $MeSO_4$
C	"	(Ni,Co,Cr) TiS_x	(Ni,Co) CrS_x	$(Ni,Co)O$* $(Ni,Co)O.Cr_2O_3$* $MeSO_4$	$(Ni,Co)O$* $(Ni,Co)O.Cr_2O_3$* $MeSO_4$	$(Ni,Co)O$* $MeSO_4$
D	"	(Ni,Co,Cr)* TiS_x		TiS_x Cr_2S_3*	$(Ni,Co)O$* Cr_2O_3* $(Ni,Co)O.Cr_2O_3$*	$Ni(VO_3)_3$* $MeSO_4$* $Me(VO_3)$*
E	"	(Ni,Co,Cr) TiS_x	(Ni,Co) $(Cr,Ti)S_x$	Ni Al_2O_3* $(Cr,Ti)O_x$	$(Ni,Co)O$* $(Ni,Co)O.Cr_2O_3$* Al_2O_3* TiO_x	$(Ni,Co)O$* $Ni(VO_3)_3$* Cr_2O_3*
F	"	(Ni,Co,Cr) TiS_x		$(Cr,Ti)S_x$ $(Ti,Mo)O_x$	NiS_x	$(Ni,Co)O$* $(Cr,Ti)S_x$ $(Cr,Ti)O_x$ $CoO.Al_2O_3$*
G	"	(Ni,Co,Cr) TiS_x	(Ni,Co) $(Cr,Ti)S_x$	Al_2O_3 $(Ni,Co)O.Cr_2O_3$* Cr_2O_3*	$(Ni,Co)O.Al_2O_3$* FeO_x SiO_2*, MnO_x	Al_2O_3 $MeSO_4$

*Phases identified by X-ray diffraction analysis, unmarked phases based on chemical composition (EMA), ** Sulfur content not exceeding 4%.

Specimen A: Solution-treated cast alloy, 90 hrs at 1450°F (773°C), synthetic atmosphere heated in electric furnace, high SO_2; Specimen B: Aged wrought alloy, 150 hrs at 1550°F (800°C), heated in combusting fuel-air mixture, low SO_3; Specimen C: Same as B, except high SO_3; Specimen D: Service corrosion in low-V, low-Na residual fuel**; Specimen E: Service corrosion in high-V, low-Na residual fuel**; Specimen F: Service corrosion in low-V, low-Na distillate fuel**; Specimen G: Service corrosion in low-V, low-Na residual fuel**, dusty industrial environment.

THE EFFECT OF NICKEL ON THE HIGH TEMPERATURE OXIDATION CHARACTERISTICS OF COPPER-BEARING STEELS

G. L. Fisher

It has been known for many years that copper-bearing steels are prone to surface hot-shortness. Other investigators have shown that when copper steels are heated above 1050°C, iron is preferentially oxidized causing an enrichment of copper at the scale-metal interface. When the copper content at the interface exceeds its solubility limit in austenite, a molten copper-rich phase forms and penetrates into the austenite grain boundaries causing them to separate during hot working.

Nickel additions to copper-bearing steels have been shown to reduce the severity of hot cracking. When a nickel:copper ratio of about 0.5 is exceeded, the incidence of cracking is sharply reduced. Although several theories have been advanced to explain the beneficial effect of nickel, the mechanism has not been fully explained.

To determine the role of nickel in preventing hot shortness five steels, each containing 1.1% copper, and with Ni:Cu ratios from 0.03 to 1.0 were oxidized in flowing moist air at 1150°C for 5 hours. After mounting and polishing to retain the scale intact, quantitative and semi-quantitative microprobe analysis was performed on phases at the interface and in the scale.

In the steels with low Ni:Cu ratios a copper-rich phase was found in the matrix at the interface. It was nearly continuous in the 0.03 and 0.10 Ni:Cu steels. As the nickel content increased further the phase became discontinuous and less prevalent. At the highest Ni:Cu ratio it had disappeared entirely. There was a minimum of 80% copper in the copper-rich phase in all steels up to and including the 0.35 Ni:Cu steel. The remainder of this phase was composed of nearly equal amounts of nickel and iron. In the 0.40 Ni:Cu steel the copper content of the phase dropped substantially to about 60% copper.

From the above, one might conclude that nickel, by alloying with the copper-rich phase, raises the melting point of the phase above the oxidation temperature. If the phase is not molten, it cannot penetrate the austenite grain boundaries and cause cracking. However, investigation of a metallic phase found occluded in the scale showed that another mechanism for the prevention of edge cracking was more important. Substantial amounts of the occluded phase were found in the scale of steels with Ni:Cu ratios of 0.10 and greater. The average copper content of the occluded phase decreased linearly with increase in nickel content of the steel. Metallographic examination shows that, in the nickel-containing steels, a row of oxide particles forms in the matrix immediately behind the copper-rich phase. These oxide particles apparently link up with each other and the surface to effectively isolate the copper-rich layer from the matrix. Thus, the presence of nickel in the steel has caused the enriched copper layer at the interface to be separated from the matrix and occluded into the scale. The higher the nickel content of the steel, the less the enrichment at the interface before occlusion occurs.

In steels with Ni:Cu ratios of 0.35 and greater, the composition of the occluded phase varied with distance from the interface. While the copper content increased with distance, there was a simultaneous decrease in both the iron and nickel content. In the 0.35 Ni:Cu steel the copper content of the occluded phase exceeded 90% at a distance of 1000 microns from the interface. Thus, if the enriched copper layer had not been isolated in the scale, it would have reached a composition sufficiently high in copper to form a molten phase.

In conclusion, nickel prevents edge cracking in copper-bearing steels oxidized in air by promoting occlusion into the scale of a copper-rich layer formed at the scale-metal interface during oxidation.

ELECTRON PROBE MICROANALYSIS OF LAMINATED METALLIZATION IN INTEGRATED CIRCUITS

J. E. Cline, R. P. Beatty and J. Gerhard

Although aluminum thin films have been used for many years for the photoengraved interconnection pattern of silicon monolithic circuits, laminated metallization, such as the gold-molybdenum system, has recently been applied to overcome some of the disadvantages of aluminum, particularly for operation at elevated temperatures.

The use of electron probe microanalysis to determine simultaneously the thicknesses of both the gold and molybdenum layers involves more complex relationships than those reported by Hutchins [1] for the thickness determination of single thin films. Successive approximations by computer programs are required in the absence of suitable mathematical analytical expressions for estimation of the effective electron penetration in the two-metal system.

Limitation of the direct measurement technique due to excessive gold thickness was extended by using beam voltages in the range 40 to 50 KV, and Mo $K\alpha$ radiation for determining the molybdenum thickness. In order to expose the underlying molybdenum, the gold layer was removed either by etching away selected areas, or by lapping the sample at an angle of $1/2°$ to the surface. Figures 1 and 2 show the presence of a triangular formation of gold-silicon eutectic, due to a defect in the molybdenum barrier layer, which appeared during a temperature-stress test of the metallization.

----

1. G. A. Hutchins, The Electron Microprobe, op. cit.
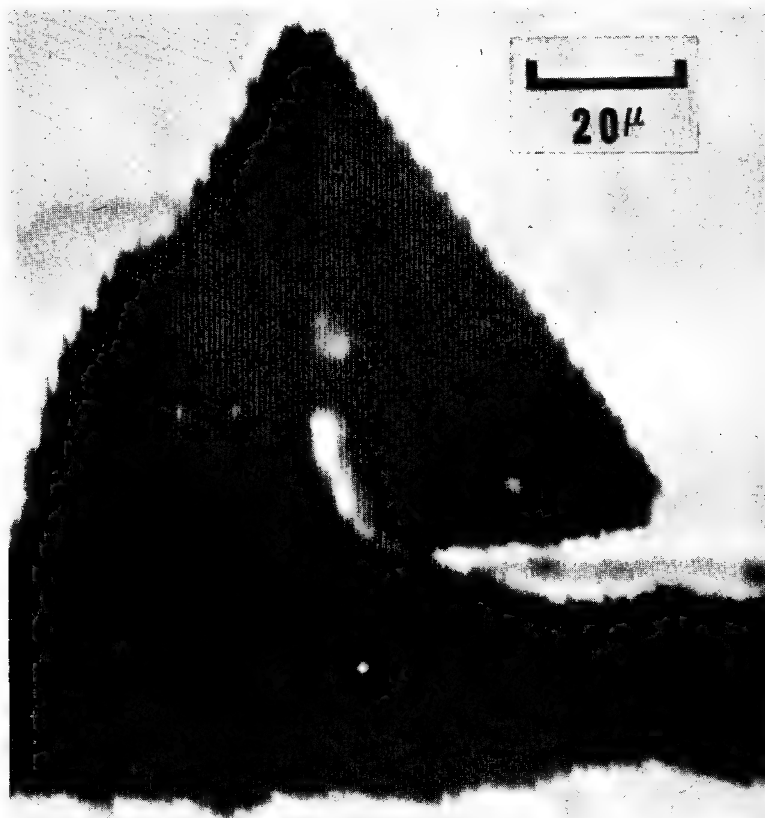
Figure 1
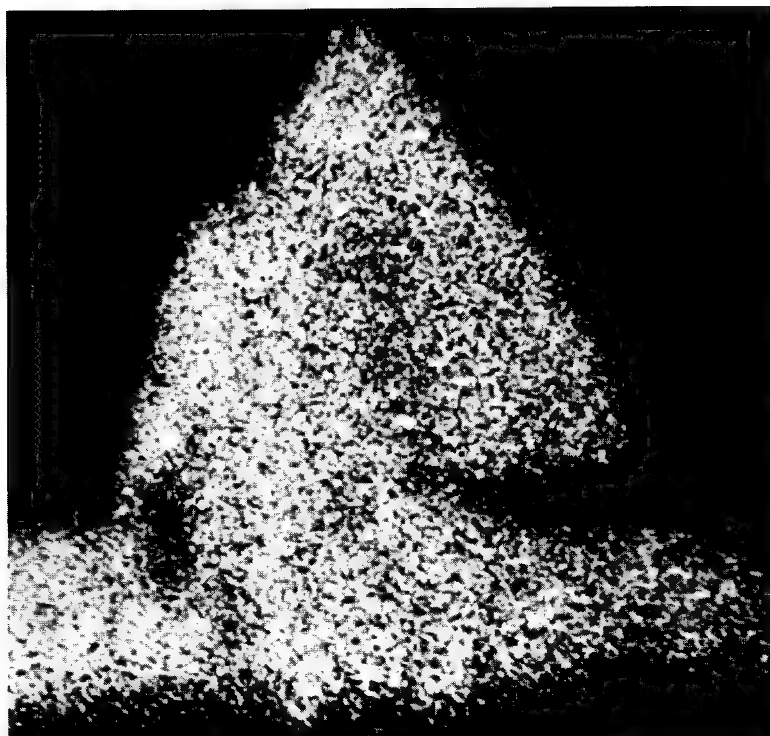
Figure 2

EFFECT OF SPECTRAL LINE SHIFT ON MICROPROBE DATA*

R. K. Hart and D. G. Pilney

It has long been recognized that the valence forces [1,2] in a chemical compound can alter the X-ray emission spectra in a number of ways. In certain oxides a wavelength shift in the spectral line has been reported to occur between the heavy element in the oxide and that of the metal standard [3,4]. The magnitude of this spectral line shift on $K\alpha$ emission spectra and its effect on microprobe intensity data have been investigated on certain oxides of aluminum, titanium, iron and cobalt.

All specimen materials were of the highest purity obtainable and were subjected to either spectroscopic or wet chemical analysis. Only well crystallized oxide was used since previous experience with sintered oxides showed that material in this form could not be relied upon. The various oxide crystals were mounted between two pieces of metal. Electrically conducting "DIALL 1610" was used throughout as the mounting media and all mounts after polishing were coated with a thin film of carbon by evaporation. Surface polishing was carried down to 0.25 micron diamond paste.

Apparent spectral line shifts and associated intensity changes can be produced by small alterations in the position of the specimen about the focusing plane of the spectrometer. This source of error was kept as small as possible by paying careful attention to the mounting arrangement of specimens and to the polishing procedure. The maximum vertical displacement that a specimen could encounter during a traverse was measured both mechanically and optically to be less than 2 microns.

Results were obtained with both air-path and vacuum spectrometers, which had been modified to include both coarse and fine adjustments. These fine controls had a total movement of 4° in 2θ and the smallest angular change that could be read was 0.008°. A mica analyzing crystal was used for aluminum and lithium fluoride crystals for the remainder. The lithium fluoride crystals were bent and ground to conform with the Johansson arrangement. In all cases the detector slit was opened to the half width of the spectral line, whose shape had been predetermined.

Table I lists the data obtained by $K\alpha$ radiation from four metal/oxide systems. Peak heights listed in this table were the average of 10 or more determinations and only results lying within the standard counting error were used.

The line shifts correspond to an energy change of approximately 2 eV in the exit photons. This change is of the same order as found by Fischer [4] for L emission shifts from metal to oxide. Fischer's results indicate that there is, in general, a systematic energy change with atomic number. The present results do not show such a trend although more data would be required for confirmation.

In application, these data show that considerable differences can be expected in the analyses of oxides by using standard metal conditions. When programmed settings are used in microprobes, a predetermined setting using an oxide standard should be used in preference to the standard metal setting.

----

1. J. Bergengren, Z. Physik, 3, 247 (1920).
2. A. E. Lindh, O. Lundquist, Arkiv. Mat. Astron. Fysik, 18, 2 (1924).
3. T. Mulvey, Brit. J. Sci. Instrum., 42, 57 (1965).
4. D. W. Fischer, J. Appl. Phys., 36, 2048 (1965).
5. L. S. Birks, Electron Probe Microanalysis, Interscience Publishers, New York, 1963.

TABLE I. Effect of spectral line shift on microprobe analysis of certain metal oxides.

Material	Spectrometer Settings* degrees 2θ		Metal $N_L - N_B$ c/sec	Oxide $N_L - N_B$ c/sec	Metal ** Concentration w/o	Actual Metal Conc. w/o	Deviation percent	Line Shift degrees 2θ
Al$_2$O$_3$	a	49.49	3284	1415	52.13	53.32	2.23	−0.010
	b	49.48		1429	52.64	53.32	1.27	
TiO$_2$	a	86.28	797	454	56.33	60.93	7.55	+0.014
	b	86.30		457	56.71	60.93	6.93	
Fe$_2$O$_3$	a	57.58	986	616	61.84	69.94	11.58	+0.021
	b	57.60		649	65.16	69.94	6.82	
CoO	a	52.84	3138	2310	72.80	78.22	6.92	+0.014
	b	52.86		2482	78.22	78.22	0.00	

* setting a is with spectrometer peaked on metal standard and b is with spectrometer peaked on oxide
**results corrected for absorption only using Birks absorption data[5].

AN EMPIRICAL METHOD FOR THE ELECTRON MICROANALYSIS OF SILICATES AND OXIDES

A. E. Bence and Arden L. Albee

The precision of current techniques of electron microanalysis of minerals is limited by the use of chemically analyzed standards. The poor precision of standard chemical analytical techniques and the lack of homogeneity of natural and synthetic phases make it difficult, if not impossible, to construct suitable calibration curves for some common minerals even with a large number of standards. Given suitable correction factors, the use of pure oxides and binary oxide phases as standards would make electron microanalysis independent of chemical analyses and problems of homogeneity.

Ziebold and Ogilvie [1] have shown that the calibration curve in a binary metal alloy system can, within the variance of data points, be described by the linear expression:

$$C_A/K_A = a_{AB} + (1 - a_{AB})C_A$$

where C_A is the concentration of element A in alloy AB relative to pure A and K_A is the intensity of a characteristic radiation line of A in the alloy AB relative to that of pure A. The curve is described by the parameter a, evaluated as $a = C/K$ when C goes to zero. This linear variation of the correction factor with composition can be extended to multi-component systems by using the weighted average of the binary correction factors [1].

Tabulations of correction factors applied to simple mineral systems [3,4,5] imply that correction factors are linear with concentration in these pseudo-binary or pseudo-ternary systems. It follows that empirical parameters might be derived in the manner demonstrated by Ziebold and Ogilvie [1], but using oxides rather than the elements as end-members. This is the approach followed in the present investigations.

The correction factors (a) were calculated for characteristic lines of nine major elements (Na, Mg, Al, Si, K, Ca, Ti, Mn, Fe) in the corresponding oxides using the standard procedures of both Ziebold and Ogilvie [2] and Smith [6]. Factors calculated using the two techniques differed by as much as 80%. Consequently, most of them have been measured using phases on binary and pseudo-binary joins, i.e.:

$$SiO_2 - FeSiO_3 - Fe_2SiO_4 - FeO$$

$$SiO_2 - MgSiO_3 - Mg_2SiO_4 - MgO$$

$$CaMgSi_2O_6$$

$$SiO_2 - CaSiO_3 - Ca_2SiO_4 - CaO$$
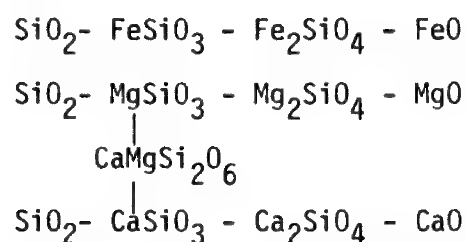
Where available, synthetic minerals were used as standards, but natural minerals verified to be nearly stoichiometric by the absence of other elements as

established in wavelength scans and to be nearly homogeneous by step and electron beam scanning were also used. The correction factors determined in this manner are given in the following table with differing significant figures to represent the confidence levels achieved at this time. There are no suitable phases to establish certain interactions such as Na-Mg and K-Fe and such parameters are necessarily based on the theoretical calculations and interpolation from adjacent oxides.

The simplicity of the weighted average correction factor makes it convenient for both hand and machine data reduction. Provided that a constant series of standards is used, the concentrations and correction factors for the standards may be entered into storage and do not have to be entered for each new analysis. For many minerals, the analysis of three elements plus a knowledge of the stoichiometry makes it possible to calculate approximate correction factors without a total analysis.

----

1. T. O. Ziebold, R. E. Ogilvie, Anal. Chem., 36, 322 (1964).
2. T. O. Ziebold, (ed.), The Electron Microanalyzer and its Applications, M.I.T., Department of Metallurgy, Lecture notes for summer course, 1966.
3. J. V. Smith, J. Geology, 74, 1 (1966).
4. R. A. Howie, J. V. Smith, J. Geology, 74, 443 (1966).
5. J. V. Smith, P. H. Ribbe, J. Geology, 74, 197 (1966).
6. J. V. Smith, J. Geology, 73, 830 (1965).

EMPIRICAL CORRECTION FACTORS (a)

Radiation	Na₂O	MgO	Al₂O₃	SiO₂	K₂O	CaO	TiO₂	MnO	FeO	Fe₂O₃
Na	1.0000	(1.00)*	1.010	1.035	1.150	1.289	(1.30)	(1.38)	(1.40)	
Mg	(1.5)	1.0000	1.0102	1.0979	(1.13)	1.2418	(1.30)	1.38	1.400	
Al	1.234	1.536	1.0000	.9989	1.0526	1.2376	(1.25)	(1.30)	1.330	
Si	1.234	1.293	1.316	1.0000	.977	.9956	1.0574	1.088	1.1647	
K	1.05	(1.13)	1.185	1.207	1.0000	(.95)	(.96)	(.98)	(.99)	
Ca	1.040	1.108	1.111	1.180	(1.2)	1.0000	.937	.95	.960	
Ti	(1.11)	(1.14)	(1.15)	1.161	(1.165)	1.170	1.0000	(.95)	.908	
Mn	(1.20)	(1.21)	(1.22)	1.239	(1.13)	1.16	(1.13)	1.0000	.948	
Fe	(1.12)	1.14	(1.17)	1.19	(1.12)	1.15	1.147	1.000	1.0000	1.0187
									.9788	1.0000

*Numbers in parentheses determined from theoretical calculations
and by interpolation from adjacent oxides.

ELECTRON MICROPROBE ANALYSIS OF ZIRCON CRYSTALS FOR TRACE AMOUNTS OF LEAD,
URANIUM AND THORIUM

A. A. Chodos and L. T. Silver

Zircon, $ZrSiO_4$, is a trace mineral widely used in the lead-uranium age dating
of igneous rocks from less than a hundred million to billions of years old.
Uranium and thorium are present in concentrations from one hundred to several
thousand parts per million. Radiogenic lead accumulates in concentrations up
to several hundred parts per million. Analysis of zircon crystals by isotope
dilution mass spectrometry commonly yields evidence of disturbance of the iso-
topic systems. Optical microscopic examination of zircon crystals shows that
many are zoned. To understand the distribution of lead, uranium and thorium
and their chemical stability in zoned zircon crystals, which bear both on the
phenomena that govern the distribution of elements during the crystallization
of igneous rocks and age interpretations, it was necessary to develop a micro-
probe technique capable of giving accurate values for the above elements from
a two to three micron area. Both of these problems had been approached using
other techniques but none were capable of studying variations on a micron scale
in individual crystals. The technique must be capable of handling grains which
are often only 10 microns in diameter and must allow examination of the grains
by transmitted light so that zoning can be seen in specific orientations.

The technique which has been developed meets all these requirements and permits
reproducible traverses to be made of zircon crystals with a present limit of
detection of approximately 25 ppm for all three elements. This has been
achieved by the use of a special sample mounting technique, high specimen cur-
rent, essentially drift-free electron optics and extremely reliable standards.

The zircon grains to be analyzed are mounted in a copper mesh, imbedded in
clear epoxy plastic and polished. The mesh, of a size appropriate to the size
of the crystals, serves two purposes. First, to hold the grains in the orien-
tation parallel or perpendicular to the c axis of the crystal, and second, to
serve as a heat sink for the heat generated by the one microampere specimen
current used. The high specimen current is necessary because of the low con-
centrations involved and the low sensitivity of the M lines used. The stan-
dards are grains of gem quality, homogeneous zircons which have been carefully
analyzed by isotope dilution mass spectrometry. These standards and a natural
crystal blank are analyzed at the beginning and end of each series to assure
accuracy.

Repeated traverses over the same area of a crystal indicates high reproduci-
bility of location of a specific spot on the sample. Repeated measurements of
the standards using 200 second counting times indicates an average deviation of
less than 50 ppm at higher concentration levels and 25 ppm at values near the
lower limit.

CHANGES IN THE COMPOSITION OF PETZITE ($AuAg_3Te_2$) DURING ANALYSIS BY ELECTRON PROBE

John Rucklidge and E. F. Stumpfl

During an investigation of naturally occurring gold silver telluride minerals, several specimens of petzite ($AuAg_3Te_2$) from widely separated localities were examined by electron probe methods. The electron probe results indicated considerable variation in composition within and between specimens, while published wet chemical analyses showed no such variation. Optically no zoning could be detected nor were differences apparent between specimens. More detailed study on the probe indicated that the composition obtained in analysis of this phase was dependent on the specimen current used, and at low specimen currents (0.005 microampere at 25 KV) all specimens appeared homogeneous with the correct stoichiometry. The effect of various specimen currents was investigated by plotting the intensities of Au $L\alpha$, Ag $L\alpha$, and Te $L\alpha$ X-radiations with respect to the time the electron beam was applied. For currents less than 0.01 microampere the intensities remained constant for times up to 20 minutes, while for higher current loadings the counts varied in the initial stages, coming to a steady state after a period of minutes. Figure 1 shows how the Au intensity drops, and the Ag and Te intensities rise. The Au appears to diffuse 5 to 10μm away from the impact area, forming a phase with composition approaching AuAgTe, while the electron bombarded spot tends towards $Au_{0.2}Ag_{3.8}Te_2$.

Experimental work in the system Au - Ag - Te [1] provides an interesting correlation. The phases petzite ($AuAg_3Te_2$) and hessite Ag_2Te) coexist below 50° ± 20°C, but above this temperature the stable assemblage is petzite with "x phase," where "x" is $(Au,Ag)Ag_3Te_2$ having from 2.5 to 14.5 weight percentage Au and is stable within the approximate temperature limits 50° to 415°C. Although petzite is stable up to 210°C it appears that the heating effect of the electron beam is sufficient to cause a change to "x phase" at temperatures which probably do not approach the upper limit of stability of petzite. Perhaps a steep temperature gradient around the impact spot is responsible for the rapid diffusion of Au out of and Ag into the area. It has not been possible to measure the temperature of the impact area, but it seems unlikely that it would reach 210°C in such a metallic material though a temperature above 50°C does not seem unreasonable. All other phases in the system are quite stable in the electron beam at currents far in excess of that causing changes in petzite.

Such low temperature phase changes may lead to completely misleading analyses if the operator is unaware of them. However, they also provide the opportunity of performing qualitative experimental work within the electron probe.
----

1. L. J. Cabri, Economic Geology 60, 1569-1606 (1965).
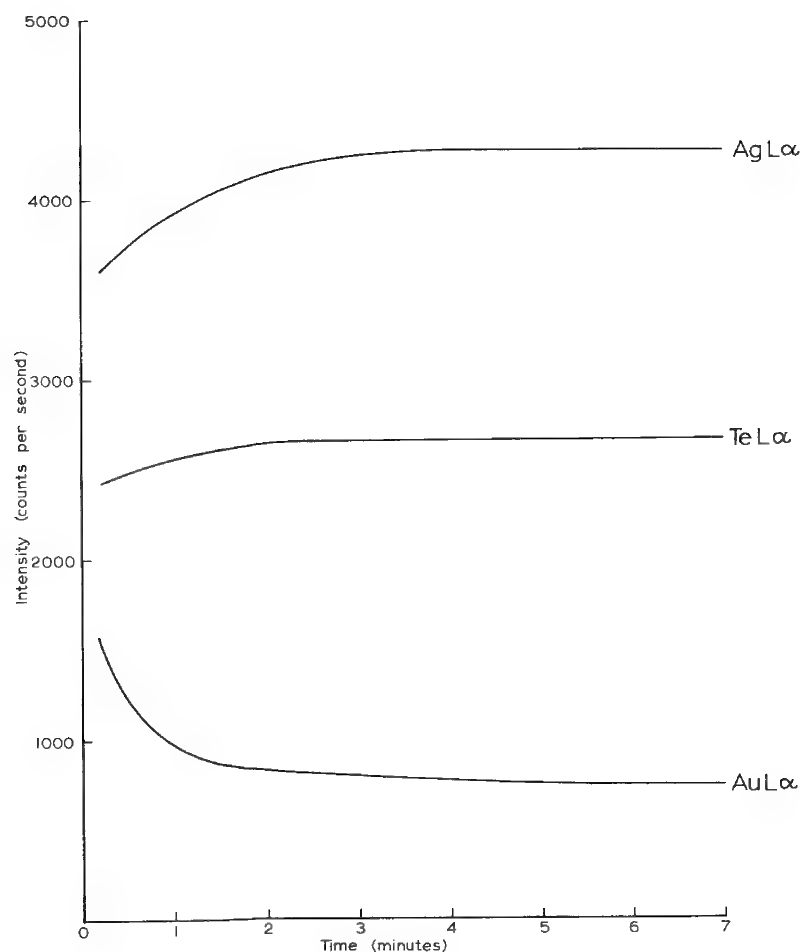
Figure 1 Change with time of intensity of AuLα, AgLα and TeLα emissions from petzite with sample current 0.025μA at 25 Kv.
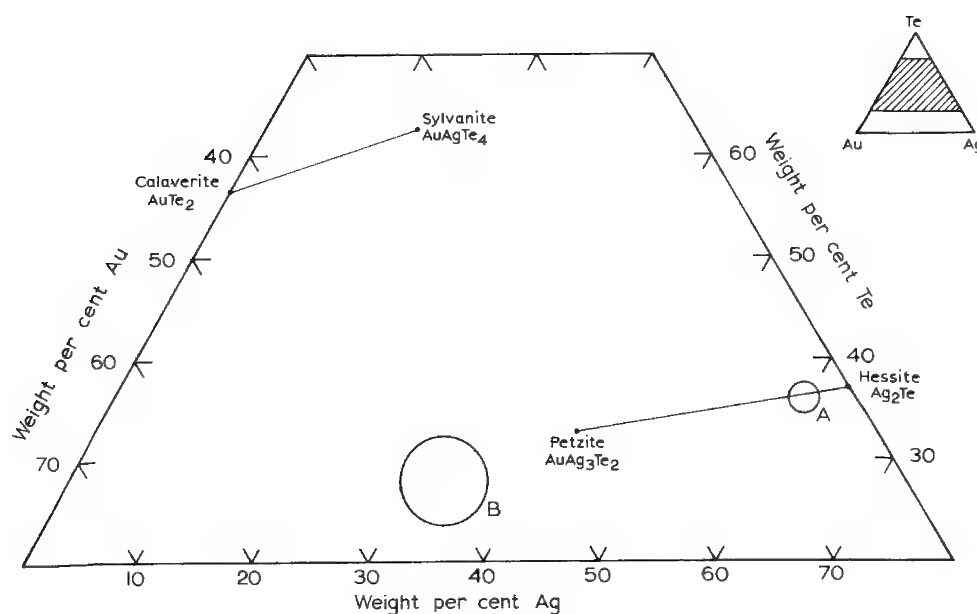
Figure 2 Some natural phases in the system Au-Ag-Te. Circle A indicates the composition of the point of electron bombardment after coming to a steady state. Area B encloses high Au compositions found in the vicinity of the spot after bombardment. No natural or synthetic phases are known in this region.

SURFACE DAMAGE EFFECTS IN ALKALI SILICATE GLASSES DURING ELECTRON MICROPROBE ANALYSIS

M. P. Borom and R. E. Hanneman

Measurements of compositional changes of a $K_2O-SrO-SiO_2$ glass with time during electron microprobe analysis were recently reported by Varshneya, Cooper, and Cable [1]. These changes were described entirely in terms of a mechanism proposed by Lineweaver [2] in which incident electrons from the microbeam stop at some finite depth in the glass producing a field that causes the positively charged alkali ions to migrate into the bulk with an associated evolution of oxygen at the surface. The purposes of this paper are threefold: 1) to present experimental data on compositional changes in similar glasses which are inconsistent with the Lineweaver mechanism and which illustrate that the drift problem can be more complex than indicated by [1], 2) to suggest that other effects can result in real or apparent composition changes and 3) to discuss methods of minimizing the problem of compositional changes during microprobe analysis.

In recent microprobe work on a variety of K_2O-SiO_2 and $Na_2O-FeO-SiO_2$ glasses, the authors have observed two important nontrivial types of local compositional drifts that are caused by the effects of the electron beam on glasses. These two general types of drift behavior are illustrated in Figure 1 where the X-ray intensities normalized to zero time are plotted vs. the time that the electron beam is focused on a given spot. The curves in Figure 1A behave in a manner analogous to that reported by [1] (i.e., the silicon X-ray intensity increases with time while the alkali metal X-ray intensity decreases with time). This behavior is consistent with the Lineweaver mechanism and results when local heating effects are small. On the other hand, the curves shown in Figure 1B exhibit a reversal in the slope of normalized X-ray intensities vs. time which is not predicted by the Lineweaver mechanism. Such behavior is shown to be associated with crater formation -- i.e., a depression surrounded by a rim higher than the original surface.

The cratering effect is due primarily to thermal effects including surface diffusion and vaporization caused by local beam heating, and the local compositional drift is directly related to the cratering process. Interference micrographs of cratered specimens show that the volume of material removed from the crater depressions exceeds the volume found in the hump which builds up around the edge of the craters. This indicates that substantial vaporization of the glass and/or local densification occurs due to the electron beam damage.

The type of drift reversal illustrated in Figure 1B is shown to result from competition between two drift mechanisms. The Lineweaver effect dominates in early stages and crater-related effects in the latter stages. A decrease in voltage, current density, and the associated local heating will decrease the drift problem due to either the Lineweaver mechanism or the cratering effects if other factors are held constant.

----

1. A. K. Varshneya, A. R. Cooper, M. Cable, J. Appl. Phys., 37, 2199 (1966).
2. J. L. Lineweaver, J. Appl. Phys., 34, 1786 (1963).

SMALL PARTICLE IDENTIFICATION BY ELECTRON MICROPROBE

Michael Bayard

McCrone Associates does considerable work in air and water pollution control, clean room monitoring and contamination analysis. This requires the identification of small single particles from a wide variety of sources. One of the most powerful single tools for this is the electron microprobe. During the past year over 1300 analyses have shown that conductive particles can be analyzed with reasonably quantitative results down to a size range of two to five microns, depending on density. With conductive particles, X-ray intensity falls off below this range, though smaller samples can be analyzed by ratios or by a known size correction.

It is much more difficult to work with nonconductive samples. The charge built up by small particles tends to defocus and deflect the beam from the particle, and, if the charge is large, the beam can be decelerated by the potential on the particle. As much as 80% of the incoming electron beam can be deflected in the extreme case of a very good small insulator with pointed surface features which tend to concentrate the charge. The sample current may drop to only 10-20% of the value found on a large sample of the same substance, indicating that much of the beam has been deflected through more than 90°. (See Figure 1.) Carbon coating helps, of course, but the beam "sees" some of the charge beneath the surface of the particle.

The contamination pattern around the particle indicates that with a nonconductor a large electron flux comes from the particle. Small irregularities in the surface of the beryllium plate on which the particle is mounted, or particles immediately adjacent to the particle under the beam, will show a radial shadowing pattern where the beam has been scattered. Conducting particles with the same backscatter coefficient show much less of this contamination.

Another way to demonstrate the effect of charge on particulates, and also to correct quantitatively for the electron loss, is to place the sample on a substrate which emits X-rays. Then with a proper correction for fluorescence caused by radiation from the sample, we can get a fairly good idea of the number of electrons not exciting the sample.

Geometric effects with conductors are not too important. In general, most particles show no more than a five percent variation in intensity due to different shapes. With nonconductors, the effect is slightly greater, usually about eight percent. Within these limits, we can usually treat conductors as bulk samples and apply the usual corrections. With nonconductors, ratios and empirical curves of size vs intensity on similar substances are used. The accuracy is correspondingly lower than for conductors.

Composition of 316 steel spheres

Raw I/I_0 values are uncorrected for backscatter and absorption. The standards are pure Fe, Cr and Ni.

Diameter, μ	% Fe	% Cr	% Ni
30*	67	21.7	11.5
17*	68.1	21.4	11.3
10*	67.5	20.5	11.3
19.6	68.1	21.2	11.2
12.6	68.3	21.0	11.5
7	67.2	20.1	10.9
5	67.8	20.9	11.8
2.8	68	21.4	12

*Polished hemispheres in Bakelite

Size versus intensity
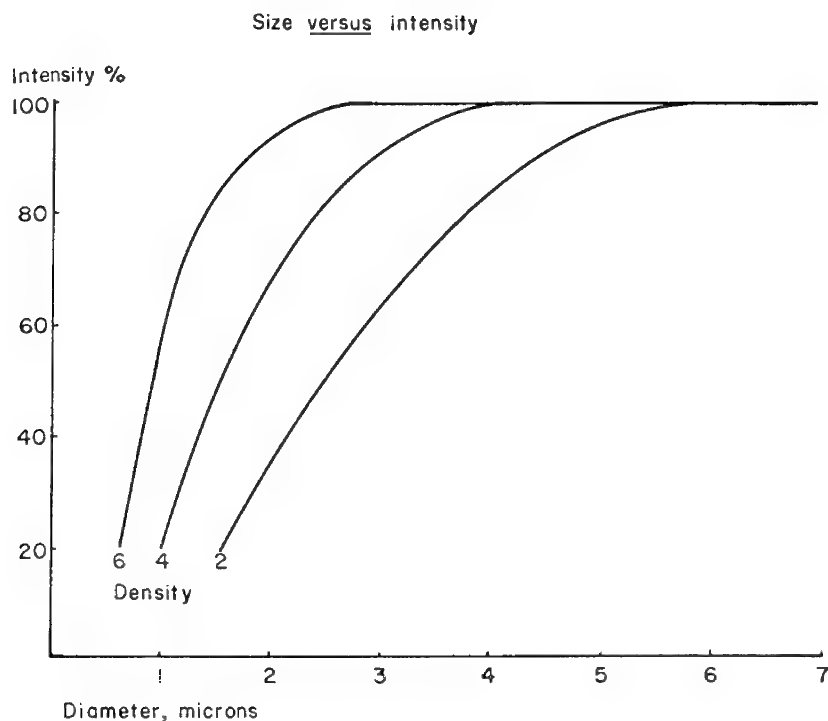
Figure 1   Size and intensity relationship for various sized spherical particles, with surface electron losses eliminated. The data are based partly on measurements on actual particles and thin films and partly on theoretical calculations.

IRON AND MANGANESE DISTRIBUTION IN SOIL CONCRETIONS

E. H. Tyner, M. P. Cescas, L. J. Gray, and F. U. Luehrs

Ferromanganiferous concretions such as the one shown in Figure 1 and 2 occur in many soils. The X-ray intensity sweeps and line scans for iron and manganese in these figures show a high iron content in the core and a high manganese content in the outer shell. The core contains 36% iron and 5.4% manganese. The outer shell has 20% iron and 21.6% manganese. Many concretions analyzed show compositional zoning but the zones are not always as well defined as the one taken for illustration. Some concretions have a greater number of composition zones indicating differential growth rates in changing environments.

Iron and manganese are subject to oxidation-reduction reactions. The environment becoming more reducing, iron precipitates first usually as hydrated oxide which explains why the core content is high in iron. With more reducing conditions, manganese will also precipitate. Even with the more reducing conditions iron will still continue to precipitate if it is available in the soil solution. The zonal distribution of iron and manganese in concretions reflects past climatic fluctuations as these influence redox states. World-wide climatic fluctuations in temperature and precipitation in the post glacial era have been shown by lake-cycle chronology, pollen profiles in non-glaciated regions and recent changes in sea level. Thus, it might be possible from concretion growth history to deduct the number of climatic cycles affecting redox potentials (ring numbers), their relative duration (ring area) and the intensity (Fe/Mn ratios) of past weathering cycles associated with present day soils, and possibly geosols developed during interglacial periods.
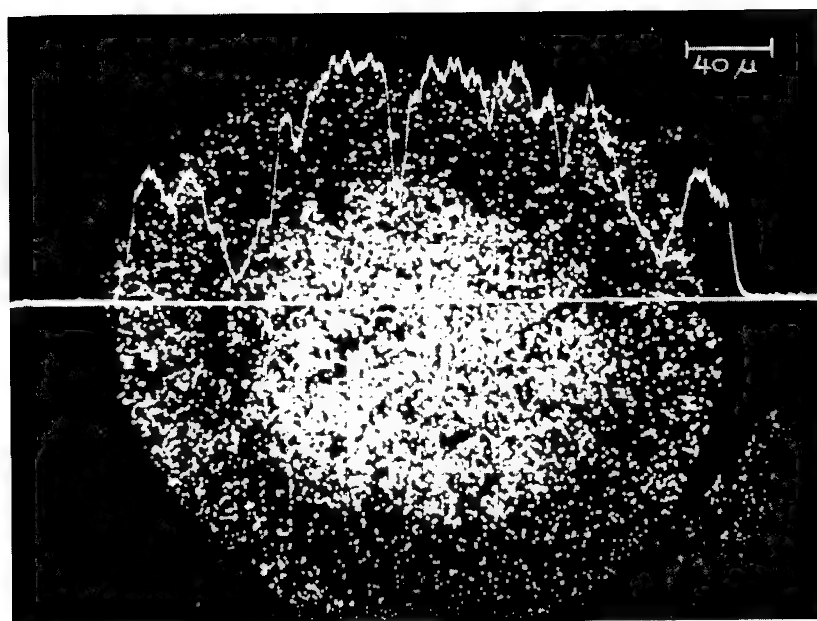
Figure 1   X-ray intensity sweep and line scan profile for iron.
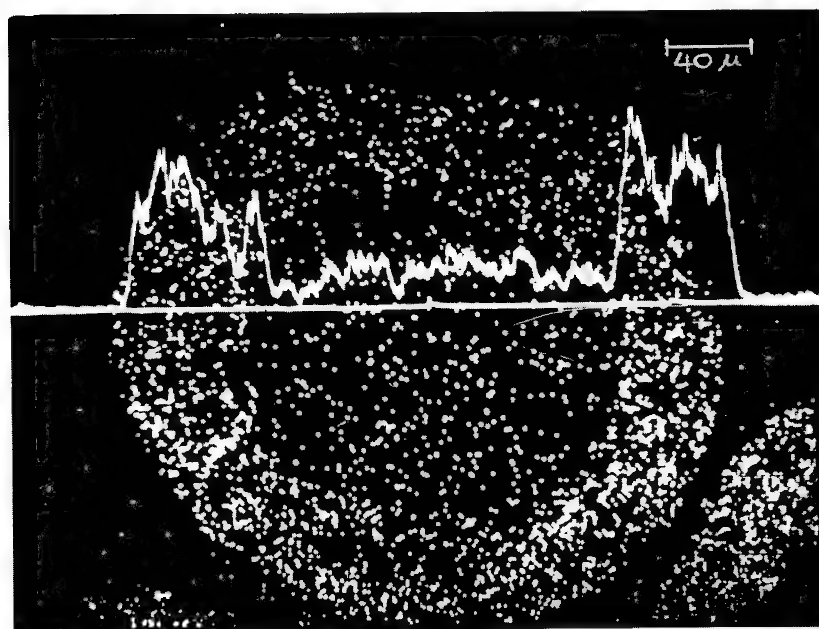
Figure 2   X-ray intensity sweep and line scan profile for manganese.

THE EFFECTS OF DIET ON THE MICROSTRUCTURE OF TEETH

Arthur J. Saffir and Robert E. Ogilvie

The electron probe may well be the instrument that will aid in solving the age old problem of tooth decay. Although the relationship of sugar in the diet and tooth decay (dental caries) was felt to be obvious (a fermentable substrate for bacterial production of organic acids which dissolved the tooth mineral), the effects of dietary manipulations such as addition of fluoride or phosphate, which inhibit the caries process, remains obscure. The probe, however, has revealed some striking changes in the microstructure of tooth mineral upon addition of supplements to a control cariogenic diet.

Teeth were obtained from a nutritional study of dental caries in the white rat. The 2 x 2 factorial design included a control group on a cariogenic diet, a test group receiving the cariogenic diet supplemented with fluoride, a test group receiving the cariogenic diet supplemented with sodium trimeta phosphate and a test group supplemented with both fluoride and phosphate. Significant caries reductions were observed in each of the test groups as compared with the unsupplemented control group. While gross chemical analysis could not detect any change in the total phosphate concentration of teeth within the different groups, the probe revealed that the microdistribution of several elements was markedly altered in teeth from animals on the phosphate supplemented diets. This effect was not observed in teeth from animals on the fluoride supplemented diet, and thereby indicated different modes of cariostatic action for fluoride and phosphate.

In the teeth of the control animals, the concentration of potassium is relatively uniform throughout the enamel (see Figure). At the interface between the dentin and enamel, the concentration of potassium rises sharply reaching a maximum within 10μ into the dentin and remains constant throughout the remainder of the dentin. The distribution of potassium is not altered in the dentin of the phosphate supplemented rats; however, the probe revealed a gradient in the distribution of potassium within the enamel. The outer enamel surface contained 35% less potassium than the enamel close to the dento-enamel junction.

Chlorine, which is normally present in higher concentration in enamel than in dentin, also maintains a uniform concentration in the enamel and the dentin. However, in the phosphate supplemented animals a chlorine gradient was found with the maximum concentration near the enamel surface.

By means of an X-ray absorption technique with the electron probe (discussed at last year's conference) it has been discovered that the calcium concentration, expressed in grams per cm^2, normally decreases in the dentin near the dento-enamel junction. This zone of reduced calcification was found to be of lesser extent in the phosphate supplemented animals.

CROSS SECTION OF A TOOTH

DENTIN   ENAMEL   PULP   CONTACT POINT
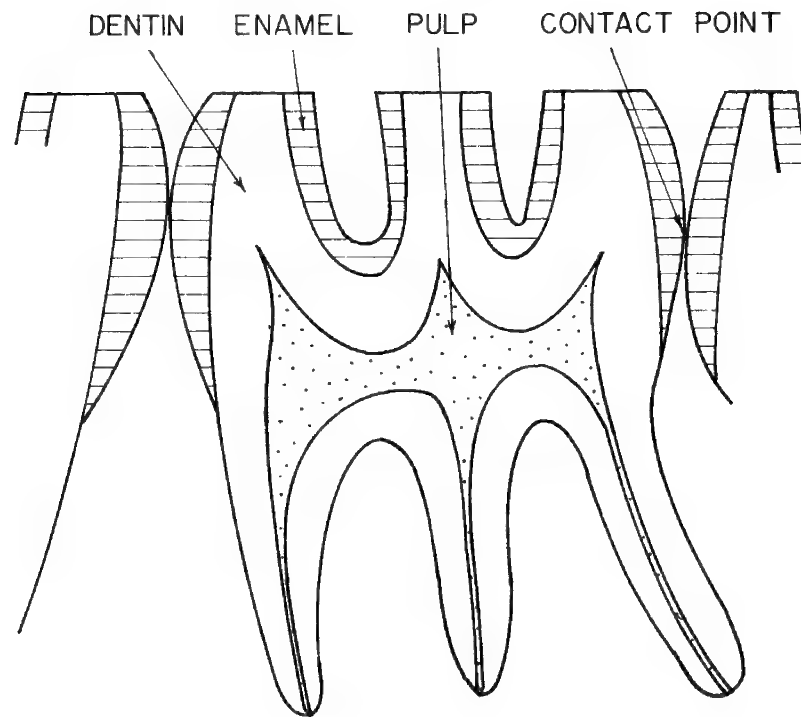
ELECTRON MICROPROBE DISPLAY OF DIFFUSABLE CONSTITUENTS (K,Cl, & Na) IN BIO-LOGICAL TISSUES*

C. Adrian M. Hogben and M. J. Ingram

In the application of the electron microprobe to elemental analysis of biological specimens, we have employed the following operating conditions: acceleration voltage 10 kv, specimen current 0.05 microamps and a minimal electron spot size. For the elements potassium, chlorine, and sodium, we have used 4" crystals of LiF (slit half width 7×10^{-3} angstroms), NaCl (half width 10^{-2} angstroms), and KAP (with a pulse height discriminator).

Both standards and tissue are frozen in liquid propane, dried under vacuum from -70°C to -30°C over four days and embedded in epoxy Epon 826 (Cl content 30 mM/kg). After polymerization, 3 micron sections are cut and mounted flat on a quartz slide prior to light carbon shadow casting. With an acceleration potential of 10 kv, these sections are infinitely thick.

The standards were solutions of salt in 20% albumin. Droplets of known salt concentration were ejected into liquid propane, providing the following values:

KCl Concentration	Net counts/sec per mM/kg	
mM/kg	$K_{K\alpha}$	$Cl_{K\alpha}$
10	.11	.21
25	.12	.18
50	.12	.20
100	.14	.20
150	.15	.22
	counts/sec	
Background	.51	.68

Tissue specimens such as frog skeltal muscle and gastric mucosa are cut to about a 1 mm cube before being plunged into liquid propane. When care is exercised, tissue can be rapidly frozen without the formation of ice crystal artifacts resolvable by light microscopy.

This sample preparation is compatible with the retention of the marked difference between intracellular and extracellular concentrations of potassium. The mean intracellular concentration of potassium calculated for probe analysis is within 10% of that estimated from conventional chemical analysis of frog skeletal muscle, 120 mM/kg.

When the electron spot is driven to scan the specimen surface, the spatial resolution has been 3 microns. With this resolution and mode of specimen preparation, we have not encountered any inhomogeneity of intracellular potassium but obviously cannot exclude this possibility.

Working with the tissues of the frog where the fluid between the cells may have a low protein content, we have not maintained the expected uniform distribution of extracellular chloride. Instead of encountering a uniformly higher extracellular chlorine signal, there are peaks of greater concentration at the extracellular boundaries, as if salt had been absorbed at the cell margins. Models have been tested employing chamois skin to provide a coarse organic matrix. Portions of chamois skin were soaked in salt solutions with varying concentrations of albumin, 0 - 20%, and then subjected to the usual sample preparation. Below 1 - 2% albumin, salt did not remain diffusely distributed.

The frozen dried tissue can be fixed in vacuum with osmium. After osmium fixation, the specimen sample current display provides a recognizable picture of tissue structure.

40

CHEMICAL CONSTITUTION OF BACTERIAL SPORES*

Kenneth G. Carroll

Resting spores of Bacillus Megaterium are living organisms which can persist for years without appreciable metabolism in a dry environment. In such a state they are remarkably resistant to heat, dessication, toxic chemicals, and ionizing radiation. When placed in a proper nutrient medium, these spores are transformed into dividing vegetative cells which germinate and reproduce by cell division. Trace elements such as manganese and cobalt in the surrounding medium have a profound effect upon the rate of post-germinative development, as documented by Levinson [1]. Electron probe microanalysis offers the possibility of illuminating the basic chemical facts underlying the biological behavior of spores by virtue of its unique ability to analyze the chemical composition of a single spore, which weighs about 10^{-12} grams.

For analytical purposes, spores were dispersed in a 1% Parlodion solution in amyl acetate on a substrate of spectrographically pure carbon. Individual spores of about 1 micron in size could be selected for analysis. Accelerating voltage was usually 15 kilovolts, and specimen current from one hundred to three hundred nano amperes. X-ray intensity measurement was accomplished by diffraction from a gypsum crystal, and by detection with a flow proportional counter with a Mylar window of one quarter mil thickness. The spectrograph was evacuated to about 10^{-5} Torr.

Examination of large clusters of spores revealed the presence of Ca, K, P, and Si. X-ray intensities were found to be independent of the time of irradiation. Single spores had X-ray spectra with peak-to-background ratios between one and ten for K-alpha lines. Measurable variations were found among individual spores, and these were studied statistically by observations on groups of 10, measured under constant instrumental conditions. The total X-ray intensities for each spore were normalized to account for size differences, and the resulting distributions were found to be Gaussian. Measured standard deviations for Ca, K, P, and Si were found to be respectively 15, 30, 18, and 29% of the amounts present. The statistical uncertainty of a single observation had a standard deviation of about 3 percent. Thus the biological variability observed among individual spores was from 5 to 10 times as large as that ascribable to purely statistical considerations of the X-ray counting process.

Preliminary observations suggest that the chemical variability of resting spores changes with age, e.g. the width of the phosphorous distribution increases markedly with time.

----

1. Bacterial Spore Germination with Special Reference to Bacillus Megaterium. H. S. Levinson and M. T. Hyatt, Annals of the New York Academy of Sciences Volume 102, p. 773 (1963).

ELECTRON PROBE MICROANALYSIS OF BIOLOGICAL ULTRATHIN SECTIONS

P. Galle

The applications of electron probe microanalysis to the study of histological sections poses special problems which differ according to the thickness of the sections to be analyzed.

When one examines thick sections (greater than 1 micron), the principle problem is to prepare the sample in such a way that it is not destroyed by the beam; this problem has been resolved, for several years now, in different ways [1,2]. It is sufficient to state here that the tissues are imbedded in a plastic material having the highest possible melting point: paraffin is almost unusable, methacrylate or, better still, araldite or epon are generally used, and are cut in relatively thin sections (1 micron) so that the heating effect will be minimal. In order to make the sample an electrical conductor, a very thin metallic layer of 100 Å is deposited on its surface.

When one examines ultrathin sections (less than 1000 angstroms) the problems are different; these sections absorb fewer electrons and therefore are much more resistant to intense electron beams. On the other hand, they can no longer be seen with the light microscope, and it becomes necessary to include a device for visualizing the sample, an electron microscope; several instruments combining an electron microscope and a system for electron probe analysis by X-ray spectometry have been constructed [3,4]. We have personally used the new apparatus made by C.A.M.E.C.A. This instrument is described in detail in another communication; however, to summarize simply here, it was constructed with the primary concern of keeping the system of electron probe analysis at its maximum sensibility, since analysis must be made on extremely small quantities of material. On the other hand, the electron microscope part was voluntarily simplified: a resolution power of the order of 200 Å was considered sufficient to detect inclusions of analyzable dimensions.

Obtaining an ultrastructural picture of the preparation being examined is particularly important for three reasons: 1) intra- or extracellular inclusions, being as a rule very small, are, for this reason, undetectable with the light microscope, 2) it is always necessary to be able to establish a precise relationship between the ultrastructural picture and the results of electron probe analysis, 3) the quantities of material detected are, generally, very small and very localized; it is therefore indispensable to have a visual control of the preparation at a very high magnification in order to eliminate all artifacts and to be certain that the analysis is not being done on a colloidal speck of dust present on the sample.

Results obtained on ultrathin sections are presented; they concern the study of the pathological kidney (nephrocalcinosis, heavy metal intoxication: lead, bismuth, uranium, and human nephropathies of unknown origin).

----

1. A. J. Tousimis, I. Adler, J. Histochem. Cytochem. 11, 40 (1963).
2. P. Galle, Rev. franc. Etudes clin. biol., 9, 203 (1964).
3. W. C. Nixon, Proceedings of the European regional conference on Electron Microscopy (Delft, 1960).
4. P. Duncumb, 5th Int. Congress for Electron Microscopy (1962).

SAMPLE SELF ABSORPTION OF ELECTRON EXCITED SOFT X-RAY SPECTRA

William L. Baun and David W. Fischer

It is recognized by most microprobe workers that there are sample self absorption effects, but the magnitude of these effects is not generally appreciated. Recent work by Fischer [1] on L spectra of first transition elements showed large variations in relative intensities of L_{II} and L_{III} with changes in voltage. These changes can be correlated with the depth of electron penetration. For instance, the ratio L_{II}/L_{III} for Cu is shown to vary linearly with electron penetration. However, it does not vary as one might expect. Generally, it would be expected that as electron penetration increases and the effective X-ray production depth increases, the relative intensity of softer radiation compared to harder radiation would decrease. This is what happens for K_α and $K\beta$ where the absorption edge lies to the short wavelength side of both lines. CuL_{II} and L_{III} behave in an opposite manner, with the harder radiation (L_{II}) being selectively absorbed in the sample with increasing electron penetration. The position of the strong L_{III} absorption edge between the L_{II} and L_{III} emission bands accounts for this behavior. This same effect may be seen by varying the takeoff angle and is illustrated in Figure 1. This example, which shows an appreciable absorption effect, as well as others which are shown in the paper, indicate the advantage of high takeoff angles. It is also shown that high takeoff angles improve intensity of soft X-rays and data are shown concerning the apparent (but not real) change in peak to background ratio with different takeoff angles.

It is shown that each of the effects on X-ray spectra ascribed to chemical combination can, in many cases, be explained by changes in absorption spectra and self absorption in the sample. Examples are given using L spectra from Cu, Cu_2O, and CuO. Very large effects are also seen in M spectra of rare earth elements, where self absorption causes line splitting and large intensity variations. Such an example is shown in Figure 2 where the dysprosium M emission spectrum is plotted along with the absorption spectrum to emphasize the coincidence of spectral features. This multiplet effect in rare earth M spectra was observed over 35 years ago and since then has been ascribed to electron vacancies in the incomplete 4f shell. Major changes in M spectra with changes in electron penetration are observed and it is shown that the self absorption effect could be used to determine absorption features with materials or spectral regions where it is difficult to prepare absorption samples.

From the data presented here it is not surprising that X-ray emission spectra obtained by different people with different voltages and takeoff angles do not always agree. Further, it is evident that intensities and line and band shapes reported in the literature are reproducible only at the same voltage and geometry as in the original work.
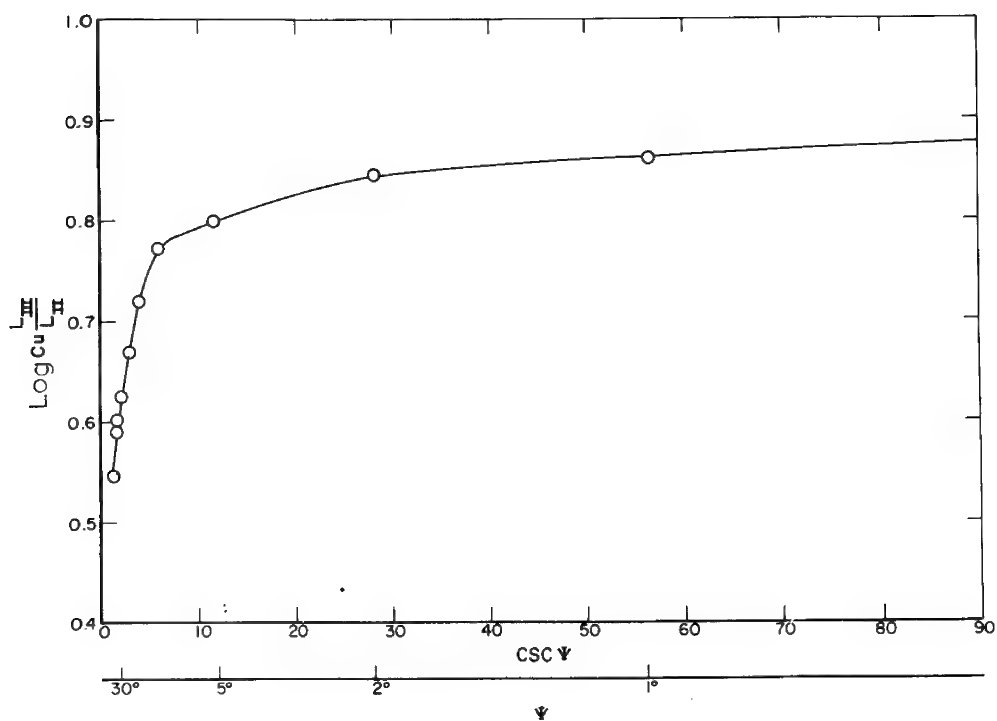
Figure 1
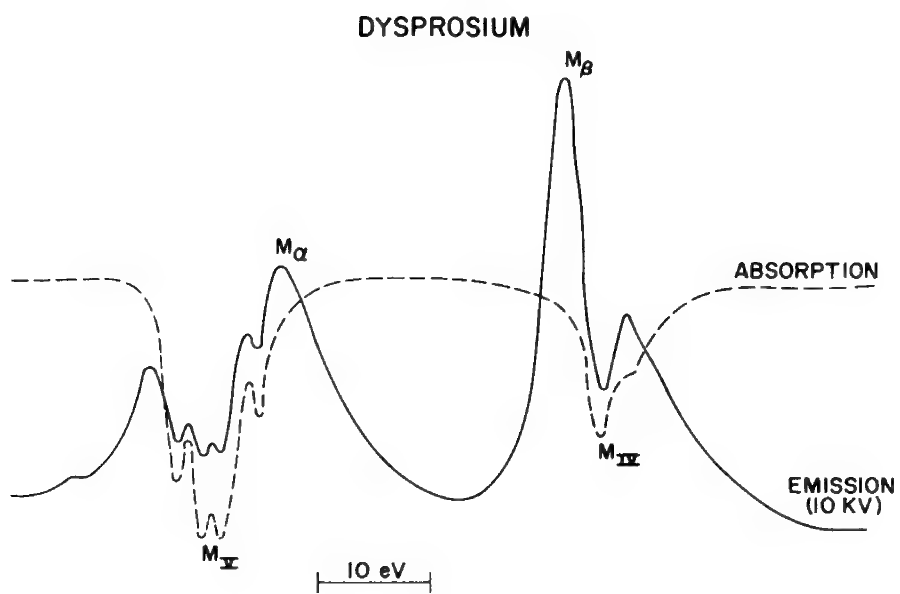
Figure 2

LIGHT-ELEMENT ANALYSIS WITH MULTI-LAYERED Pb-STEARATE

Horoshi Okano and Teruichi Tomura

Electron probe microanalysis is a non-destructive method for light-element analysis. The most important problem in such analysis by the dispersive-method is the efficiency of the diffraction crystal. In this report, we will discuss the characteristics of a multi-layered Pb-stearate diffraction crystal and show examples of its use in light-element analysis.

The multi-layered Pb-stearate was prepared on a curved glass surface. Each monomolecular layer was built up under strictly controlled conditions, with careful cleaning of the base and removal of the impurity metal ions from the solution on whose surface the monomolecular layer was spread.

The diffracted intensity of C K X-rays from this Pb-stearate crystal was measured with a 100 mm radius focusing type spectrometer and found to be 1.84×10^4 cps at 10 KV and $0.1\mu A$. This value was obtained after a careful setting of the discrimination level of the measuring circuit to avoid spurious counts. The misorientation, estimated from the beam breadth of diffracted X-rays at the focusing point of the spectrometer, was less than 3 min.

In the case of C K X-rays the natural breadth is converted for the Pb-stearate crystal to 1.45×10^{-2} radians, which is larger than the misorientation of the crystal. Therefore, when a sufficiently wide receiving slit is used, the peak height of the spectra corresponds approximately to the integral reflection intensity. On the basis of this consideration, the integral reflection coefficient was obtained from measurements of the intensity of the characteristic X-rays incident upon the crystal and the peak intensity of the diffracted beam. The integrated reflection coefficient, ρ is related to the integrated intensity, I, as follows:

$$\rho = \frac{I}{2d \cos \theta_0 \ E(\lambda_0)},$$

where d is the lattice spacing of the diffraction element, θ_0 the Bragg's angle, and $E(\lambda_0)$ the peak height in the intensity profile of C K X-rays. $E(\lambda_0)$ was deduced to be 7.66×10^7 cps/ Å/ sterad. from the incident intensity of 1.66×10^{-4} quanta/ electron/ sterad. at a 10 KeV electron energy which was measured by the non-dispersive method. A peak intensity of 2.5×10^4 cps was obtained from the aforementioned value by correcting for the efficiency of the detector. From these values and the above equation, an integral reflection coefficient of 2.0×10^{-4} radians for C K X-rays was calculated. This coefficient agrees satisfactorily with a theoretical value, 3.2×10^{-4} radians, which includes the correction of the second extinction effect.

Many light-element analyses have been performed with an electron probe micro-analyzer using this Pb-stearate crystal. Some results will be presented.

44

A COMPARISON OF THE NETWORK METHOD OF PULSE-HEIGHT ANALYSIS WITH CRYSTAL SPECTROMETRY FOR LIGHT ELEMENT ANALYSIS

G. V. T. Ranzetta and V. D. Scott

The importance of being able to microanalyse for the light elements such as boron, carbon, nitrogen, oxygen and fluorine has long been acknowledged but it is only in recent years that techniques have been developed for this purpose. One method, pulse-height analysis, has been in use at AWRE (Aldermaston, England) for the past five years and more recently, large d-spacing crystals such as KAP and stearate have become available. In the present paper the performance of both methods for qualitative and quantitative studies is compared.

In this evaluation, quantitative measurements have been carried out firstly on a number of metal carbides, SiC, TiC, WC and UC, and then on some oxides, Al_2O_3, ZrO_2 and UO_2. The advantage with using carbides was that the samples were conducting and that a standard was readily available in the form of carbon. The oxides, however, had to be coated with a minimal thickness of gold to avoid the surface charging up, and with these materials beryllium oxide was used as a standard.

In general, clear differences were found between the values given by the two techniques. It is considered that the network method of pulse-height analysis has potential errors which arise from the basic assumption that the shape of the X-ray emission spectrum from a particular element differs only in intensity according to the amount of the element present. The shapes of the spectrum, however, are frequently not the same for sample and standard as a result of the different X-ray absorption characteristics, with wavelength, of the respective targets. This can lead to over- or under-compensation for the background and, in practice, is worse when discriminator settings of the pulse-height analyser have to be used. This problem does not arise with the crystal spectrometry method but, with both techniques, some additional complications may occur as a result of soft X-rays from heavier elements overlapping the light element X-ray spectrum.

These difficulties are discussed in relation to the experimental results and it is concluded that crystal spectrometry is preferable for quantitative analysis, especially when working at high kilovoltages of 8-10 kV or above.

The conversion of the measured values into quantitative data is also investigated with reference to atomic number and X-ray absorption corrections, which are large in most of the systems considered.

The final section of the paper deals with some practical applications in metallurgy including inclusion identification and oxygen penetration into corroded metals.

These illustrations are used to compare the performance of the two techniques for qualitative microanalysis, for example, the formation of scanning X-ray images. The network unit is shown to have the advantages here of complete elimination of background as well as speed of image formation.

ELECTRON MICROSCOPE - MICROPROBE FOR ANALYSIS OF SMALL PARTICLES

Robert A. Skrivanek

Recent interest in the study of cosmic dust particles in the size range 0.1 to 10 microns has necessitated the modification and extension of existing microprobe techniques. In its simplest form, the problem reduces to being able to positively identify a micron-sized particle as being "Real," i.e. not a contaminate and then obtaining its chemical analysis. In most cases, the presence or absence of a shadow next to the particle, resulting from a low-angle, evaporated, metal coating applied immediately before and after particle collection, is the primary criteria for distinguishing between real and contaminate particles. In order to see a particle between 0.1 and 10 microns, and determine whether or not it possesses such a shadow, usually requires the use of an electron microscope operating in a magnification range between 1,000 and 10,000X.

In order to perform a chemical analysis on such a particle, the sample would first have to be removed from the electron microscope and then placed in a standard electron microprobe which utilizes some kind of visible light optics to find the particle of interest. If the particle is very small, it will never be seen in these optics and one can never positively know that the beam is on the right particle or even on any particle at all. A solution to the problem has been quite apparent for some time, namely, an instrument which combines an electron microscope with an electron microprobe analyser. However, the actual production of such an instrument was quite an undertaking and only recently has it been completed.

The instrument has a variable accelerating voltage of 0-75 KV, a magnification range of 2,000X to 14,000X and a resolution of approximately 40 A°. The image can be viewed directly on a phosphor screen or recorded on either 35mm film or 2" x 2" plates. When a particle of interest is found, the beam is merely focused to a small spot and centered about the particle.

A nondispersive analysis of the particle can be obtained using a gas proportional counter and a 400-channel pulse height analyser; or a dispersive analysis of the particle can also be obtained using the vacuum crystal spectrometer connected to an X-Y recorder. In addition, X-ray and specimen current scanning displays on a cathode-ray tube are also possible, but as yet have not been found to be of great use in small particle work.

In most high-altitude rocket and satellite particle collection work to date, thin, nitrocellulose films supported on 200-mesh grid and shadow-coated with a metal, have proved to be the most popular particle collection surface. These surfaces are usually sealed in a vacuum-tight container and exposed only during certain periods in space. In spite of extreme cleanliness precautions, the presence of many contaminate particles still tend to cloud the chemistry of the true extraterrestrial particles.

Other workers, using a nondispersive system attached to an electron microscope, have been able to obtain some chemical data from collected particles. However, the chemistry of the collected particles on the flight samples does not tend to be any different from that of the ones on the control. Thus far, particles that have been analysed on this instrument also tend to confirm this.

Additional samples from previous flights are still being scanned and analysed in an effort to determine if there is some specific characteristic that can be used to differentiate extraterrestrial particles from terrestrial contamination.

While the instrument was initially designed with the small particle problem in mind, it has proved quite useful in both biological and metallurgical applications.

AN X-RAY SPECTROMETER ATTACHMENT FOR THE PHILIPS EM-200 ELECTRON MICROSCOPE

D. M. Koffman, M. Schippert, S. H. Moll, and S. Hamill

An X-ray spectrometer has been developed to extend the analytical capability of the Philips EM-200 Electron Microscope to studies of sample chemistry. It attaches directly to the objective aperture port of the rotating/tilting specimen stage.

Shown in Figure 1, the spectrometer is a high resolution instrument, employing a mica crystal which is continuously curved to fulfill the X-ray focusing conditions over the entire angular range. Equipped with a flow proportional counter, it is capable of analyzing characteristic X-ray lines of any element from Mg through U. With the rotating/tilting specimen stage and a replacement aperture installed in the microscope, the spectrometer may be attached to or removed from the instrument in less than five minutes. It may also be left in situ during normal use of the microscope.

Supplementing the present ability of the electron microscope to investigate morphology and crystal structure (by electron diffraction), the spectrometer allows the simultaneous determination of chemical composition by X-ray fluorescence analysis. One typical application of the spectrometer is associated with its ability to analyse small particles originally imbedded in a matrix of similar chemistry. Figure 2 is an electron micrograph of an extraction replica obtained from a sensitized stainless steel. Examination of the X-ray emission spectral pattern (shown in Figure 3) obtained from one of the fine precipitates in the grain boundaries identified it as chromium carbide.

The instrument has demonstrated capability in the chemical analysis of: precipitates removed from bulk specimens by extraction replication; particle dispersions, thinned metal specimens, and biological tissue sections. Specific examples are presented which illustrate the applicability of the instrument for material studies in the biological metallurgical and mineralogical fields.
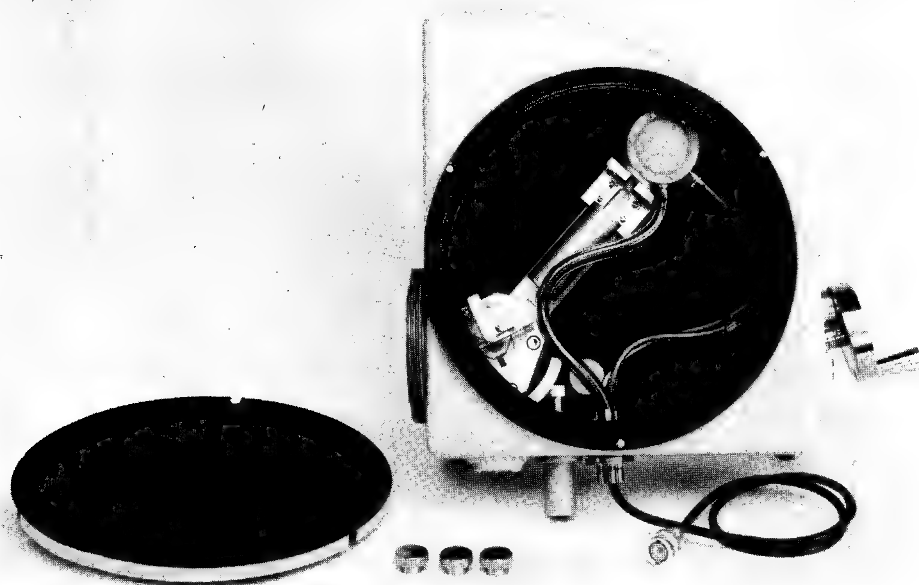
Figure 1   AMR Spectrometer Attachment
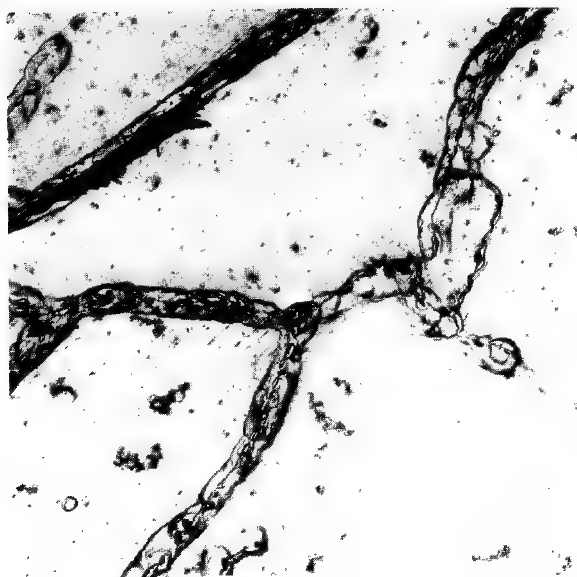
Figure 2   Electron Micrograph
(Mag. 4500X) of an Extraction
Replica from a Sensitized
Stainless Steel. A series of
fine precipitates ranging in
size from 0.2 to 3μ are
observed along the grain bound-
aries. These precipitates
should be chromium carbides.
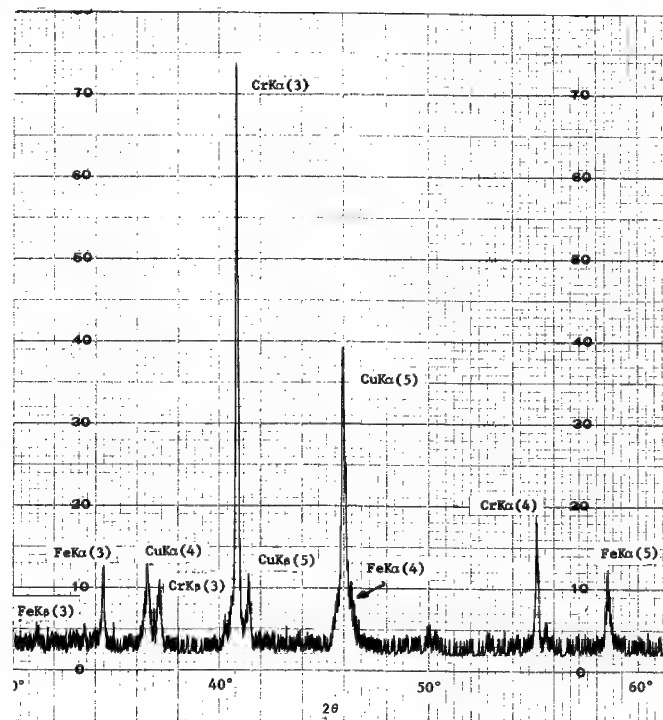
Figure 3   Spectral Pattern from Chromium
Carbide taken with 1.5μ probespot
on 0.8μ diameter particle. Note
Fe content of carbide. Full
scale 200 counts/sec.

47

DESIGN AND APPLICATION OF A COMBINED INSTRUMENT "ELECTRON MICROPROBE ELECTRON MICROSCOPE"

Claude Conty and Pete Finley

The microanalyser is commonly used in metallurgical and biological research. In the case of biological specimens and metallurgical replicas, however, the use of an optical microscope for visual examination is not satisfactory. As Duncumb [1] has shown, the use of a combined instrument, the "Electron Microscope, Microanalyser," overcomes this difficulty. For this reason a new attachment for the CAMECA MS 46 Microanalyser has been developed. This instrument is an electron microscope which permits superior specimen observation while retaining the capabilities of the microanalyser.

The system consists of two lenses (objective and projector) with a magnification of about 6,700 on the viewing screen and 8,000 on the film plate with a resolving power close to 100 angstroms. The device is inserted in place of the standard specimen chamber and can be taken out very easily. The viewing window is at table level allowing easy observation. A vacuum camera is placed below the fluorescent screen.

Some characteristics of the probe (astigmatism, diameter) have been measured. For a given probe size, the intensity of the electron beam with and without an anode aperture is compared to the theoretical intensity which would be obtained with a gun of theoretical maximum brightness. A study of the precipitation phenomenon in high strength stainless steel, utilizing extraction replicas, shows the potentialities of this apparatus.

---

1. P. Duncumb, Tech. Rpt. 182, Tube Investments Research Laboratories, Essex, England.

ANALYTICAL APPLICATIONS OF A COMBINED ELECTRON MICROSCOPE/ELECTRON MICRO-ANALYZER

M. A. Schippert, S. H. Moll and R. E. Ogilvie

The Advanced Metals Research (AMR) Probescope consists of an electron optical column combining the resolution and magnification capability of an electron microscope with the electron beam intensity and small probe spot size of a high quality electron microprobe. Data retrieval facilities include dispersive (for high resolution) and nondispersive (for high sensitivity) X-ray detection system.

This instrument is especially suited for submicron area or particle investigations, where the specimen is electron transparent, as in electron microscopy, or where the particles are mounted on a nitrocellulose or carbon film. Such a specimen may be investigated in order to determine simultaneously its morphology, its crystal structure (by electron diffraction) and its chemical composition (by X-ray analysis). The analytical capabilities of this instrument allow its application to materials studies in the metallurgical, mineralogical and biological fields. Specimens suitable for normal electron microscopy can be examined in the probescope. A schematic cross-section of the electron optical column is shown in Figure 1. A minimum probe spot of $0.2\mu m$ can be formed.

Specimens are mounted, as in most conventional electron microscopes, between the objective lens pole pieces which results in an electron microscope resolution of 50 angstroms. The vacuum X-ray spectrometer is a focusing curved crystal device equipped with a flow proportional counter. The nondispersive X-ray system consists of a high resolution flow proportional counter coupled with a 400 channel pulse height analyzer.

A typical application would involve a determination of the chemistry of an extremely fine particle. The $0.8\mu m$ particle shown in Figure 2 was found on a gold coated micrometeorite collection grid. The two nondispersive spectrums reveal that the lower energy peak represents the X-ray emission from the particle. The spectrometer scans through several elements exhibiting spectral lines of about the energy of these peaks indicate a high magnesium level in the particle and gold from the background (see Figure 3). Other metallurgical and geological applications involving determinations of chemistry in fine particles or extractions are presented. The determination of element distribution in biological specimens is also discussed.

Section A-A

A M.R. PROBESCOPE No. 4-301

Figure 1

60 KV, I.0μ Probespot

Particle Shape

0.8μ

X-Ray Energy Spectrum of suspected Micrometeorite (Particle 3) on Au coated Formvar Film
NONDISPERSIVE ANALYSIS

Figure 2

X-Ray Spectrometer Scans through Au, Mg, Al, S and Si Peak Positions for
Suspected Micrometeorite (Particle 3)
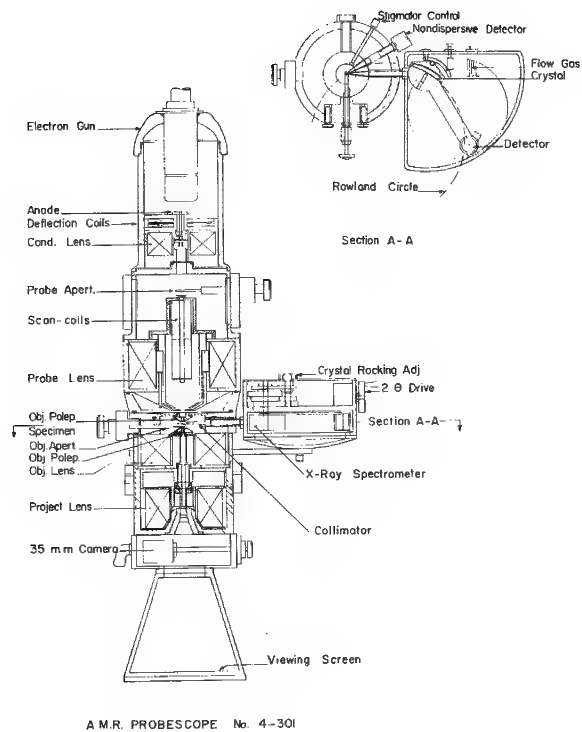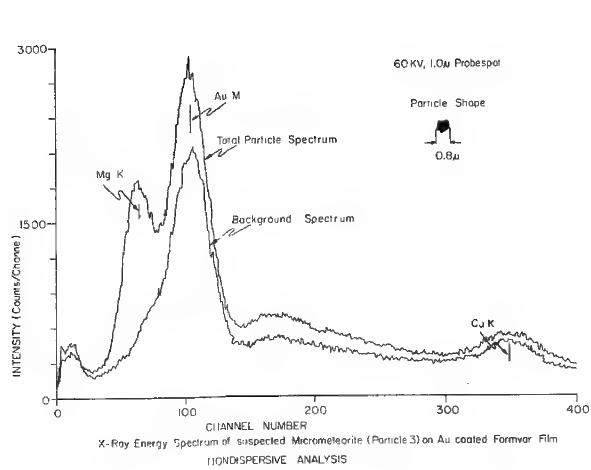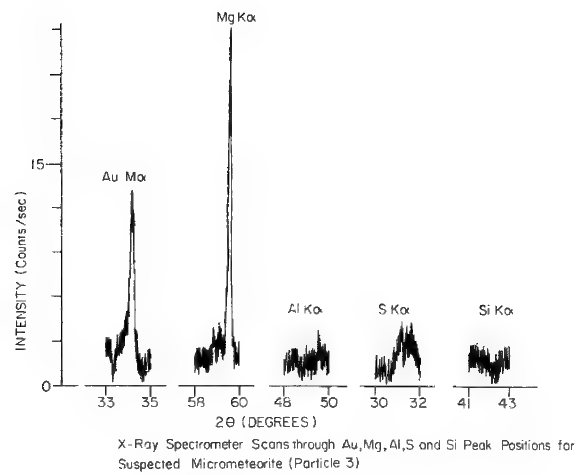
Figure 3

APPLICATIONS OF A COMBINED ELECTRON MICROSCOPE AND ELECTRON PROBE MICRO-ANALYSER - EMMA

C. J. Cooke and P. Duncumb

The design and basic performance of EMMA have been described previously by Duncumb [1,2]. It is the purpose of the present paper firstly to review the application of the instrument as a combined electron microscope and electron probe microanalyser and secondly to illustrate the possibilities of rearranging the instrument, by virtue of its modular construction, to enable it to be used for a variety of other techniques.

In the EMMA mode of operation the specimen must be at least partially electron transparent at the highest accelerating potential available (70 KV); carbon extraction replicas, evaporated metallic films and micro-tomed sections have been examined. The small probe size obtainable (0.2_{μ}m for 2 nanoamperes probe current at 30 KV), combined with efficient full range (1 to 100 angstroms) crystal spectrometers, have made possible the identification of particles down to below 1000 angstroms in size. Selected area diffraction can be carried out simultaneously with the analysis with an accuracy of area selection better than 0.2μm, and this facility, combined with the morphological information available in transmission electron micrographs (100 angstroms resolution) and in the electron scanning image ($0.1 - 0.2\mu$m resolution), has made the instrument a useful tool in the examination, for example, of precipitation occurring in stainless steels [3]. In the biological field, the reliable histological identification of areas of interest for analysis provided by the transmission electron microscope image has proved particularly important for specimens consisting of micro-tomed sections, giving low contrast or poor resolution in the electron scanning or optical microscope image of the conventional microanalyser. Applications which will be described include the examination of a variety of precipitates in stainless and alloy steels, the identification of particles collected by rocket from the upper atmosphere and a study of the mechanism of bone formation in chick embryos [4].

The instrument has also been used as a conventional solid specimen microanalyser in preference to a standard instrument because of the high spectrometer efficiency and the resolution obtainable in the electron scanning image; such an application was the investigation of titanium boride and other inclusions, often less than 0.5μm in size, in an aluminium alloy. Other modes of operation which have been investigated include scanning electron microscopy, Kossel line X-ray diffraction and X-ray projection microscopy.

It is intended that this paper will demonstrate the viability of a universal instrument for electron imaging and microanalysis, an instrument which can rapidly be adapted to suit the immediate needs of any investigation and still provide near optimum performance in any one mode of operation.

----

1. P. Duncumb, Proc. 5th Int. Conf. on Electron Microscopy, Philadelphia (1962).
2. P. Duncumb, The Electron Microprobe, op. cit.
3. V. B. Nileshwar, "The Metallography of the V Phase in Type 3.2.1. Stainless Steel, (in press).
4. H. J. Hohling, T. A. Hall, C. J. Cooke, P. Duncumb, "Studies of the Early Stages of Bone Formation by Means of Conventional and Electron Microscopic Electron Probe X-ray Microanalysis," Naturwissenschaften (in press).

SOME OPTICAL SIGNAL DETECTION TECHNIQUES FOR ELECTRON MICROPROBE INSTRUMENTS*

D. F. Kyser, J. McCoy, and D. B. Wittry

Optical signals produced by focused electron beams have been useful in a variety of investigations including cathodoluminescence of semiconductors [1], selective oxidation of metals [2], characterization of phosphors [3], mineralogical investigations [4], and studies of biological specimens [5]. In these investigations photographic films and electron multiplier phototubes have been used to obtain qualitative information on the spatial distribution of the radiation while quantitative information has usually been obtained by the use of monochromators [1,3] combined with choppers and phase-sensitive demodulation [1]. In the present work, two additional techniques have been used to increase the utility of optical signals from electron probe instruments.

The first technique involves chopping of the electron beam and measurement of the decay of luminescence to determine the lifetime of excited states or of excess carrier [3]. In this technique the electron beam is gated off or on in a time less than a nanosecond, and the decay or buildup of the luminescence is observed with a fast electron multiplier phototube and sampling oscilloscope. The transit-time spread of available multiplier phototubes is the limiting factor in the present system. With an Amperex CVP 150 electron multiplier phototube accurate values of the decay constant τ can be obtained only for $\tau >$ 10 nanoseconds. Signal averaging has been employed to facilitate the study of luminescence decay at low intensities.

A second technique that has proved useful in investigations of optical radiation is that of single photon counting. While photon counting has been used in cathodoluminescence microscopy [3] and in other applications involving low light levels [6], the advantage of photon counting for the detection of low intensity optical signals is not well known. Photon counting techniques are useful even for near infrared radiation if a small image of the radiation source can be focused on the photocathode. In this case, it is possible to use commercially available electron multiplier phototubes (such as ITT Model FW118) in which an electron image of the photocathode is formed on an aperture in front of the electron multiplier. With this type of multiplier phototube, the effective photocathode area can be of the same order as the size of the focused image of the radiation source.

The background counting rate of a focusable photocathode with S-1 sensitivity and an effective area of 10^{-7} cm^2 was found to be approximately 500 c/sec at room temperature, and this background can be reduced one or two orders of magnitude by cooling the photocathode and by using pulse-height discrimination. Assuming a photocathode efficiency of 0.3% in the near infrared region and a measurement time of 100 seconds, it is possible to detect infrared signals corresponding to only 200 photons/sec. The overall sensitivity for infrared radiation can then be two to five orders of magnitude higher than that obtained using a chopper with phase-sensitive demodulation of the current generated by a room-temperature electron multiplier phototube with a 1 inch diameter photocathode. The increased sensitivity makes it possible to study many phenomena

involving visible and near infrared radiation that cannot be observed by more conventional techniques. As an example, the cathodoluminescence excited in a GaAs specimen at 30 KV was measurable with the specimen current as low as 10 picoamperes.

----

1. D. F. Kyser, D. B. Wittry, The Electron Microprobe, op. cit.
2. K. F. J. Heinrich, Advances in X-Ray Analysis, W. M. Mueller (ed.), Plenum Press, Inc. N.Y., 1960, vol. 3, p. 185.
3. J. P. Davey, Thesis, University of Cambridge, 1964.
4. J. V. Smith, R. C. Stenstrom, J. of Geology, 73, 627 (1965).
5. R. F. W. Pease, T. L. Hayes, Nature, 210, 1049 (1966).
6. E. H. Eberhardt, IEEE Transactions on Nuclear Science, 11, 48 (1964).

MICROPROBE ATTACHMENT FOR QUANTITATIVE STUDIES OF CATHODO-LUMINESCENCE*

Raymond T. Greer and Eugene W. White

A versatile monochromator-photomultiplier attachment to an electron microprobe has been developed. It has facilitated the study of a number of cathodo-luminescence phenomena including: 1) recording of luminescence spectra, 2) distribution of luminescent phases in specimens, 3) growth and decay of "F-center"-induced luminescence and 4) relation of luminescent intensity to composition within a phase. This paper describes the salient features of the attachment and illustrates its application to several pertinent problems.

The attachment consists of a monochromator housing, a monochromator, an ocular tube, a selection of interchangeable slits and interchangeable photomultiplier detectors. The interchangeable components are readily permuted so that one can perform a variety of experiments or use the microscope in the normal manner without having to remove the attachment. For visual microscopic examination, the ocular is inserted in the attachment. Then the specimen can be viewed either through the monochromator, in which case the specimen is displayed in any color light desired, or alternatively, the monochromator can be bypassed for normal microscopic observation. Defining slits for the monochromator are inserted in place of the ocular, and then photomultiplier tubes in light-tight housings are slipped onto the attachment for electronic detection of light intensities.

The attachment replaces the ocular tube of the optical microscope on the microprobe. The monochromator within the attachment is an inexpensive Bausch and Lomb wedge interference filter of narrow band width and high transmission (average linear dispersion of 5.5 millimicrons per mm) with a useful wavelength range of 400 to 700 mu. An odometer is used to read wavelength directly to the nearest 0.1 mu. The visible spectrum is scanned by use of a synchronous motor drive on the monochromator with strip chart recording of the signal. A complete spectrum of a luminescent area, within the contour of interest can be obtained. The amplified photomultiplier signal can also be displayed on the oscilloscope in a fashion analogous to the conventional electron backscatter image as described earlier by Heinrich [1]. However, with this attachment light intensity displays at a particular wavelength can be photographically recorded.

Measurements of the luminescence of individual enstatite grains from a suite of enstatite chondrite and achondrite meteorites, produced by moderate-energy electron excitation (less than 40 keV), have established spectral energy distributions and excitation efficiencies as a function of mineral composition, irradiation time, and electron energy within individual grains. Striking variations of composition and luminescence spectra within the individual grains have been found, indicating the importance of precise localized investigation of a phase assemblage to provide an understanding of the bulk luminescent response of the material. The influence of increasing manganese

activator ion concentration and specimen purity is demonstrated with a shift of wavelength to longer wavelengths and higher intensity, and the quenching influence of iron is confirmed. The signals from these weakly luminescent silicates are adequate and do not require photomultiplier-differential current amplifier circuits or photomultiplier unit cooling for their detection and quantitative measurement.

In many instances, the cathodo-luminescent pattern has been used as a "marker" to establish the original reaction interface in solid state reactions of oxide materials.

The authors wish to thank Professors J. N. Weber, V. Vand, and R. Roy for their interest and assistance in this research.

----

1. K. F. J. Heinrich, "Oscilloscope Readout of Electron Microprobe Data," Advances in X-ray Analysis, Vol. 3, University of Denver, Plenum Press, New York, 1962, pp. 291-300.

MICROANALYSIS OF ELECTRON MICROSCOPE IMAGES WITH A NEW TYPE ELECTRON VELOCITY ANALYZER

Takeo Ichinokawa

A normal, cylindrical magnetic lens, in strong excitation, has been applied to the velocity analysis of electron microscope images. The cylindrical magnetic pole-piece shown in Figure 1 was inserted into the large bore of the intermediate lens of an electron microscope and was energized by the stabilized current of that lens.

The cylindrical magnetic lens in strong excitation has two focal points on the X-plane, with no lens action in the perpendicular plane (Y), as shown in Figure 2. If the lens current of the cylindrical lens is adjusted so that the magnification is the same in both directions on the screen and the image of the objective lens is focused on the object plane of the analyzer lens, the final image resembles the image formed by an electron microscope exhibiting some astigmatism. An example is shown in Figure 3 (a) for a micro-grid. Since the depth of focus is quite large in the intermediate image, the astigmatism is not bothersome. In this experiment, 2,450 ampere-turns were required in the cylindrical lens at 50 KV and 3,100 ampere-turns were required at 80 KV; the value of $NI/\sqrt{V}$ was 11 for both accelerating voltages. It should be noted that the lens excitation parameter for a cylindrical lens, $NI/\sqrt{V}$, is half that of the normal axially symmetric lens. With a lens of this strength, the chromatic aberration constant, C_{cr}, becomes positive and large for off-axis rays. If a slit is placed at the object plane of the cylindrical lens lying parallel to the Y-plane but a distance r from it as shown in Figure 1, the displacement δ on the final screen of the slit image caused by energy loss is given by

$$\delta = M \cdot C_{cr} \cdot r \cdot \Delta V/V \tag{1}$$

where M is the total magnification. The position and width of the parallel slit may be adjusted while observing the final image by using the locating mechanism of the intermediate lens selector aperture of the electron microscope. Figure 3(b) shows an energy spectrum obtained by placing the slit several microns from the optical plane. The optical plane is indicated by the dotted line in Figure 3(a). An energy resolution of about 1 eV at 80 KV is obtained. This is comparable to that obtained with an electrostatic lens (Mollenstedt type [1]).

The advantage of the system shown is that changes in instrumental arrangement are not necessary, it is easy to use, and specimen films of various kinds may be analyzed simply by providing a cylindrical magnetic pole-piece. Moreover, this system may be applied to any high voltage electron microscope and to the energy analysis of microdiffraction patterns. Examples of further applications will be shown.

----

1. G. Mollenstedt, Optik, 5, 473 (1952).
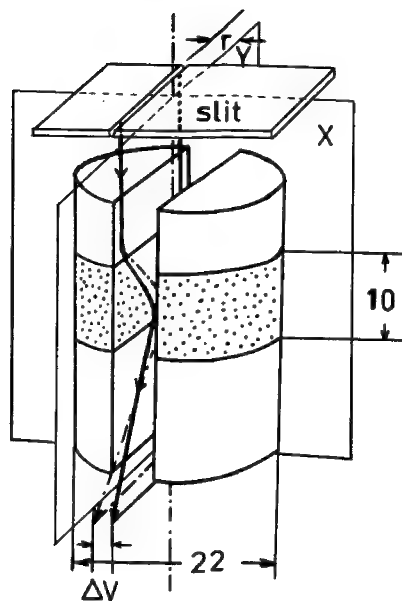
Figure 1 The cylindrical mag-
netic pole-piece used
as an electron velocity
analyzer.
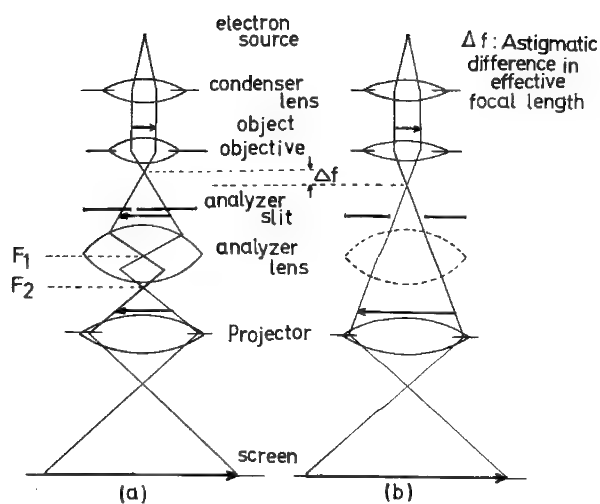
Figure 2 Electron ray paths for image
formation when the analyzer lens
operated: (a) X-plane, (b) Y-plane.

(a)

(b)
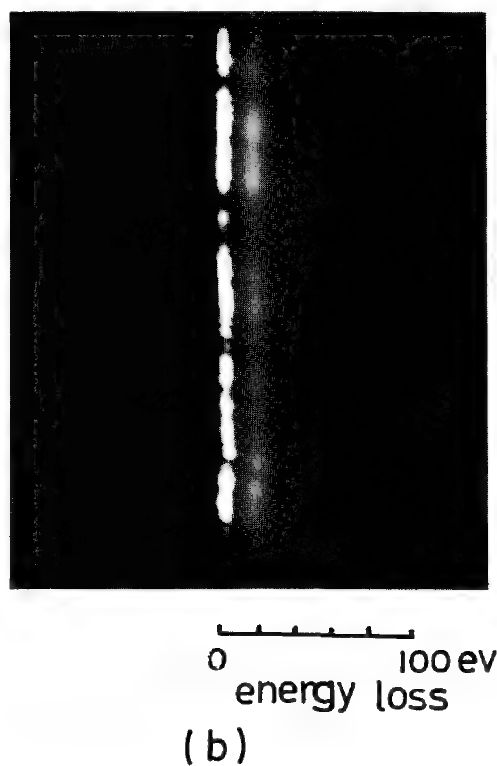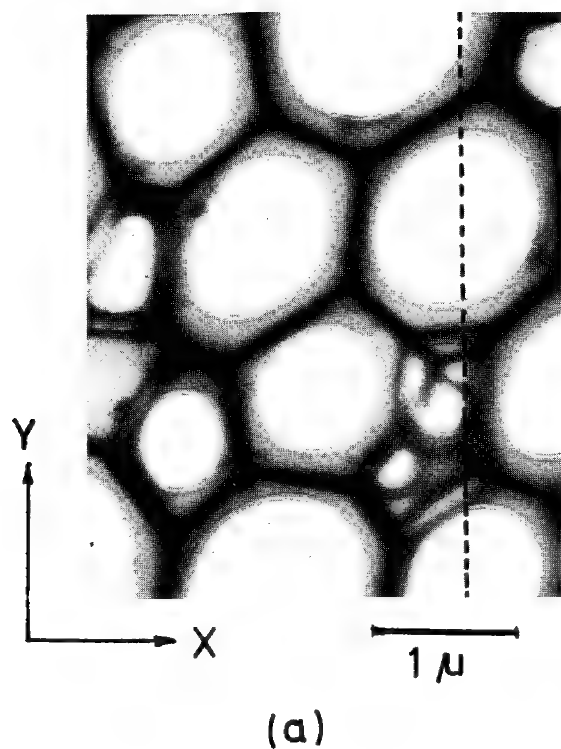
Figure 3 (a) Electron micrograph of micro-grid with analyzer lens operated.
Astigmatic difference between X and Y-axes is small because a small
objective aperture was used. Dotted line shows optical axis of
cylindrical lens. (b) Energy loss spectrum obtained by placing the
slit several microns from the optical axis.

OBSERVATION OF THE TRANSMITTED ELECTRON IMAGE OF THIN FILMS WITH A SCANNING
ELECTRON MICROSCOPE

Shizuo Kimoto, Hiroshi Hashimoto, and Susumu Tanaka

Transmitted electron images of thin films were observed with a scanning elec-
tron microscope. The construction of the detector system is shown in Figure 1.
In order to separate the transmitted and diffracted beams, an aperture and a
diaphgram were placed between the specimen and detector. The angle of the
detector aperture is about equal to or a little larger than that of the inci-
dent probe aperture. The contrast of the image depends on the aperture angle
of the detector. In order that the diffracted beams on a selected lattice
plane may form an image, the aperture is placed in the path of selected beams.

Figures 2 and 3 show the extinction contours and the equal thickness fringes
of an aluminum wedge. A replica film and crystal imperfections, such as dis-
locations, can also be observed as in an ordinary electron microscope.

The scanning electron microscope has the following advantages over the conven-
tional electron microscope.

1) In the scanning electron microscope, the aperture angle and its
   position can be easily varied or selected without changing the
   characteristics of the incident probe.

2) The deformation or the damage of the specimen due to the electron
   bombardment is negligible, as the incident probe current is in
   the range of $10^{-12} - 10^{-9}$ amperes.

3) A bright image is obtained since the probe current density is high
   for each picture element, and the photomultiplier of the detector
   works as an image intensifier.

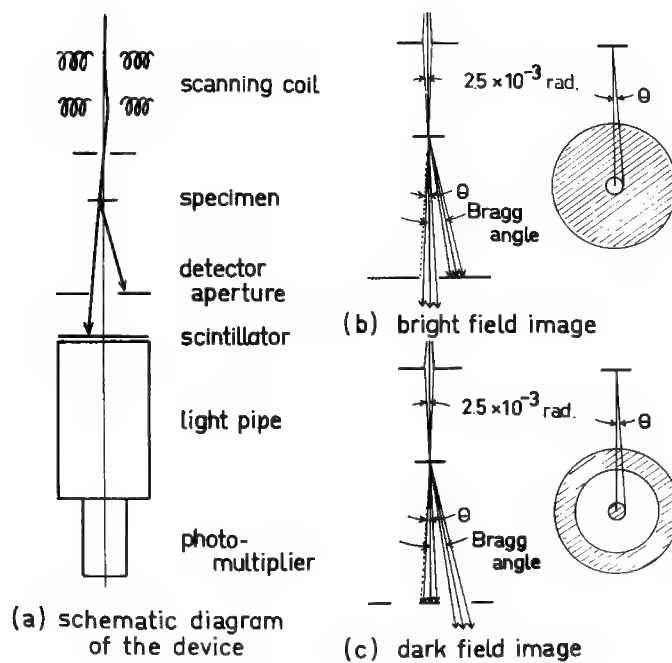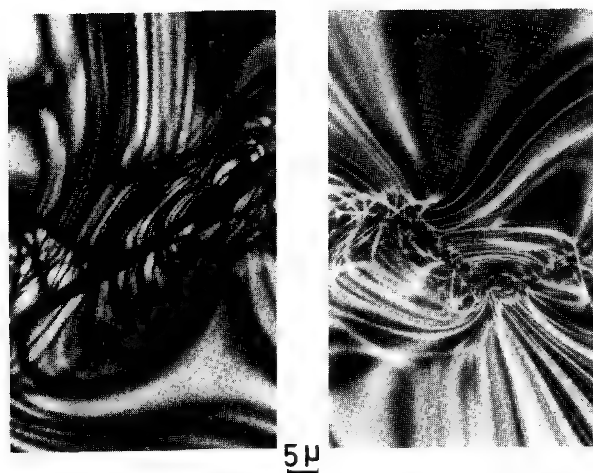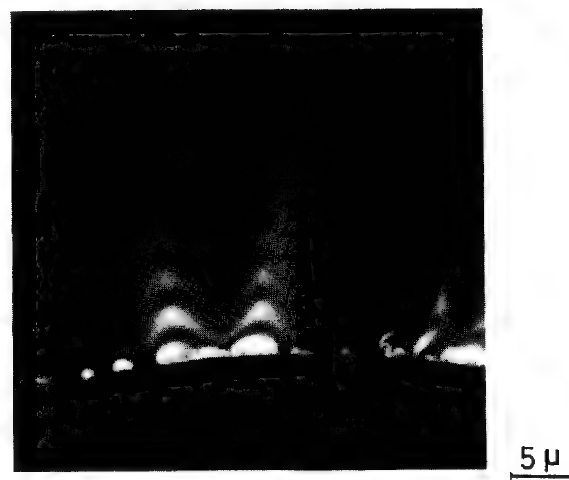|	
scanning coil	2.5×10^{-3} rad. θ
specimen	θ Bragg angle
detector aperture	
scintillator	(b) bright field image
light pipe	2.5×10^{-3} rad. θ
photo-multiplier	θ Bragg angle
(a) schematic diagram of the device	(c) dark field image

Figure 1

(a) Bright field   (b) Dark field
(Aluminum   45 KV)

Figure 2

Equal thickness fringes in Aluminum
Dark field.   45 KV

Figure 3

54

DECONVOLUTION: A NEW TECHNIQUE TO INCREASE ELECTRON MICROPROBE RESOLUTION

Eugene J. Rapperport

The concept of using the techniques of deconvolution to increase electron microprobe resolution to sub-beam sized dimensions is currently being explored in detail. The initial phase of this work has been previously reported [1]; the recent work has been devoted to refinements in the methods of deconvolution and the generation and analysis of reliable specimens of known geometry.

By the use of deconvolution techniques applied to appropriate data it may be possible to obtain composition profile information to a resolution of one-tenth of beam diameter, or smaller. This may be done by examining the interaction of a known (measured) incident electron spatial profile with an unknown (desired) concentration discontinuity to yield a known (measured) transmitted or backscattered electron spatial profile. Analyzing the interaction of these three distributions as a superposition problem, one finds the profile of the observed backscattered (or transmitted) current distribution, $h(t)$, as the convolution of the concentration discontinuity profile, $g(t-x)$, and the incident electron profile, $f(x)$. Using x as a distance variable and t as an auxiliary distance variable to relate the geometry of $f(x)$ to $g(t-x)$, one may write:

$$h(t) = K \int_{-\infty}^{\infty} f(x) \, g(t-x) \, dx \qquad (1)$$

where K is a constant whose value is determined by experimental conditions.

The deconvolution of the desired concentration profile, $g(t-x)$, from the other two is a mathematical problem involving the solution of the given integral equation relating the three profiles. The deconvolution technique that is now being explored is a modification of one proposed by Rice [2]. The essence of Rice's method is the use of Laplace transforms of the functions of equation (1) to obtain a series of n simultaneous equations involving a lesser number, m, different values of the unknown $g(t-x)$. The solution of these simultaneous equations, in general, requires the use of an additional constraint, such as minimizing the maximum deviation or minimizing the sum of the squares of the deviation.

Rice's solution was found to work well in the deconvolution of a mathematically simulated electron probe problem; however, when a small amount of random noise (0.5% of peak) was analytically introduced, the solution became unacceptably degraded. At this juncture, Ridge Analysis [3,4] was successfully applied to Rice's solution as an effective analytical tool. Ridge Analysis, applied to the matrix inversion required in Rice's solution, introduces additional statistical constraints in order to determine how stable the exact analytical solution is and simultaneously shows the best compromise if it proves unstable.

Examples of deconvolution operations on simulated data with various degrees of noise introduced will be shown and discussed. Examples of deconvolution of real electron probe data taken on specimens of known geometry will also be shown to illustrate the principles and applications of the method.

The development of the mathematical analysis and its reduction to a form suitable for digital computer processing has been done by D. Morris of the Kennecott Copper Scientific and Engineering Computer Center.

----

1. E. J. Rapperport, First Nat'l. Conf., (College Park), op. cit.
2. R. B. Rice, Geophysics, 27, (1), 4 (1962).
3. A. E. Hoerl, Chem. Eng. Prog., 55, (11), 69 (1959).
4. A. E. Hoerl, Chem. Eng. Prog., 58, (3), 54 (1962).

MECHANISM OF GAIN SHIFT IN PROPORTIONAL COUNTERS

N. Spielberg

Counting rate dependent shifts of the pulse height distribution have been rather troublesome for flow proportional counters used to detect soft X-rays, particularly when employed with the electron microprobe X-ray analyzer. These shifts are present in sealed counters also. When shifts occur, counting rates may be kept low to avoid complex correction procedures. This paper reports further studies of factors affecting the shifts, and conclusions as to the basic mechanism [1].

Several mechanisms may be considered: A. Space charge effects: (1) Due to low mobility of positive ions generated in the avalanche, at sufficiently high counting rates and gas gain the large amount of uncompensated positive charge within the tube volume will induce a negative charge on the anode wire, decreasing the electric field, and hence the gas gain. (2) The space charge of electrons in the final stages of an avalanche reduces the field for immediately subsequent nearby avalanches. B. Recombination effects: At sufficiently high gas gain and counting rates, the density of positive ions near the anode wire is high enough to recapture electrons from the final stages of the avalanche. C. Contaminant effects: Electronegative atoms, such as oxygen or chlorine, can decrease the number of electrons in the avalanche.

The admissibility of these mechanisms may be considered in the light of the following experimental conclusions: (1) If the proportional counter is operated so as to reduce the number and size of avalanches per unit area of anode wire, shifts may be reduced or eliminated. Thus it is better to use conditions (pressure, composition, X-ray optics) to give X-ray absorption throughout the counter volume, rather than through a very narrow cross-section or between the anode wire and entrance window. Increasing the anode diameter (and hence its surface area) dramatically reduces the shifts, and the use of low gas gain is helpful. (2) Doping noble gas mixtures with a small percentage of heavier noble gas atoms to inhibit the formation of molecular ions (which have extremely high recombination rates) has no effect on the shifts. Shifts are observed in gas mixtures containing no noble gas, such as pure methane. (3) The material of the anode and its treatment have large effects on the magnitude of the shifts. Treatment of the wire material may be only temporarily effective, with gradual deterioration under continued operation until shifts are as large as with untreated material. (4) In some cases, shifts do not take place immediately upon changing the counting rate, but the pulse height distribution can be seen to be changing from one equilibrium position to another. The transition time varies inversely with pressure, and can be as long as a few minutes at 50 torr.

It thus seems that the most likely cause for the shifts is the presence of adsorbed gases on the anode wire, which are driven off under the action of the avalanches. These adsorbed gases either capture electrons from the final stages of the avalanche or increase the amount of energy required to create

ion pairs in the final stages of an avalanche. The amount of adsorbed gases driven off depends upon the number of discharges per unit area of anode wire and upon the wire material and treatment; and the transition time depends upon the time to achieve equilibrium between adsorbed gas driven out and gas being re-adsorbed on the wire. One source of gas to be adsorbed would be debris from the quench gas.

----

1. N. Spielberg, Rev. Sci. Instr. $\underline{37}$, 1268 (1966); Rev. Sci. Instr. $\underline{38}$, to be published (1967).

PULSE HEIGHT PROGRAMMED X-RAY WAVELENGTH SCANNING

Kurt F. J. Heinrich, Mary Ann M. Giles and Donald L. Vieth

Several publications describe single channel pulse height selectors synchro-
nized with a scanning crystal X-ray spectrometer [1-4]. In such devices the
first order reflections are maintained within the pulse height selector window
during the scanning operation, while the higher order reflections are excluded.
The elimination of higher order reflections simplifies the interpretation of
spectra. This advantage is considerable in electron probe microanalyzers
covering the wavelength region from 10 to 70 angstroms where many higher order
lines appear.

As mentioned elsewhere [1], it is advantageous to adjust for this purpose the
pulse amplification rather than the pulse height selector parameters. In the
case of a wavelength change which is constant in time, this can be obtained
simply by driving at uniform speed a linear potentiometer regulating the linear
pulse amplification. A device for an electron probe based on this design will
be described.

This device incorporates also a circuit permitting the registration of reflec-
tions higher than the first in a distinctive manner. This is achieved by
periodic switching from the integral mode to the differential mode of the
pulse height selector. The first order reflections remain within bounds of
the selector regardless of the mode, while higher order lines are detected in
the integral mode only. As a result, they appear as periodically interrupted
traces, which can be used for confirmation of lines detected in the first
order.

The effectiveness of this device is limited only by possible excessive pulse
height shrinkage at high counting rates, and by occasional effects of escape
peaks in higher orders of reflection. In spite of these limitations, the
interpretation of such spectra is considerably simplified, and the possibility
of misinterpretation of reflections in higher orders is avoided.

To assist the interpretation of wavelength scans, we use a combination of
wavelength tables and graphs. This task is complicated by the fact that the
spectrometers of the instrument used have crystal changers. Since the wave-
length scale is used for two crystals of different spacings, the readings of
at least one crystal must be multiplied by a factor to yield wavelengths in
angstrom units. Tables incorporating these conversion factors were calculated
by E. W. White et al. [5]. These tables include numerous satellite lines not
normally observed in electron probe analysis; the section ordered by atomic
numbers of the emitting element does not contain higher order reflections.
Hence, while these tables are extremely useful they are too cumbersome for
routine wavelength scan interpretation.

Using data extracted from White's tables, we have constructed a simplified set of tables and graphs for the mentioned purpose. We have experimentally scanned several elements in order to determine which lines and orders of lines can be expected to be found commonly in wavelength scans. A table containing only these reflections was then constructed. In order of increasing atomic number, all reflections of a given element which are observable by means of the crystals installed in our instrument are listed. The crystals taken into consideration are the following: LiF, EDDT, ADP, KAP, and lead stearate. This table is complemented by a series of graphs showing the position on the spectrometer scales of the X-ray emission lines.

The interpretation is started by tentatively identifying the strongest line appearing on the wavelength scan registration, using the graph, and then determining with the aid of the table the position of all other lines of the same element. This confirms the original diagnosis and permits the rapid identification of a great number of higher order reflections. The second strongest, first order line is used next, and the process is repeated. The entire operation is very fast and effective, even without the use of the pulse height programmed wavelength scanning device described above. Combined with this device, the interpretation of wavelengths scans is rendered extremely simple even if a great variety of complex spectra must be dealt with.

----

1. K. F. J. Heinrich, Advances in X-ray Analysis, Vol. 4, University of Denver, Plenum Press, N. Y., 1961, p. 370.
2. F. B. Riggs, Jr., Rev. Sci. Instr. 34, 312, 1963.
3. M. L. Salmon, Advances in X-ray Analysis, Vol. 7, University of Denver, Plenum Press, N. Y., 1964, p. 604.
4. K. Weber and J. Marchal, J. Sci. Instr. 41, 15 (1964).
5. E. W. White, G. V. Gibbs, G. G. Johnson, Jr., G. R. Zechman, Jr., X-ray Wavelengths and Crystal Interchange Settings for Wavelength Geared Curved Crystal Spectrometers, 2nd Ed., The Pennsylvania State University, University Park, Pa., 1965.

GAS JET SAMPLE DECONTAMINATION IN THE ELECTRON MICROPROBE

S. H. Moll and G. W. Bruno

The level of analytical detectability of the elements boron, carbon, nitrogen, oxygen and fluorine has been severely limited by the formation of the carbon contamination spot. The thickening spot yields not only an increasing $CK\alpha$ X-ray intensity, but in addition, it strongly absorbs CK_α or $NK\alpha$ X-rays produced in the sample. Investigation of the sample light element contents is limited to short time X-ray counting which limits both the precision of the result and the detectability.

The authors recently proposed a technique [1] in which the carbon X-ray intensity is measured as a function of time. An extrapolation to zero time yields the true sample X-ray intensity. Ong [2] has developed the use of a cold "finger" which very effectively reduces the rate of carbon contamination. Castaing and Descamps [3] described the use of a gaseous flow directed through a capillary tube at the point of excitation. This procedure is successful both in eliminating carbon contamination and in cleaning previously contaminated surfaces.

This paper describes an examination of the phenomenon of gas jet cleaning carried out with argon, air and other gas streams on a variety of sample surfaces.

A plot of the rate of carbon contamination on copper indicates that a flow rate of 1 cc/minute of air eliminates carbon deposition. However, a flow of 1.4 cc/minute of argon is required to reduce the contamination rate to zero. Although the rate of carbon contamination on Si is lower with no gas flow, the gas flow rates required for the complete elimination of carbon contamination are essentially the same as those required for copper.

The use of air as a decontaminating gas is most convenient. However, the possibility of surface oxidation must be examined. Recent data [1] showed that oxygen is deposited along with carbon in the contamination spot. As expected, the initial oxygen contamination rate is more rapid when the air gas stream is utilized. The rate of contamination appears to level off after a few minutes, however, and the net $OK\alpha$ intensity increase is about twice that observed when no air gas jet is used for the same time interval. Surprisingly, a high oxygen contamination rate is also noted when the argon gas jet is used. A series of different gases and various surfaces have been examined in order to determine the mechanism of oxygen contamination and to eliminate its presence.

The surface cleaned by the gas stream is relatively less susceptible to subsequent carbon contamination and acid etching. Practical application of the gas jet appears to be entirely feasible and no systematic errors are discernable when it is used. Filament life is reduced when the gas jet is used, but not drastically so.

Further work aimed at determining the mechanism of gas cleaning involved the use of various gases and substrates and application of various potentials to the sample surface. Interaction of the gas stream and electron beam must occur, with possible ionization, since a loss of incident electron current occurs.

----

1. S. Moll, G. Bruno, First Int. Conf. (College Park) op. cit.
2. P. S. Ong, J. F. Moskal, P. Crean, 14th Annual Denver Conf., Applications of X-ray Analysis, 1965.
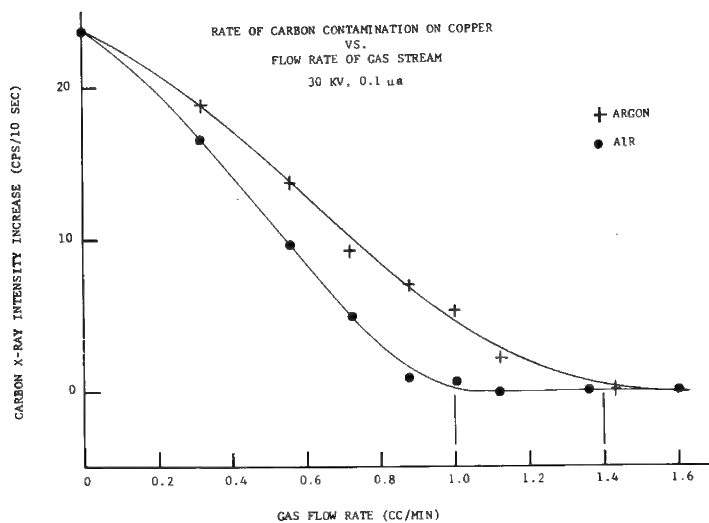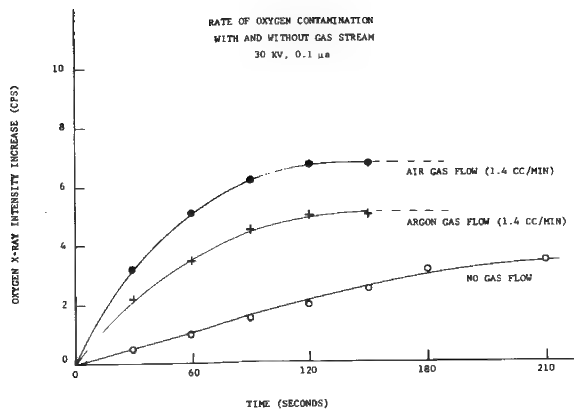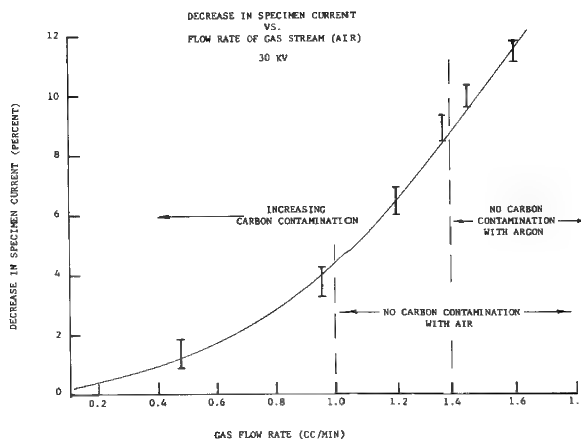3. R. Castaing, J. Descamps, Comptes Rendus, 238, 1506 (1954).

Figure 1

Figure 2

Figure 3

STATISTICAL EVALUATION OF PHOTOGRAPHIC, OPTICAL AND ELECTRONIC INTEGRATION OF X-RAY SCANS
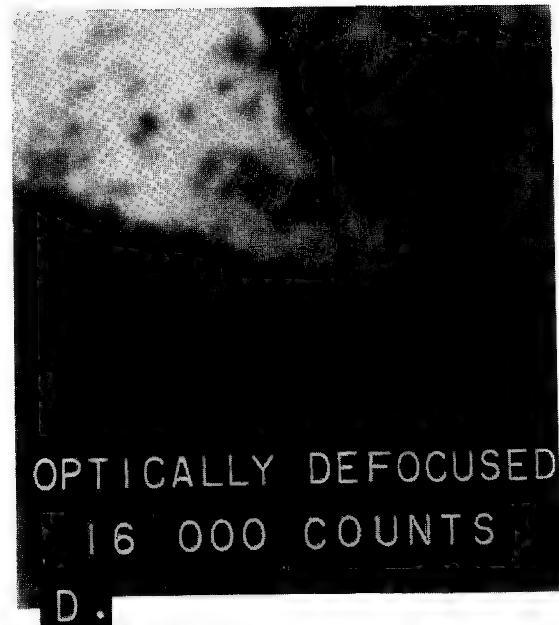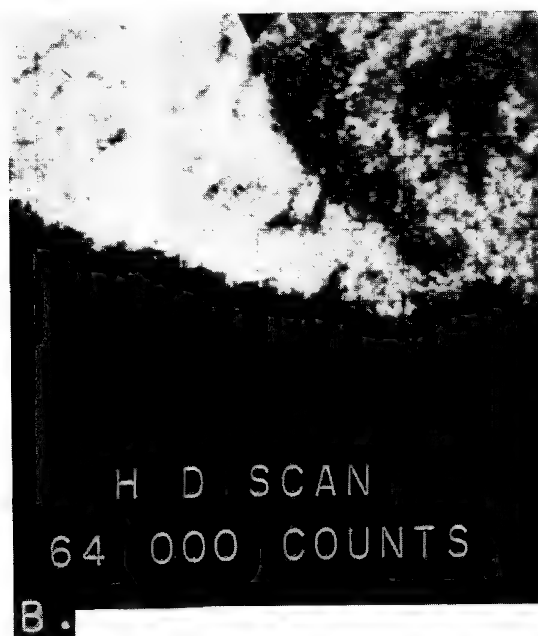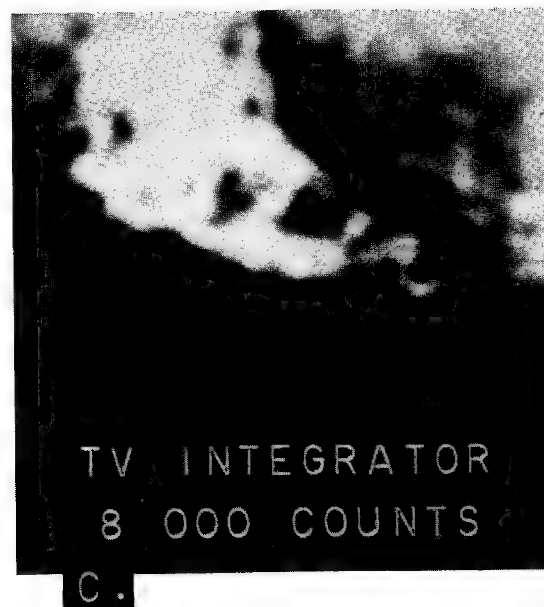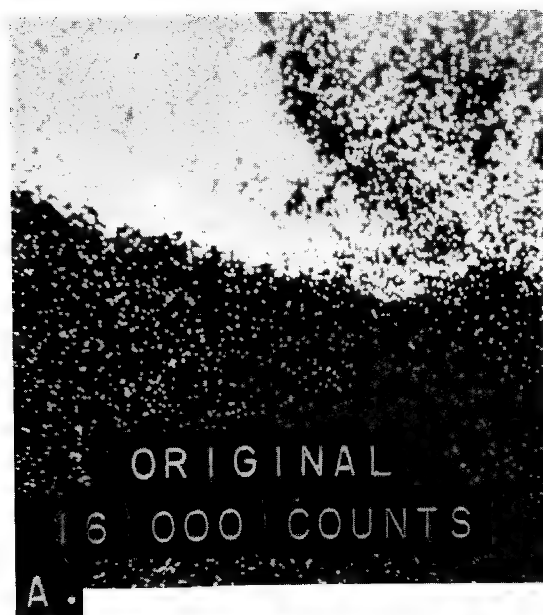

William R. McMillan

An investigation of possible improvements in X-ray raster scans and in treating the completed scans was made. In particular, techniques available for enhancement of the real structure which the scan represents, and also the preparation of back-ground-free scans suitable for viewing by nontechnical people were examined.

A previously reported study [1] explored methods of obtaining concentration contour maps from suitable X-ray raster scans and presenting these in black and white or color on a TV screen. The success of those methods depends upon the number of events registered on the film. For that reason, films with different numbers of photons registered on them were used as a basis for the present work.

Several Fe $(K_\alpha 1,2)$ scans were made of the same area in which the total numbers of counts recorded on each film were distributed in the range from 1,000 to 64,000. For these films, four different cases were considered: (a) Every count (true signal plus background) was recorded on the film. (b) The cathode ray tube was defocused slightly and the camera exposure reduced so that only nonrandom true structure would reproduce. Since this method of treating the data uses the low exposure end of the Hurter and Driffield photographic sensitivity curve, it will be called here the H & D scan. (c) Completed scans were treated in Gregg's [2] closed circuit TV data integrator. (d) The same scans were photographed while optically defocused with a one-half diopter lens inserted in the otherwise one-to-one copying system and with the lens set at the optimum aperture.

Careful comparison of these prints indicated that the TV integrator (c) did as well for fine structure duplication with only half the number of counts as the original (a). Second, while the H & D scans (b) by design gave the best pictures, they required four times as many counts to compare with the TV (c) scans. Third, the optically defocused scans (d) were not appreciably better than the original scans (a).

---

1. W. R. McMillan, Pittsburgh Diffraction Conference, November 9-11, 1966.
2. E. C. Gregg, et al, Am. J. of Roentgenology, Radium Therapy and Nuclear Medicine, 93, 733 (1965).

A. ORIGINAL 16 000 COUNTS

B. H D SCAN 64 000 COUNTS

C. TV INTEGRATOR 8 000 COUNTS

D. OPTICALLY DEFOCUSED 16 000 COUNTS

A SPECIMEN HEATING DEVICE FOR AN ELECTRON PROBE MICROANALYZER

Shizuo Kimoto, Hiroshi Hashimoto and Kazuko Tada

A specimen heating device has been developed for an electron probe microanalyzer. The furnace consists of a beryllia porcelain crucible provided with a tungsten heater. The temperature of the specimen can be raised to 1,100°C.

When measuring the absorbed, backscattered and secondary electrons on the specimen at high temperatures, it is necessary to consider the effect of the thermal electron emission which disturbs the measurement.

The thermal electrons which are emitted from the specimen and from the furnace produce a net current between these two components which electrically couples the specimen with the circuit which supplies power to the heater. Circuit noises are therefore induced in the specimen, producing current fluctuations in the absorbed current signal. The quality of an absorbed electron image will, therefore, deteriorate.

This paper discusses a method which eliminates this disturbance in the absorbed electron image. Electrical shielding has been effectively achieved by providing a conducting shield in the furnace.

Figure 1 shows a schematic diagram of the furnace. The furnace is a double crucible construction with a thin tantalum foil between the inner and outer crucible. The foil is grounded via the lead shown, thus protecting the specimen from signals induced through the heater.

Some AC noise is picked up even when the shielded furnace is used. Figure 2 shows the relation between temperature and noise. The noise results chiefly from stray fields which are picked up by the heater circuit. The AC noise is appreciably reduced by shielding, however, the effect of furnace shielding on an absorbed electron image is illustrated by applying 1 kc square waves with amplitudes of 1 and 10 volts to the heater. In the case of the unshielded furnace, the noise predominates over the signal such that a clear image cannot be obtained. With the shielded furnace, the noise almost disappears.
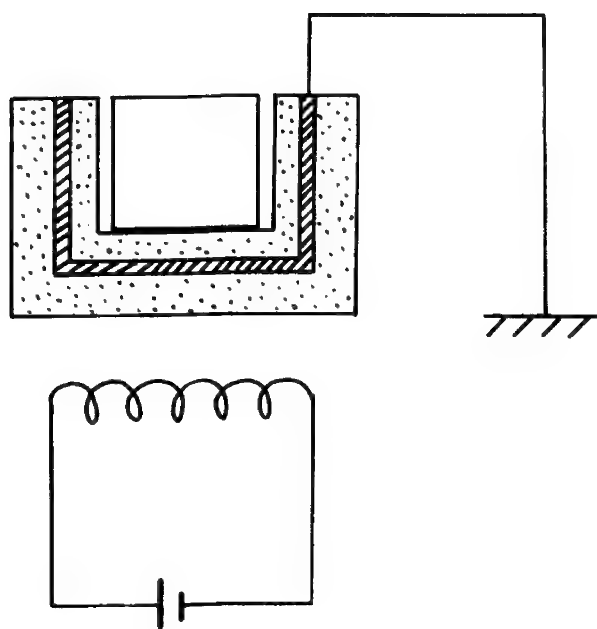
Schematic Diagram of Furnace

Figure 1
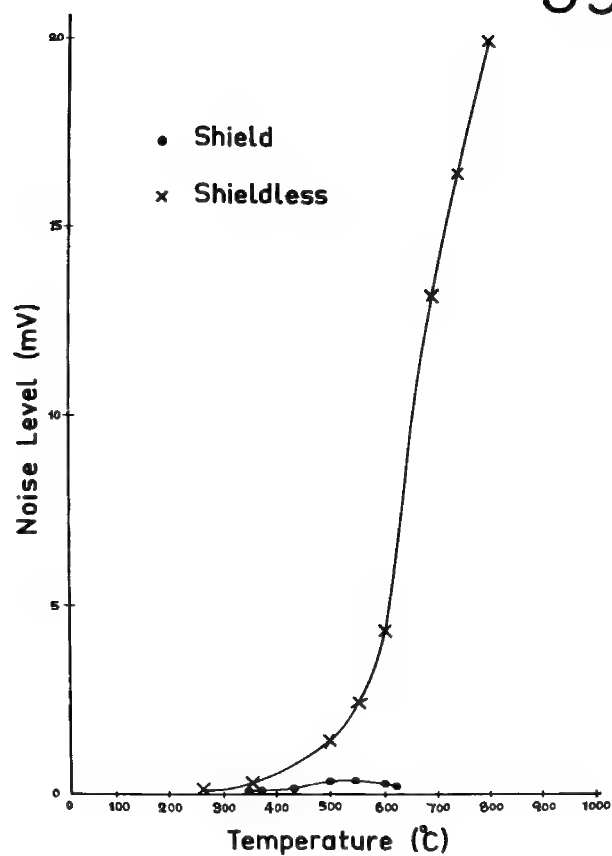
Figure 2

A SIMPLE CAMERA FOR TAKING STERO PROJECTION X-RAY MICROGRAPHS WITH AN ELECTRON MICROPROBE

J. C. Robinson and M. J. Mitchell

A simple method has been devised to take stero projection X-ray micrographs in the electron microprobe. A standard Applied Research Laboratories microprobe sample holder was used to house the camera. The sample holder, with a light tight base, is capped with a washer, the central hole of which is covered with a thin metal foil of the appropriate target material to produce a divergent beam of X-rays under electron bombardment. The specimen is placed beneath the foil at a distance depending on the magnification desired. A disk of X-ray sensitive film with emulsion on the upper surface only is placed in the bottom of the camera. An X-ray image is formed on the film by the differential absorption of X-rays in the specimen. The exposed film is removed from the camera, developed and printed by standard enlargement techniques or rephotographed in a microscope using transmitted light.

An almost unlimited depth of field is permitted by this method. Stereo pairs (Figure 1) may be produced by taking pictures of the same sample with the X-rays originating from different points on the target.

Primary magnification of 100X have been made, and pictures with magnifications of 4 or 5X have been optically enlarged to several thousand times with good results. The resolution is limited by the size of the excited volume in the target and the film emulsion.

Pictures can be made of organic or biological specimens as well as metals. This technique has been used to find the spatial distribution of metal particles in a filter material, to determine the phase relationships in metal and fiber composites, to determine the morphology of single fibers and filaments and to photograph biological specimens. These pictures can also be of aid in selecting areas for thinning for transmission electron microscopy.

Figure 1   Plastic Foam, Au target, 2.5 min exposure, Kodak type M single side film, primary magnification 4x enlarged to 20x, 15 Kv.
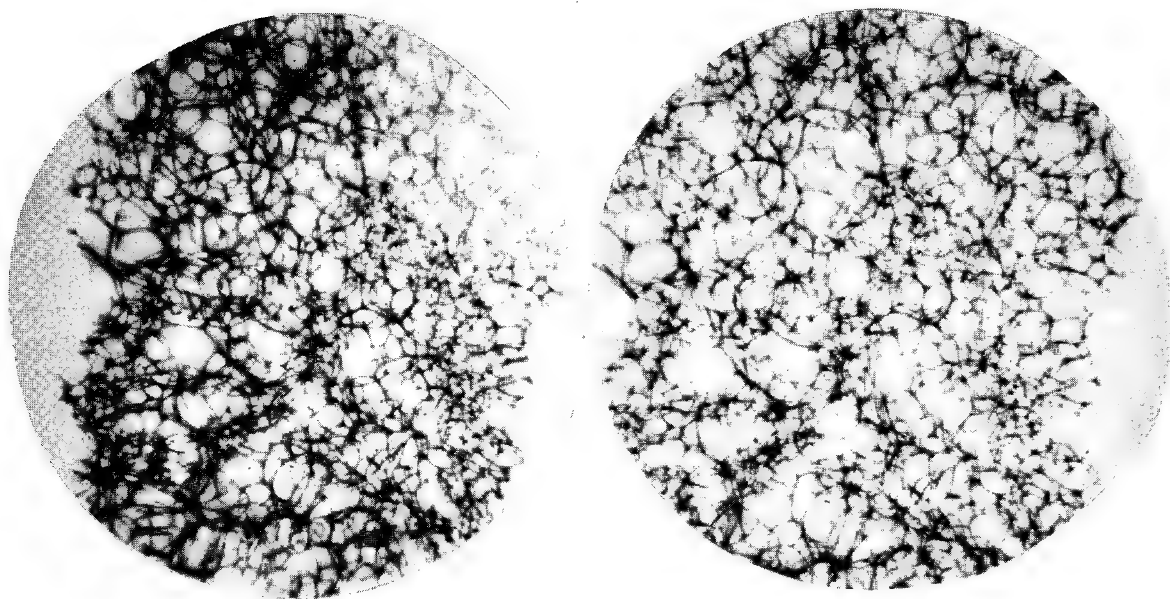
61

ON THE USE OF A FOCUSING SPECTROMETER WITH A CAMBRIDGE ELECTRON PROBE

D. R. Beaman and H. A. Diehl

An Acton Laboratories X-ray spectrometer has been installed on a Cambridge Mark II electron probe microanalyser in an attempt to obtain the resolution, peak to background ratios and intensity/current values associated with focusing spectrometers. In this spectrometer the crystal moves away from the target along a straight line, at a constant take-off angle, and tangent to the focusing circle. A supporting frame was constructed to hold the spectrometer at a 20° take-off angle and to provide complete translational freedom. An X-ray port was made that would offer a minimum target to crystal distance, contain a Mylar window and accept apertures of various sizes. The new spectrometer was operated in air, no permanent modifications of the column were made, and the Cambridge counting circuitry, including the preamplifier, was utilized.

Comparative measurements were made on Fe, Cu, Ni, Zn, Mn, Cr, W, Pt and Pb at 20 and 30 KV with different spectrometer slit openings. The tables show some results obtained on Cu and W with and without pulse height selection. As expected, a notable improvement in performance is obtained with the new spectrometer; e.g., peak to background ratios at the same peak intensity levels are increased considerably. Even better results could be attained by using different crystals (1011 quartz), sealed detectors, high pressure flow detectors, and by operating in vacuum. Use of the spectrometer without modification of the column restricts slightly the lower wavelength limit because the minimum target to crystal distance of 92 mm cannot be realized; however, this situation could be alleviated by redesigning the column base.

Combining a focusing spectrometer with the specimen stage in the standard Cambridge unit in which the control of specimen height is limited makes it necessary to refocus the spectrometer whenever the electron beam or sample is moved. The problems encountered in the analysis of an alloy as a result of this requirement will be discussed.

Photographs of the arrangement, construction details, complete performance data, cost information, spectrometer ranges, and possible improvements will be discussed.

Copper ($K\alpha 1$ radiation)

Unit	Acton	Acton	Cambridge	Cambridge
Medium	air	air	air	vacuum
Aperture	3mm dia.	3mm dia.	71% slit	68% slit
Crystal	quartz	LiF	LiF	LiF
Baseline only				
%*	100	100	100	100
P	3960	10550	9150	9950
P/B	465	382	159	174
R	1.0	3.6	4.0	4.0
With pulse height selector				
%	59	43	51	53
P	2340	4560	4650	5250
P/B	1650	8280	365	353

* % is the percentage of the total peak accepted by the pulse height analyser; P is the peak intensity in cps; P/B is the peak/background ratio; and R is the peak width at half peak intensity in minutes.

Tungsten ($L\alpha 1$ radiation)

Unit	Acton	Acton	Cambridge	Cambridge
Medium	air	air	air	vacuum
Aperture	3mm dia.	3mm dia.	82%slit	85% slit
Crystal	quartz	LiF	LiF	LiF
Baseline only				
%	100	100	100	100
P	2610	7020	5810	6640
P/B	111	102	44	47
R	1.4	3.6	4.8	4.8
With pulse height selector				
%	56	44	54	55
P	1462	3075	3140	3630
P/B	268	943	96	105

PROGRESS IN FULLY AUTOMATIC SCANNING ELECTRON PROBE MICROANALYSIS

G. W. Browning, D. J. Cooknell, K. Heathcote, I. K. Openshaw, J. L. Williams
and P. W. Wright

At the present time the vast majority of microanalysis is carried out with
manual instruments. The concessions to automation are limited to motor scan-
ning of specimens or the spectrometer. Few instruments have the facility to
allow conversion to automatic operation. Most of the automatic microanalysis
is concerned with computer calculation of analysis from raw data produced by
X-ray counting. There are many examples of such computer programs and the
nearest example of a microanalyser on-line was described at the First National
Conference [1].

However, the analysis process in many problems for a microanalyser may be
represented as a fairly complex routine:

1. Locate specimens
2. Select areas for analysis
3. Choose best kilovoltage for analysis
4. Select analysis lines
5. Set spectrometer angles for peaks and backgrounds
6. Select appropriate crystals
7. Find pulse height analyser conditions
8. Select counting times for peaks and backgrounds
9. Record counts
10. Repeat for standards
11. Calculate analyses

Such a program can be applied to such quantitative problems as (1) the analysis
of inclusions in metals, (2) the analysis of multicomponent diffusion, and (3)
the survey of different geological zones in specimens from a given site.

In the AEI SEM2 Scanning Electron Probe Microanalyser an automatic servo con-
trolled spectrometer and fully integrated control cubicle has allowed the pro-
vision of a tape programming control unit called P.E.R.M.A. (Programed Electron
probe for Routine Microanalysis). This unit uses a punched tape digital con-
trol system and provides for setting all of the facilities in the control cubi-
cle. The quantitative analysis processes covered are:

1. Selection of spectrometer angle for peak of analysis lines.
2. Selection of spectrometer angle for backgrounds of analysis lines.
3. Selection of appropriate crystal and detector for analysis lines in
   range from BK upwards.
4. Selection of pulse height threshold voltage, with a fixed gate width,
   for each analysis line.
5. Choice of counting range with preset time or preset pulses.
6. Print accumulated pulses or time.
7. Repeat program as appropriate for standards.

Other facilities which can be included in the tape program include (1) selection of specimen position and appropriate standard, (2) scanning photography of both electron and X-ray pictures, and (3) line scanning and recording of semi-quantitative data.

A routine program for the analysis of 12 elements has been applied to inclusions in steel. With a counting time of 10 seconds on peaks and backgrounds, the program takes 9 minutes to analyse each point. Results from such a routine show good agreement with manual analysis.

Our conclusion is that the microanalysis of many problems can be accomplished automatically, the calculation of all quantitative results can be programed and therefore, the next stage in the automation of a microanalyser is to have the instrument on-line with a computer. This unit will allow, among other facilities, suitable feed-back from the calculated results to control the analysis procedure and optimize the time taken to produce true concentrations from a sample.

----

1. E. Lifshin, R. E. Hanneman, First Nat'l. Conf. (College Park), op. cit.

REPORT OF THE NEW YORK METROPOLITAN PROBE USERS GROUP ON ANALYSIS OF Fe-Ni AND Fe-Cr STANDARDS

G. L. Fisher, J. J. Fischer, A. Noetzel, and W. Sutkowski

The New York Metropolitan Probe Users Group was organized over two years ago. The group is open to all probe users in the New York area and its members represent fourteen private companies and two government laboratories. The main purpose of the group is to provide a forum for the interchange of ideas and information about electron probe microanalysis. This is accomplished largely by guest speakers, talks by members on their special areas of interest, and by cooperative studies such as reported here.

For the past year, the group has analyzed several binary alloy standards. Three iron-nickel and two iron-chromium compositions were prepared at the Paul D. Merica Research Laboratory of The International Nickel Company. The alloys were vacuum melted and then hot and cold worked and annealed to homogenize them. Chemical analyses were obtained from two laboratories. Microanalysis of twenty spots taken at random on each standard gave an average σ(experimental)/ σ(theoretical) of less than 1.6. The standards were analyzed by each member using the same operating conditions. Each member corrected the data using his choice of correction procedures. Results for one of the iron-nickel compositions are shown in the accompanying table.

The results are typical of those obtained with the other Fe-Ni standards. The agreement between the chemical analysis and the average of the microprobe analyses was about one percent. The intensity ratios were also corrected by applying the same correction procedure to all of the intensity ratios. Philibert's absorption correction, modified by Duncumb and Shields, and Castaing's fluorescence correction were used. These results are shown below the table.

The variation of intensity ratio with X-ray take-off angle was also investigated. A computer program, using Philibert's absorption and Castaing's fluorescence corrections, calculated the intensity ratio to give the true chemical composition for each standard for different take-off angles. A plot of these intensity ratios versus the cosecant of the take-off angle produced a straight line. Comparison was made between this line and the experimental points.

RESULTS OF MICROANALYSIS OF AN IRON-NICKEL STANDARD

INSTRUMENT TAKE-OFF ANGLE	INTENSITY RATIOS		CORRECTED COMPOSITIONS	
	Nickel	Iron	Nickel	Iron
52.5°	0.527	0.494	56.7	45.0
	0.519	0.488	56.6	43.4
41.0°	0.489	0.494	55.6	44.2
	0.517	0.506	56.4	43.6
20.0°	0.462	0.496	56.0	45.9
	0.452	0.475	56.6	43.4
16.0°	0.441	0.478	56.5	43.5
15.0°	0.472	0.456	57.2	42.8
AVERAGE			56.5	44.0
CHEMICAL ANALYSIS			56.4	43.7
MOD. PHILIBERT'S ABS., CASTAING'S FL.			57.4	42.8

64

REPORT ON THE ACTIVITIES OF THE MIDWEST ELECTRON PROBE USERS GROUP

D. R. Beaman*

The primary objective of the Group since its formation in June of 1966 has been the study of binary standards of known homogeneity and composition. The Group has completed its analysis of an Fe-Ni alloy provided by the New York Metropolitan Users Group and a cast brass (C-1102) provided by the National Bureau of Standards. Preliminary data on an Fe-C alloy have also been collected.

Each investigator determined the experimental X-ray intensity ratio for each component in the system. Corrections for deadtime, drift and background were made and the concentrations were calculated using the investigator's choice of correction procedures. In addition the concentrations were calculated using the following correction scheme on each measured intensity ratio: all intensity ratios were corrected for absorption using the Duncumb and Shields modification of the Philibert technique and the Fe and Cu (fluorescence of $CuK\alpha$ by $ZnK\beta$) intensity ratios were corrected for characteristic fluorescence using Reed's technique. The results are summarized in the accompanying tables.

The first Group analysis on Fe-Ni was performed using optional conditions of analysis while the second Fe-Ni and brass analyses were carried out under predetermined conditions. The following items were specified: beam voltage, sample current, pulse height analyzer settings, sample preparation, beam size, counting statistics, type of detector, measurement of background, and standards. The second analysis of the Fe-Ni sample resulted in a significant improvement in the results and gave data similar to those obtained by the Metropolitan Users Group. The relatively large number of measurements resulted in an accuracy of better than 0.5% and a precision of better than $\pm2.3\%$ of the amount present. These values were obtained using a variety of correction procedures. The use of a constant correction scheme on all data caused a slight degradation of some of the results.

A complete tabulation of results indicating the effect of take-off angle, dead time correction, and choice of correction procedure will be discussed. The Fe-C results and some probe performance data collected by the Group will also be presented.

---

*Reporting for the Midwest Electron Probe Users Group

SECOND TRIAL ON AN Fe-Ni ALLOY[1]

	Intensity ratio		Calculated chemical concentrations			
			Variable correction[2]		Constant correction	
	k(Fe)	k(Ni)	C(Fe)	C(Ni)	C(Fe)[3]	C(Ni)[4]
No. of Measurements	9	9	8	8	9	9
Mean (wt. %)	48.5	50.1	43.5	56.8	44.2	56.5
Standard deviation	0.8	1.9	1.0	0.8	1.0	0.7
Mean (wt. %)[5]	48.2	47.7	43.9	56.6	-	-
Standard[5] deviation	1.7	3.5	1.2	0.7	-	-

1. Mean of two wet chemical analyses-43.55% Fe and 56.55% Ni
2. Investigator's choice of correction techniques
3. Duncumb and Shields', and Reeds' correction techniques used
4. Duncumb and Shields' correction technique used
5. Results obtained by Metropolitan Users Group

NBS BRASS ALLOY - C1102[1]

	Intensity ratio		Calculated chemical concentration			
			Variable correction[2]		Constant correction[3]	
	k(Cu)	k(Zn)	C(Cu)	C(Zn)	C(Cu)	C(Zn)
No. of measurements	12	12	11	11	12	12
Mean (wt. %)	73.3	26.9	73.0	27.1	73.4	27.0
Standard deviation	0.9	0.4	0.5	0.4	0.9	0.4

1. Certified analysis...72.85% Cu and 27.10% Zn
2. Investigator's choice of correction technique
3. Duncumb and Shields technique used

REPORT OF THE SCANDINAVIAN ASSOCIATION OF MICROPROBE USERS

Lennart Backerud

The Scandinavian Association of microprobe users was constituted some years ago and now has 15 members. The object of the association is to increase the understanding of microprobe techniques by mutual exchange of knowledge and experience. Seven different types of instruments are in use among the members, and this fact makes it easy to compare the possibilities and limitations inherent in the construction of the different instruments, at the same time permitting the relative skill of each operator to be assessed. A simple test program, outlined in the table below, will be discussed.

Different evaluation methods published in the literature have been applied to calculate the composition of well-defined standard samples which have been circulated among the members. Depending on the geometry of the apparatus and on the accelerating voltage used, the methods of Tong, Philibert, Birks and others give more or less reliable results. Typical values obtained are shown in the accompanying figure and will be discussed.

Another activity of the group which will be covered in more detail is the practical limits of the use of the microprobe in metallurgical research. Samples have been distributed to the members to determine the limit of detectability. A simplified theoretical definition of the detectability limit will be given, which is based on the characteristic intensity from a pure metal standard and the spectral resolution of the instrument in question. A comparison between calculated and measured values will be reported.

A SIMPLE TEST-PROGRAM FOR MICROPROBES

Property	Procedure
Environment	Influence by Temperature - pressure changes, vibrations, etc.
Vacuum System	Rough and High Vacuum pumping times, Final pressure
Beam Current Stability	Sample current measured in a simple Faraday Cage over a period of time
Beam Position Stability	Measured on a "Sandwich Sample"
Beam Diameter	Electron Beam Diameter and effective X-ray diameter measured on a "Sandwich Sample"
Sample stage stability and reproducibility of settings	Repositioning of a small particle by reading the sample stage micrometers.

Spectrometer adjustment	Check correct absolute 2θ-values for all angles
	Optimize $\theta/2\theta$ ratios for all angles
	Optimize focusing conditions for all angles
	Measure on samples of pure Al, Cu, Ag and Pb:
	    Total intensity
	    Line/Background ratio
	    Halfwidth

Limits of detection	Determine on a series of standards
Scanning system	Measure and map intensity over whole scanned area
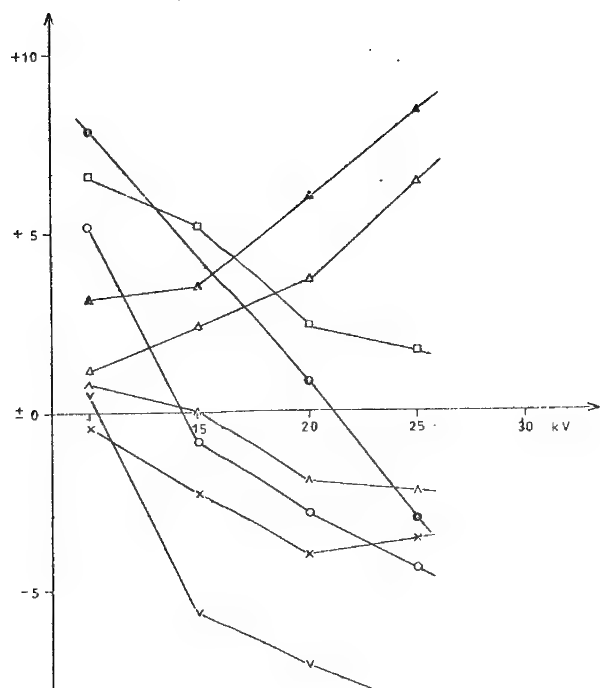
Figure 1 Corrections calculated for Al Kα in Al$_6$Mn by various methods indicated. Vertical scale is percent relative error in corrected intensity using a Geoscan.

x = Tong
o = Philibert
□ = Adler
△ = Theisen a)
▲ = Theisen b)
● = Birks
∨ = o plus atomnr. Reed
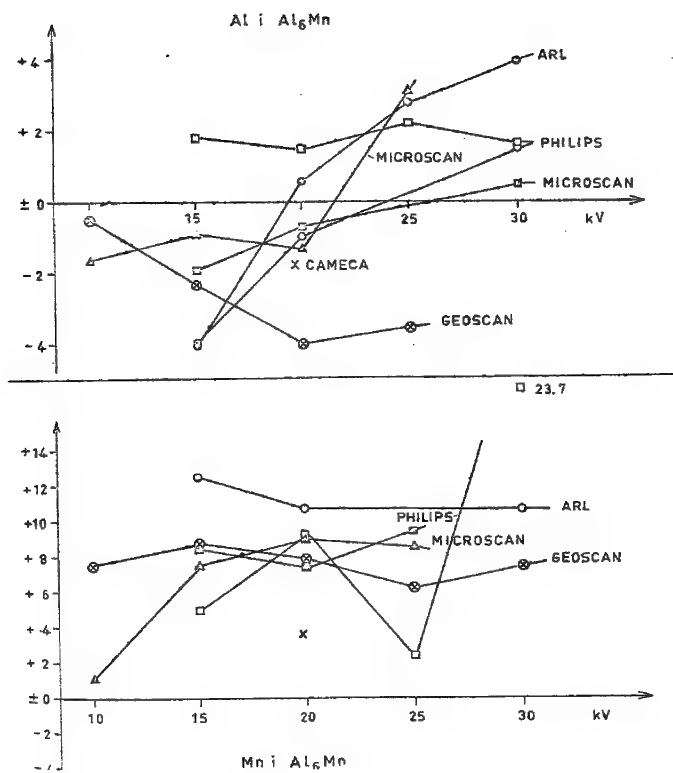∧ = □ plus atomnr. Reed

Figure 2 Absorption correction using Tong's method for Al$_6$Mn. Vertical scale is percent relative error in corrected intensity using various instruments.

PROPOSED CONSTITUTION FOR NATIONAL SOCIETY

Article I.   The name of the society shall be THE ELECTRON PROBE ANALYSIS
                SOCIETY OF AMERICA.

Article II.   The purpose of this Society shall be to provide continuity,
                advance planning and financing mechanism for annual meetings,
                to advance and diffuse knowledge concerning the principles,
                instrumentation and applications of electron probes, subject
                to the provisions of the Internal Revenue Code, Section 501(c)
                (3), (1954).

Article III.   The membership of the Society shall consist of Full Members,
                Honorary Members, Student Associates, and Sustaining Members.
                Sustaining Members may be either persons or corporations; all
                other members must be persons.

Article IV.   The officers of the Society shall be a President, a Secretary,
                and a Treasurer. Their election and term of office shall be
                stated in the By-Laws of the Society.

Article V.   The affairs of the Society shall be managed by an Executive
                Councel consisting of the three officers of the Society, three
                Members-at-large, the President-elect, and the immediate past
                President. The election and term of office shall be stated in
                the By-Laws of the Society.

Article VI.   Amendments of this Constitution may be proposed by the Council
                or by a petition to the President signed by at least two per-
                cent of the total number of current members. The text of the
                proposed amendment shall be circulated to the membership at
                least thirty days in advance of the meeting of the Society at
                which discussion is planned on the amendment. The amendment
                will be adopted if more than two-thirds of those voting by
                written ballot are in favor of the amendment.

Article VII.   In event of either voluntary or involuntary dissolution of the
                Society, the funds or assets of the Society, remaining after
                discharging all just debts of the Secretary or its officers in
                the name of the Society, shall be distributed without encumbrance
                to a non-profit group, organization or institution of learning
                within the contemplation of Section 180(c)(2) of the Internal
                Revenue Code (1954). The selection of the recipient or recipi-
                ents shall be made by the majority vote of the Executive Coun-
                cil in office at the time of dissolution, but in no event shall
                the assets be distributed to any member of the Society.

BY-LAWS

Article I. Membership

Section 1. Eligibility. Any person or corporation interested in the use of electron microprobes or related instrumentation shall be eligible for membership in this Society. Every person or corporation desiring to become a member shall in person or by authorized representative make application in writing for such membership.

i. Any graduate or undergraduate college or university student interested in the use of electron microprobes is eligible to become a Student Associate. Evidence of such interest must be certified by the faculty member advisor for this student.

ii. Any member wishing to participate in the financial obligations of the Society is eligible for election to Sustaining Membership in this Society.

iii. Any person whose contributions to the field of electron probe microanalysis are of the highest order is eligible for election to Honorary Membership in this Society. The number of Honorary Members may not be increased so as to exceed one percent of the Full Membership.

iv. Any member is eligible for election to Life Membership.

Section 2. Nomination and Election. Application for all classes of membership except Honorary Membership must be endorsed by at least two Full Members and forwarded to the Secretary. Nominations to Honorary Membership must be endorsed by at least ten percent of the Full Membership. A majority of the Members of the Executive Council present and voting at a regular or a special meeting shall constitute election to membership.

Section 3. Privileges. The right to vote at elections and to hold office shall be restricted to and vested in the Full Members of the Society in good standing. Full Members elected to Sustaining Membership or Life Membership keep their privileges as Full Members.

Section 4. Termination of Membership. Membership in the Society may be terminated at any time for cause by a two-thirds majority vote of the Executive Council present and voting.

Article II. Meetings

Section 1. There shall be an annual technical meeting whose location and dates shall be selected by the Executive Council.

Section 2. There shall be an annual business meeting held concurrently with the technical meeting.

PROPOSED BY-LAWS FOR NATIONAL SOCIETY

Article III.   Dues

Section 1.   The Executive Council shall be empowered to fix the annual dues, these dues being payable on January 1st of each year.

    i.   The dues for Full Members shall not exceed $10.00.

    ii.   The dues for individual Sustaining Members shall not exceed $100.00, and for corporation Sustaining Members shall not exceed $1,000.00.

    iii.   The dues of Student Associate members shall be 1/2 that of a Full Member for the first five years of membership. After five years, a Student Associate must apply for Full Membership.

Section 2.   A person elected to membership becomes a member in good standing upon payment of the designated dues. If the dues of any class of member remain unpaid for two consecutive years, the Executive Council shall be empowered to remove his name from the membership list.

Section 3.   For dues and other fiscal purposes, the fiscal year shall be January 1st to December 31st.

Article IV.   Election and Tenure of Officers

Section 1.   Any Full Member of the Society shall be eligible for election to any office in the Society. Each year a Nominating Committee, selected in the manner specified below, will nominate one or more candidates for each of the offices of the Society. The Secretary shall inform the members of the nominations made, distribute ballots and invite the members to suggest additional nominations for the various offices. The closing date for the ballots shall be November 1st of each year. Election shall be by a plurality of those voting. If there are no competing candidates, the nominees shall be declared elected at the annual meeting.

Section 2.   Terms of office will begin January 1st and end December 31st. All officers, except the Members-at-large, shall be elected for one year. The first year one of the Members-at-large shall be elected for one year, one for two years and one for three years. In the ensuing years, one Member-at-large shall be elected for a period of three years. No officer except the Secretary and Treasurer may succeed himself in the same office. If a vacancy occurs, the President shall be succeeded by the President-elect. If a vacancy occurs in any other office, the Executive Council of the Society shall be empowered to appoint a member to serve out the unexpired part of the term of the original officer.

Article V.   Committees

Section 1.   The Executive Council shall have the power to establish such committees as it may deem desirable to aid it in the management of the Society. The President shall appoint the Chairman and members of each committee and state the terms of appointment.

Section 2.   Standing Committees. Any committee established to provide continuing assistance to the Executive Council may be considered as a standing committee and its Chairman shall be a member of the Executive Council and with all the prerogatives of the members thereof.

Section 3.   Nominating Committee. The Nominating Committee for officers shall be appointed by the Executive Council immediately after the annual meeting, but not later than September 1st of each year, and shall include at least two Full Members of the Society who are not members of the Executive Council. It shall consist of at least four but not more than six members.

Article VI.   Regional Divisions

Section 1.   The Executive Council may, upon petition by members of the Society, authorize the formation of local chapters, or of regional sections of the Society. Such chapters or sections shall elect executive committees, who shall report at least once a year its activities and needs to the Executive Council of the Society. The chapters or sections shall have the power to collect dues.

Article VII.   Affiliation with other Societies

Section 1.   Affiliation of this Society with other scoieties may be implemented by an amendment to the Constitution or By-Laws according to the procedure of Article V in the Constitution.

Article VIII.   Amendments to the By-Laws

Section 1.   Amendments to these By-Laws may be proposed by the Executive Council or by a petition to the President signed by at least two percent of the total number of current members. The text of the proposed amendment shall be circulated at least thirty days in advance of the meeting of the Society at which discussion is planned on the amendment. Members shall vote by written ballot and the amendment will be adopted if it is favored by 3/5 of the members voting.